TABLE OF CONTENTS

Page

LIST OF TABLES

Page

LIST OF FIGURES

Page

LIST OF ABREVIATIONS

2D/3D	Two/Three Dimensional Space
ACPD	Adapted Coherent Point Drift
ASME	American Society of Mechanical Engineers
ASTER	Analyses des Structures et Thermomécanique pour des Études et des Recherches
CAD	Computer Aided Design
CASCADE	Computer Aided Software for Computer Aided Design and Engineering
CPD	Coherent Point Drift
CMM	Coordinate Measuring Machine
DCS	Design Coordinate System
FE	Finite Element
FEA	Finite Element Analysis
FEM	Finite Element Method
FENR	Finite Element Non-rigid Registration
FMM	Fast Marching Method
GD	Geodesic Distance
GD&T	Geometrical Dimensioning and Tolerancing
GMDS	Generalized Multi-Dimensional Scaling

GNIF	Generalized Numerical Inspection Fixture
GPS	Geometrical Product Specifications
ICP	Iterative Closest Point
IDI	Iterative Displacement Inspection
ISO	International Organization for Standardization
LTA	Lighter Than Air
MCS	Measurement Coordinate System
MDS	Multidimensional scaling
NGD	Nominal Geodesic Distance
QC	Quality Control
RBF	Radial Basis Function
RGNIF	Robust generalized numerical inspection fixture
RM	Rapid Manufacturing
RP	Rapid Prototyping
RT	Rapid Tooling

LIST OF SYMBOLS AND UNITS OF MEASUREMENTS

$\overrightarrow{\Delta r_j}$	Displacement vector [mm]
δ/tol	Ratio between maximum profile deviation (δ_{max}) and tolerance of profile
δ_i	Profile deviations [mm]
δ_{max}	Maximum profile deviation on a defect [mm]
σ_{noise}	Standard deviation of Gaussian measurement noise [mm]
$\lambda_1, \lambda_2, \lambda_3$	Barycentric coordinates ($\lambda_1 + \lambda_2 + \lambda_3 = 1$)
A/B.S/B.F/T	Case A/B . Small/Big defects . Flexural/Torsional displacement
$Ave.\ GD_{ij}$	Average geodesic distance between a pair of holes [mm]
B_j, B'_j	Corresponding points inside each constrained area j on the CAD surface, and consequently their correspondents on the scanned data
C_{CAD}, C_{Scan}	Set of correspondent pairs between two surfaces
C_{m_j}, C'_{m_j}	Centre of mass in B_j, B'_j
e_{ij}	Deviation metrics, Algorithmic error [mm] or [%]
F	Speed function with positive values
GD_{ij}^{CAD}	Nominal geodesic distance between two determined points or features on the CAD surface [mm]
GD_{ij}^{SCAN}	Geodesic distance between two corresponding points or features on the scanned part surface [mm]

$N(0, \sigma_{noise})$	Gaussian measurement noise [mm]
P_i, P_j, GD_{ij}	Featured points on a skin panel and their geodesic distances [mm]
$\mathbb{R}^m$	m-dimensional Euclidean space
S	Set of featured points
S_{CAD}	CAD surface
S_{Scan}	Scanned part surface
T	Shortest traveling time
$Tol_{\ arc\ length}$	Tolerance of arc-length along the surface [mm]

INTRODUCTION

Thesis problem definition

One of the main aspects for manufacturing companies to survive under globalization, market pressures, and technological developments is the quality control (QC) of products. Without regarding this aspect, it is not possible to be assured of the functionality and quality of products. Due to errors that occur during the manufacturing process, manufactured parts have deviations from their nominal geometry. Therefore, one of the important sections in quality control is the geometric inspection of products. With the help of computers, time and costs can be saved during the geometric inspection process.

Inspection fixtures integrated with coordinate measuring machines (CMM) are widely used in industry for geometric inspection. Non-rigid (or flexible) parts such as aeronautic products, that are the focus of this project, include deformations in the free-state condition due to factors such as weight and residual stress which cannot be completely and exactly quantified. Therefore, non-rigid parts are considered exceptions to the rule stated in standards such as (ASME Y14.5-2009) and (ISO 1101:2004) for Geometrical Dimensioning and Tolerancing (GD&T). These geometric inspections of manufactured parts are performed in a free-state condition. For the geometric inspection of non-rigid parts in industry, special fixtures integrated with CMM are usually used and a reasonable force ($\approx$ 50 N) is imposed on the flexible parts during the inspection to compensate deformations of such parts for simulating the product's functional state. These dedicated fixtures are very expensive, heavy and complex (Figures 0.1, 2.1, and 3.1), and they should be calibrated regularly. The flexible part needs to be precisely positioned on the inspection fixture. The time required for the fixture setup and the fixation process is typically more than 60 labor-hours. The other challenges are: dedicated and complex fixture design, inspection process and setup planning, and the production line stop (Figure 0.2). The proposed solution and the objective of this thesis, dimensional inspection of non-rigid parts without specialized fixtures (in a free-state condition), will be discussed in the following sections.

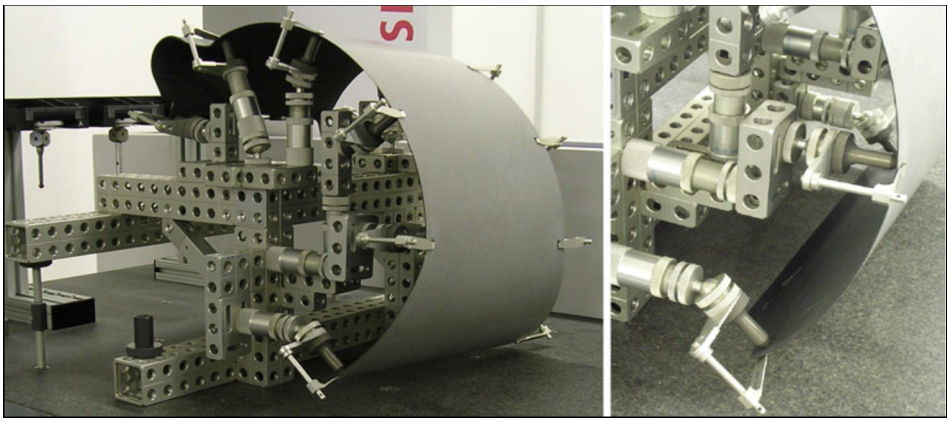

Figure 0.1 Special, expensive, heavy, and complex fixtures integrated with CMM for inspection of a flexible plate (Ascione and Polini 2010)

Cost	• Material • Operator & labor • Calibration,…
Time	• Inspection fixture setup (typical > 60 hours) • Inspection process integrated with CMM • Production line stop,…
Difficulties & Complexities	• Inspection process and fixture design • Inspection setup planning,…

Figure 0.2 Main challenges in dimensional inspection of flexible parts with dedicated fixtures in the industry

Quality control and geometric inspection of mechanical parts

With the developments and improvements in *rapid prototyping (RP)*, *rapid tooling (RT)*, and *rapid manufacturing (RM)*, it is now possible to design and manufacture products with high geometric complexity for application in industries such as aerospace and automotive. Therefore, product geometric inspection has an important role in the quality control of mechanical parts just after manufacturing, which usually consumes a large part of production lead time. Geometric specifications and design of a product are specified regarding functionality by means of Geometric Dimension and Tolerance (GD&T) of a product. The

GD&T inspection process is applied to verify the conformity of manufactured parts with the specification defined at the design stage. A reliable, efficient, and automated inspection process will decrease the product life cycle time and cost, improve industrial competition, and increase production efficiency (Gao, Gindy et al. 2006). Although geometric inspection methods and the equipment for rigid parts with regular geometric features have greatly improved and are generally available in the industry (Li and Gu 2005), the geometric inspection of non-rigid parts with free-form surfaces, especially without the use of inspection fixtures, has not been well studied.

Geometrical dimensioning and tolerancing

In mechanical engineering applications, free-form surfaces are assigned a *profile tolerance* to control surface variations (Li and Gu 2005). The surface profile should be controlled based on the principals and methods established in the standards of (ASME-Y14.5 2009) for GD&T (section 8, Tolerance of Profile). To control form or combinations of size, form, orientation, and position of a feature(s) relative to a true (nominal) profile, a tolerance zone is defined by using profile tolerances. This tolerance zone is a volume (3D), extending along the length and width (or circumference) of the regarded feature(s). The profile tolerance zone indicates a uniform or non-uniform tolerance boundary along the true profile within which the surface or its elements must lie. More details on tolerance zone boundaries, profile application, etc. are explained in the section 8, standards of (ASME-Y14.5 2009) for GD&T. Based on the application, the profile tolerance is defined with/without reference to a datum(s), which is called a related/individual profile tolerance (Li and Gu 2005). Regarding this research's main objective (fixtureless inspection), tolerances will be defined without reference to a datum(s).

Measurement methods

In traditional methods for obtaining measurement data, skillful operators use particular techniques and equipment such as special gauges; thus these methods require much time and

cost. On the other hand, due to errors resulting from operator and measurement uncertainties they have low accuracy. (Li and Gu 2004)

With developments in modern measurement systems, measuring operations have become much more accurate and quicker. Measurement data obtaining systems are divided into two main categories: contact measurement and non-contact measurement. (Savio, De Chiffre et al. 2007) presented a comprehensive review of measuring systems. A comparison of contact and non-contact measurement strategies is done in (Martínez, Cuesta et al. 2010), analyzing the applicability of contact and non-contact systems for measuring and control of tolerances.

(Beraldin 2010) proposed a more exact classification (Figure 0.3). Regarding this classification, point-by-point measuring methods are:

- generally more accurate,
- more rapid for controlling a small number of entities and dimensions,
- able to measure zones with difficult access more easily,
- not affected by reflectivity or transparency of objects.

In contrast, the non-contact measuring methods are:

- much more rapid for measuring a non-prismatic surface,
- more rapid for controlling a big number of entities and dimensions,
- able to measure, in some cases, inside and outside of a part,
- recommended for measuring flexible materials to avoid deformation of the part due to making contact.

One can choose an appropriate non-contact measuring method for a specific application regarding requirements such as accuracy, volume, flexibility, reflectivity, resolution, and portability (Beraldin 2010). For performing the fixtureless inspection in the free-state condition, the only option is the non-contact measurement because the contact measurement needs a physical fixture and positioning of the flexible part on it.

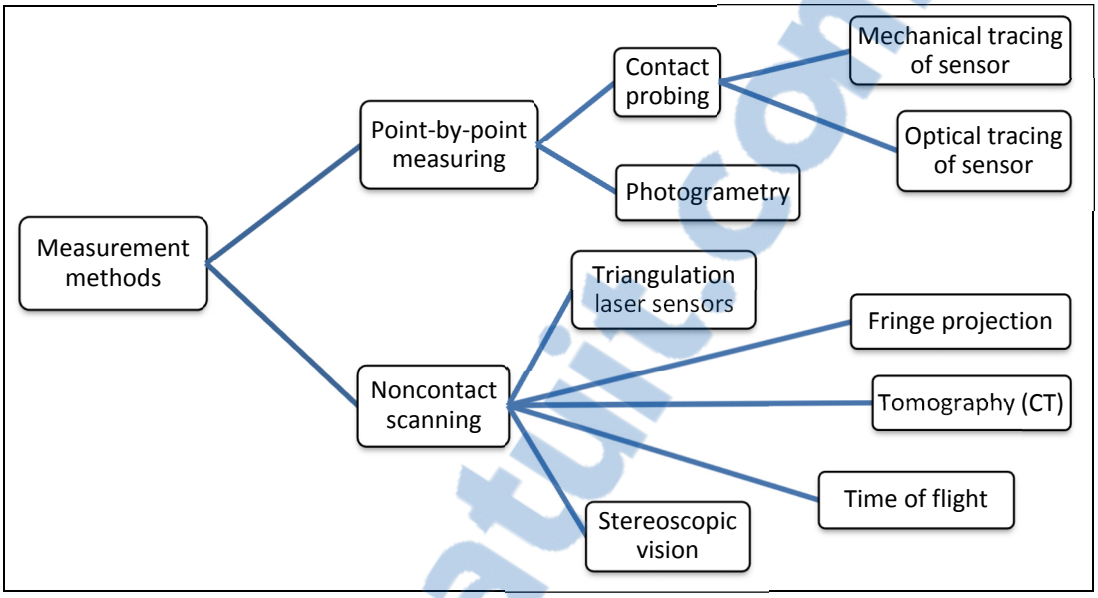

Figure 0.3 Measurement methods by (Beraldin 2010)

Registration (localization)

To compare the measurement data (point cloud obtained by a measurement method in the previous section) with the design (nominal, CAD) model for evaluating the deviations (and defects) with respect to the specified tolerance, it is essential to arrange these two surfaces in a common coordinate system. This process is called *localization* or *registration*. Traditionally, localization is performed by presenting the part at a favorite position and orientation using special tools, fixtures, etc. for inspection purpose. This kind of process is usually expensive and time-consuming, and needs time and effort to design and manufacture special fixtures. In recent and modern technologies, registration is done by the mathematical determination of a part's positions and orientations in the *design coordinate system (DCS)* with respect to the *measurement coordinate system (MCS)*. In application, registration can be done in two steps: finding the point-point *corresponding* relationship between scanned and nominal surfaces; and, finding an optimal transformation matrix between the DCS and MCS. (Li and Gu 2004), (Abenhaim, Tahan et al. 2011)

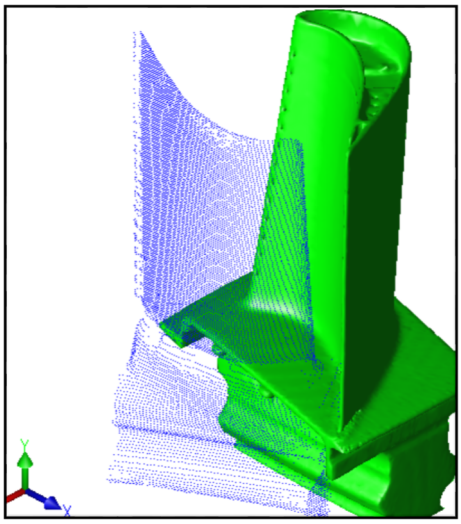

Figure 0.4 Registration of the measurement data with the nominal model (Radvar-Esfahlan and Tahan 2012)

Rigid registration (ICP)

(Li and Gu 2004) presented an extensive review of the rigid registration methods. (Besl and McKay 1992) developed the *iterative closest point (ICP)* algorithm, the most popular method for rigid registration of 3D shapes based on individual profile tolerance (without reference to a datum(s)) (Li and Gu 2005). The registration of two surfaces is performed by 3D transformations including rotations and translations. At each iteration, this algorithm calculates the optimal transformation matrix minimizing the Euclidean distance between two point clouds. Many variants of ICP have been developed improving all phases of the algorithm. Main advantages of ICP and its variants (Besl and McKay 1992):

- handling the full six degrees of freedom,
- independence from the shape representation (no need for a parametrical representation of the surfaces),
- need only for a procedure to find the closest point to a given point.

Generally, although ICP and its variations are the dominant methods for registration, they have an obvious limitation: two surfaces must be initially located close enough while

registering in order to determine the corresponding points which may be a difficult task when two surfaces have arbitrary positions and orientations in 3D space. (Li and Gu 2004)

A very recent method, *3-Points Convex Hull Matching* (3PCHM), was proposed in 2016 by (Fan, Yang et al. 2016) for fast and robust point set registration by using the invariant property of the 3D convex hull. Considering the invariant property of 3D convex hull, the algorithm is not limited to the initial pose of the point set. Compared to the widely used algorithms (ICP and its variations), this method is more efficient and robust even in the presence of noise and outliers, it is also much quicker because the number of vertexes on the convex hull is smaller than the size of the point set. This registration method is limited when 1) there are a large number of outliers or noise outside the point sets, 2) the point set is sphere-like structure.

Non-rigid registration

The rigid registration methods are only applied for rigid parts whose shapes are similar (for example, two lines). Thus, they do not cover flexible parts in which the registration problem requires application of a non-rigid registration method in addition to finding a rigid mapping. The difference between rigid and non-rigid registrations is that non-rigid registration can align different shapes (for example, a line with a curve). (Abenhaim, Tahan et al. 2011)

Many methods have been developed for non-rigid "surface / body / shape" registration such as the *Multi-Dimensional Scaling (*MDS*)* method (Borg and Groenen 2005), and the *Coherent Point Drift (*CPD*)* algorithm (Myronenko and Xubo 2010), applied in medical imaging, animation, etc. But the situation is different for the non-rigid registration of mechanical parts because of *compliance behavior* (flexibility) of a non-rigid part due to mechanical properties and material covariance. Therefore, we will take the advantage of the *finite element analysis* method to consider mechanical properties and compliance behavior of non-rigid part. In the next sections, we will discuss about non-rigid part and its compliance behavior.

Non-rigid (flexible) part, compliance behavior (flexibility)

According to the standards of (ASME-Y14.5 2009) and (ISO-1101: 2004), all tolerances are applied in a free-state condition unless otherwise specified. Exemptions to this rule are provided for non-rigid parts in the sections 4.20 and 5.5 of the ASME Y14.5 standard and by the (ISO-10579: 2010) standard.

Non-rigid parts are parts which may deform significantly from their defined tolerances due to their weight, flexibility or the release of residual stresses resulting from the manufacturing processes (*free-state condition*) (ASME-Y14.5 2009, ISO-10579: 2010). The mentioned standards allow for the application of a reasonable force (not exceeding the force excepted under normal assembly conditions) to make a deformation to conform the non-rigid parts within the specified tolerances. Depending on the functionality and design specifications, it may be necessary to assess the part subject to accepted restrained condition instead of, or in addition to, assessing the part in its free-state condition. These standards give rules for dimensioning and tolerancing non-rigid parts where the restraining of features is required during the verification of dimensions and tolerances specified on a drawing.

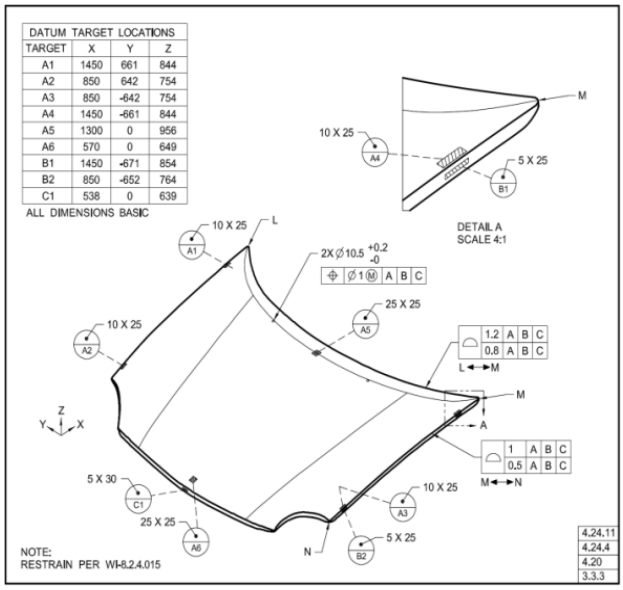

Figure 0.5 Restrained condition application
(ASME-Y14.5 2009)

The (ASME-Y14.5 2009) standard states that in some cases “it may be desirable to restrain a part on its datum features to simulate their function or interaction with other features or parts”. Figure 0.5 illustrates a non-rigid part that should be restrained to its design shape by adding sufficient reinforcement (section 4.20). The maximum allowable free-state variation should be specified with an appropriate feature control frame where an individual form or location tolerance is applied to a feature in the free-state condition. In some cases, form or profile tolerances may be restrained. Because these surfaces may be subject to free-state variation, it is obligatory to denote the maximum force necessary to restrain each of them. The amounts of the restraining or holding forces and other requirements, required to simulate excepted assembly conditions, should be determined (section 5.5). (ASME-Y14.5 2009)

Knowledge of the compliance behavior of a non-rigid part is an important factor to consider when specifying tolerances and evaluating the geometric and dimensional specifications of the part. According to the definition proposed by (Abenhaim, Desrochers et al. 2012), the compliance behavior of a non-rigid part is a relative notion based on the ratio between an applied force and its induced displacement. Based on the displacements induced by a reasonable force during inspection (around 50 N), the parts in zone A / B / C are considered rigid / non-rigid (flexible) / extremely non-rigid (see Table 2.1).

Another method for quantifying the flexibility of the mechanical part, from an industrial point of view, was proposed by Aidibe and Tahan (Aidibe and Tahan 2014). Their quantifying method is based on the ratio between the maximum displacement induced by a certain force and the profile tolerance of the non-rigid part. Our research is done on typical non-rigid mechanical parts used in the aeronautic and automotive industries.

Research objectives

The main objective is to eliminate the need for physical fixtures specialized for the inspection of non-rigid parts because of the challenges mentioned before (time, cost…). Therefore, we have to inspect such parts in a free-state (fixtureless) condition. The only option is non-contact measuring devices such as optical scanners which quickly measure the part by

obtaining a point cloud from its surface without the need for a physical fixture and positioning the part on it (free-state condition). Since the measured part and the nominal model are not in the same coordinate system, a registration process is necessary for a comparison between them to identify defects from deformations. For rigid parts, a rigid registration process is enough and any deviation from the nominal model is identified as a defect. In contrast, for non-rigid parts, a non-rigid registration technique is required in addition to the rigid registration method. As well, an identification step is critical for distinguishing between deformations and deviations. The mechanical properties as well as the compliance behavior of non-rigid parts should be considered for developing a more realistic method of fixtureless geometric inspection, which is also more practical and reliable.

Thesis organization

The methodology of this thesis is inspired by the real process of dimensional inspection of flexible parts in the industry: the flexible part should be positioned precisely on the inspection fixture to simulate the functional state. In this thesis, the nominal (CAD) model is used as the numerical (virtual) fixture (reference) that should be mapped into the scanned part for displacement compensation.

In terms of registration problems, the literature tells us that the best approach seems to be to search for the correspondence between two data sets (in our case, the CAD model and the scanned data). The GNIF method based on the isometric displacement (Radvar-Esfahlan and Tahan 2012) has some advantages that encourage us to use it to search for corresponding points between two data sets. In our previous work (Sabri, Tahan et al. 2016), presented as Chapter 2 in this thesis, we developed an approach to numerically inspect the profile tolerance of a non-rigid part using a non-rigid registration method and finite element analysis. To do so, a simulated displacement was performed using an improved definition of displacement boundary conditions for simulating unfixed parts. The developed method was applied on two industrial non-rigid parts with free-form surfaces simulated with different types of displacement, defect, and measurement noise (for one case). A conference paper entitled "*Fixtureless Profile Inspection of Non-rigid Parts*" was accepted to the proceedings

of the *43rd International Conference on Computers & Industrial Engineering 2013 (CIE 43)* at the University of Hong Kong, Hong Kong on October 16-18, 2013. The paper entitled "*Fixtureless Profile Inspection of Non-rigid Parts using the Numerical Inspection Fixture with Improved Definition of Displacement Boundary Conditions*" has been published in the *International Journal of Advanced Manufacturing Technology – Springer London*, February 2016, Volume 82, Issue 5, pages 1343-1352.

In Chapter 3, we improved the latter method and saved time by using an automatic node insertion and finite element analysis. Also, repeatability and robustness of the approach were studied. We applied the improved method on two industrial non-rigid parts; one from the previous work (case B) and a new one (case C). In addition, for repeatability and robustness evaluation, Gaussian measurement noise was introduced to each case three times (24 times for 8 cases). Therefore, the improved method was studied totally on 32 cases. The paper, entitled "*A Robust and Automatic FE-based Method for the Fixtureless Dimensional Inspection of Non-rigid Parts using an Improved Numerical Inspection Fixture*", has been accepted for the publication in the *International Journal of Advanced Manufacturing Technology – Springer London* (submission ID: JAMT-D-16-02890).

Figure 0.6 represents a comparison between the GNIF method and our proposed method (Improved Numerical Inspection Fixture). In the GNIF approach, borders are only used as a corresponding relationship for matching, by assuming them free of defects, whereas this situation generally does not conform to assembly conditions and real use state. Boundary conditions definition was improved in our approach based on assembly conditions. Also, the GNIF algorithm does not measure several defects (size, position, area) individually and only returns part's maximum deviation, whereas in our improved approach, several defects (and their size, position, and area) can be measured separately. Also in the improved algorithm in Chapter 3, we eliminated the limitation for the part size (number of nodes) in the GNIF method by modifying the GMDS algorithm from the 32b version to the 64b version.

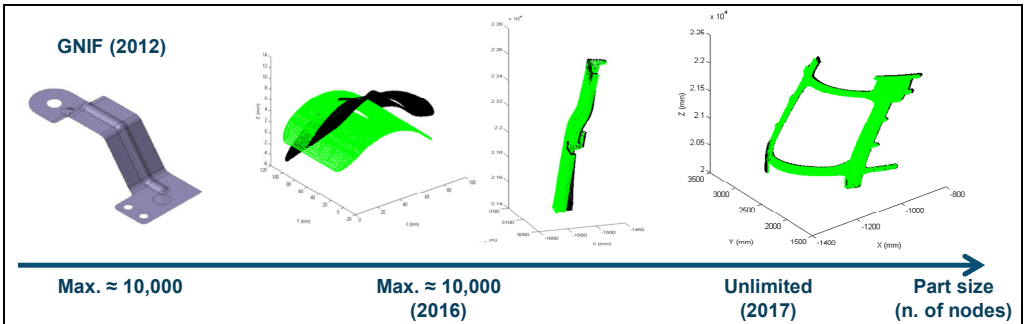

Method	Part size (n. of nodes)	Several defects	Defects size, position and area	Assemblying boundary conditions
GNIF	Max. ≈ 10,000	No (only part's max. deviation)	No (only part's max. deviation)	No (only borders)
Improved NIF	Unlimited	Yes	Yes	Yes

Figure 0.6 Comparison between the GNIF method and the Improved Numerical Inspection Fixture (NIF) approach

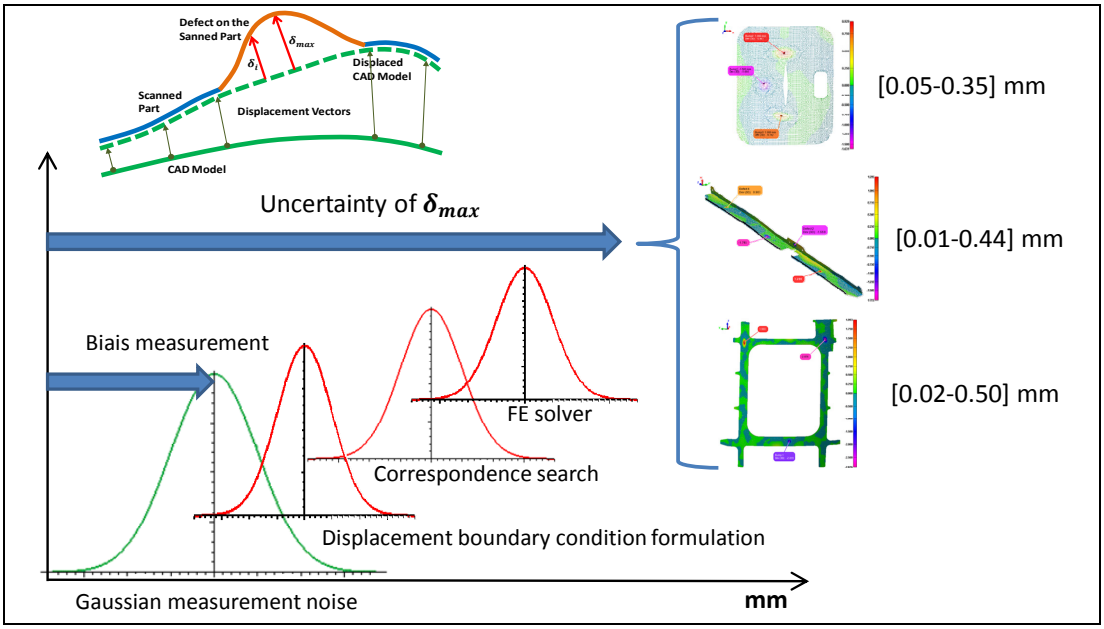

Figure 0.7 Uncertainty of defect's amplitude δ_{max} (maximum deviation)

An improved version of Figure 3.10 in Chapter 3 is represented in Figure 0.7. Uncertainty of defect's amplitude $\boldsymbol{\delta_{max}}$ (maximum deviation) is the sum of Gaussian measurement noise and uncertainties in the displacement boundary condition definition, the correspondence search, and the FE solver. Gaussian measurement noise is known in our simulation process of

case studies, but the other uncertainty sources are unknown especially when they are combined together in the method's algorithm. One solution to study these uncertainty sources could be to isolate each of them from the others and then to perform the validation research separately for each one. The minimum and maximum values (intervals) of algorithmic error (uncertainty of $\boldsymbol{\delta_{max}}$) for each part are also illustrated in Figure 0.7.

Chapter 4 represents a new approach for the fixtureless inspection of extended arc tolerance and dimensional tolerance on free-form surfaces. We took advantage of the *Fast Marching Method* (FMM) (Sethian 1996, Kimmel and Sethian 1998) for computing the geodesic distance (shortest path) between each pair of points on the surface mesh. Therefore, there is no need for any special tool or fixture. The geodesic distance between any considered pair of points on the scanned part can be calculated using the *Adapted FMM* method as well without the need for any registration procedure. The algorithm was applied on several cases with curvature for studying the extended arc tolerance, and a comparison was done between the results of the proposed Adapted FMM method and the Adapted CPD method on the study cases in (Aidibe and Tahan 2015). The paper entitled "*A method for Dimensional Metrology of Non-rigid Parts based on Arc Length Measurement at Free-state Condition"* has been accepted with revisions to the *International Journal of Advanced Manufacturing Technology – Springer London* (submission ID: JAMT-D-16-03929).

We have added some preliminary modifications to the third paper (Chapter 4) before final submission of its revised version. Figure 0.8 represents a comparison between the Dijkstra's algorithm (Dijkstra 1959) and the Fast Marching Method (Sethian 1996, Sethian 1999, Sethian 2008) in finding multiple short paths or the optimal diagonal (shortest) path between two points. A brief flowchart of the proposed methodology is presented in Figure 0.9. Figure 0.10 is dedicated to the methodology proposed in the cases with hole features. Figure 0.11 illustrates a set of featured (strategic) points on a free-form part surface as well as their pairwise geodesic distances along the surface.

At the end of the thesis, we will present a conclusion and summarize the contributions made within the framework of our PhD study as well as our key recommendations for future works.

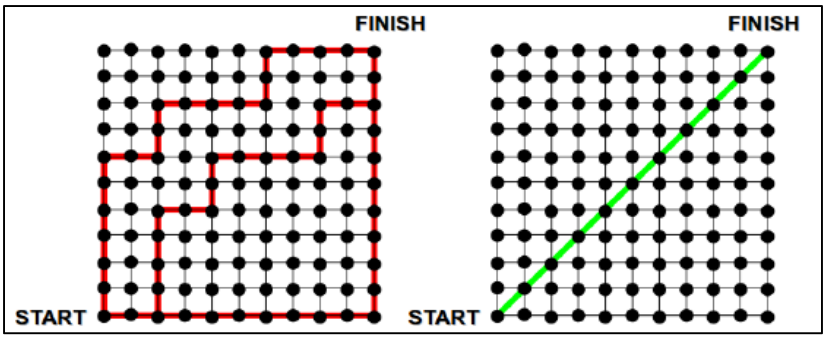

Figure 0.8 The Dijkstra algorithm offers multiple short paths following always the connections between the nodes. Fast Marching Method finds the optimal diagonal (shortest) path using the interpolation. (Garrido, Moreno et al. 2011)

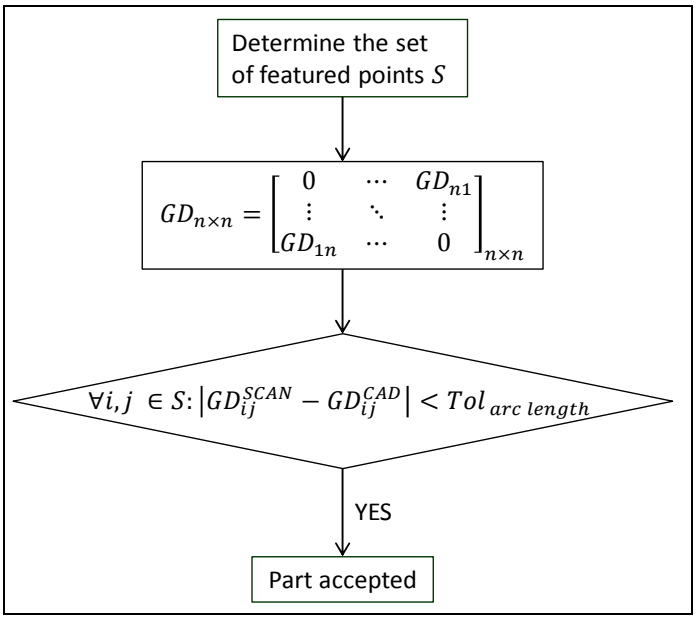

Figure 0.9 Flowchart of the methodology in Chapter 4

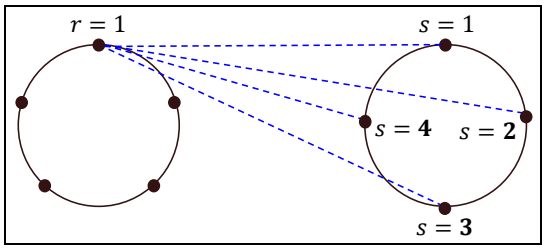

Figure 0.10 The methodology proposed in the cases with hole features.

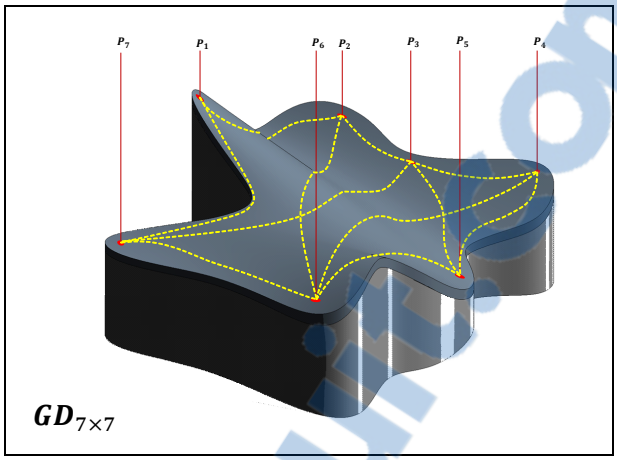

Figure 0.11 A set of featured (strategic) points on a free-form part surface as well as their pairwise geodesic distances along the surface

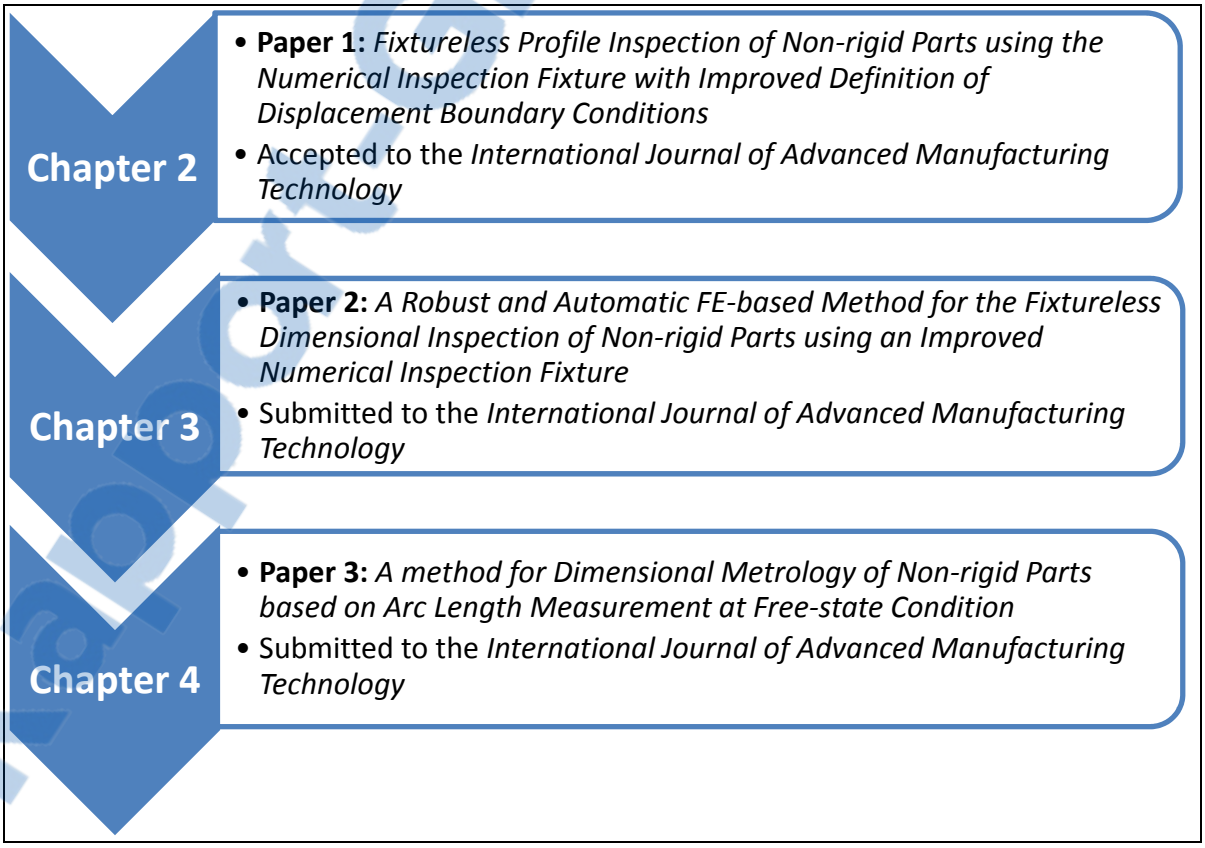

Figure 0.12 Thesis organization

CHAPTER 1

REVIEW OF PREVIOUS RESEARCH

(Ascione and Polini 2010) dealt with the inspection of free-form surfaces belonging to non-rigid parts with inspection fixtures combined with CMM. In the following, the main methods based on *simulated displacement* approach developed for geometric inspection of non-rigid parts without the use of inspection fixtures, are described.

First effort for the fixtureless dimensional inspection of non-rigid parts was done by (Weckenmann and Gabbia 2006, Weckenmann and Weickmann 2006). They proposed the *virtual distortion compensation* method in which the distorted part was deformed virtually into the nominal model by displacing the point cloud obtained by non-contact scanning (fringe projection). They used feature extractions such as holes and edges for the corresponding relationship between the CAD model and measurement data, assuming the fixation points are free of defects. A triangle mesh of the surface from the obtained point cloud was generated, and then was transformed into a FEM model for simulating the fixation process using the information about the deviation of the assembly features from their actual position to their nominal position. The proposed method had some disadvantages; it was not completely automated due to the need for human challenges to identify the correlation between some special points and assembly conditions to find the boundary conditions of the FEA problem. Therefore, boundary conditions can be improved to simulate a real model of the fixation system. In addition, transforming the point cloud into a computer-aided analyzable model is a very time-consuming process. As well, parts with hidden structure or other details at the backside of a scanned surface cannot be easily modeled as a FEM model.

(Weckenmann, Weickmann et al. 2007) improved the shortcomings in their last work by deforming the CAD model towards the measurement data in the *virtual reverse deformation* method. They enforce the boundary conditions on the nominal FE model using the known position of the fixation points on the scanned part. Therefore, pre-processing of the measurement data is not needed. By this method, they decreased the time of inspection and obtained results that are more precise. However, the proposed method still needed human

intervention in order to find the corresponding relationship between the CAD model and the measurement data. Moreover, modeling of the boundary conditions in the FEM dataset needs to be improved to simulate the unfixed part. Limitation of the method is uncertainties in measurement, model building and accuracy of the FEM simulation.

Similar to the virtual reverse deformation method, (Jaramillo, Boulanger et al. 2009, Jaramillo, Boulanger et al. 2011) proposed an approach which requires significantly less computing power, using the Radial Basis Function (RBF) to minimize the finite element mesh density required to predict correctly the behavior of the part. Recently in (Jaramillo, Prieto et al. 2013), they improved their method by performing flexible part registration using only partial views from areas that have to be inspected. They applied an interpolation technique based on RBFs to estimate positions of the missing fixation points since the partially scanned data may not contain all of them. During that same year, (Jaramillo, Prieto et al. 2013) proposed an approach for performing the inspection without the need for scanning the complete part's surface or the areas near the fixation positions. In this algorithm, instead of typical fixation positions, surface feature points are used for computing the non-rigid transformation.

(Gentilini and Shimada 2011) proposed a new computational method for inspecting the final shape of a flexible assembly part by virtually mounting it into the assembly. After data acquisition from the shape by laser scanner, FEA is used to predict the post-assembly shape. First, a laser-digitized dense mesh is smoothed and decimated to be suitable for FEA. Then the part's material properties are determined by a calibration process if not available. Next, specific displacement boundary conditions are applied to reproduce and simulate the assembly process. After FEA is executed, the quality inspection of the *simulated post-assembly* shape is done using visualization tools such as *light-reflection patterns* and *contour plots* of the distance between the computed geometry and the *target* computer-aided design (CAD) geometry. In addition, for validating the proposed method's accuracy, the simulated post-assembly shape is compared with the *actual* post-assembly shape measured after physically assembling the part. This method can predict numerically the final shape of an assembled flexible part, reducing the time and the cost of product quality inspection.

However, the proposed method has the shortcomings mentioned before for the virtual distortion compensation method; the polygonal mesh data acquired by a laser digitizer requires post-processing steps, smoothing and decimation, because it suffers from uncertainties, noise and an excess number of polygons. The primary sources of noise are: physical phenomena such as the object's spectral properties, surface texture, and lighting; and hardware-related issues such as digitizer calibration, lens typology, and camera resolution.

(Radvar-Esfahlan and Tahan 2012) introduced the *Generalized Numerical Inspection Fixture (GNIF)* method which is based on the property that the inter-point shortest path (geodesic distance) between any two points on the parts remains unchanged during an *isometric deformation* (*distance preserving property* of non-rigid parts), in spite of large deformation. Taking advantage of this property and inspired by a real industrial inspection process (locating the flexible part on the inspection fixture to simulate the use state), this method looks for some correspondence between the distorted part and the CAD model as the numerical inspection fixture. Through the ability of introducing a similarity measure using Multidimensional Scaling in order to find correspondence between two metric spaces, *finite element non-rigid registration (FENR)* can be performed knowing some boundary conditions as prior information and finding the correspondence to make the displacement. The geometric deviations between a deformed CAD model and measurement data can be calculated after finite element non-rigid registration. The main advantages of the GNIF method are the ability to inspect the parts with large displacements, taking the advantage of geodesic distance for finding correspondence, and using FEA method for making simulated displacement considering compliance behavior and mechanical properties. Another significant specification of GNIF is the capability for isometry-invariant partial surface matching in the existence of missing data. Correspondence search is also completely automatic. The main shortcoming of this method is that they use the borders as a corresponding relationship for matching, by assuming them free of defects, whereas this situation generally does not conform to assembly conditions and real use state. Boundary conditions can be improved based on assembly conditions. The authors in (Radvar-Esfahlan

and Tahan 2014) robustified the GNIF method by filtering out points that cause incoherent geodesic distances. The improved method is able to handle parts with missing data sets.

In contrast to the aforementioned methods, (Abenhaim, Tahan et al. 2011) proposed the *iterative displacement inspection (IDI)* algorithm that is not based on the use of a FE analysis module. This method deforms iteratively the meshed CAD model until it matches the scanned part (measurement data). The proposed IDI algorithm is based on optimal step non-rigid ICP algorithms (Amberg, Romdhani et al. 2007) which combine rigid with non-rigid registration methods, as well as a developed identification method, to distinguish the surface deviations from the part's distortion. This method essentially deforms the mesh in such a manner to assure its smoothness that prevents concealing surface defects and measurement noise during the matching process. (Aidibe, Tahan et al. 2011, Aidibe, Tahan et al. 2012) improved the identification module of the IDI algorithm, by proposing the use of a maximum-normed residual test to automatically set the identification threshold. However, the IDI method has some drawbacks. Due to lack of a FE analysis, the method depends on identifying some flexibility parameters, which are dependent on the thickness. In addition, they used the same number of nodes in the two point clouds.

(Aidibe and Tahan 2014) presented an approach that combines the curvature properties of manufactured parts with the extreme value statistic test as an identification method for comparing two data sets and to recognize profile deviation. This approach was tested on simulated typical industrial sheet metal with satisfactory results in terms of error percentage in defect areas and in the estimated peak profile deviation. As the core of the algorithm is based on the Gaussian curvature comparison, application of the method is limited to relatively-flexible parts where small displacements are predictable. The authors in (Aidibe and Tahan 2015) proposed the ACPD (*Adapted Coherent Point Drift*) method for optimization of the CPD algorithm in order to adapt it to the relatively-flexible parts problem, introducing two criteria: the stretch criterion between the nominal model and the aligned one, and the Euclidian distance criterion between the aligned nominal model and the scanned part.

(Abenhaim, Desrochers et al. 2015) introduced a method that registers the point cloud to the nominal model using information recuperated from the FE model of the nominal model. This is done by embedding a FE-based transformation model into a boundary displacement constrained optimization. The boundary displacement constrained optimization tries to minimize a distance-based similarity criterion between points in unconstrained areas whereas this criterion between points in constrained areas is maintained in a specified contact distance, and simultaneously, the restraining forces are limited. The latter allows for the inspection of non-rigid parts for which their functional requirements obligate to limit the restraining forces imposed during assembly. In addition, the point cloud does not need to be pre-processed into a FE model. Also, there is no need for manual identification of fixation positions in the point cloud. Furthermore, as long as the point cloud includes the restraining areas, a partial view of the part can be enough for the method.

The authors in (Wang, Zhou et al. 2016) used a 3D scanner to inspect a plate in the stamping forming process and to compensate the spring-back. The point cloud is converted to a polygonal object (mesh) of the part. The mesh is improved by repairing and filling the holes. Then by comparing the deformed part with the design model using the Geomagic Qualify software, its deviation and spring-back angle were obtained. This method is more accurate and complete than the traditional method (special fixture), and the spring-back compensation by this method can effectively reduce die tryout time.

Recently in (Thiébaut, Lacroix et al. 2017), an approach was proposed to evaluate shape deviations of flexible parts, using optical scanners, in a given measuring configuration for which the setup is known (whatever configuration, independent from the assembly conditions). The CAD model was displaced by the FE simulation of the part's displacement due to its own gravity considering the known configuration used for the measurement. Having applied to a simple part, the form deviations were recognized by subtracting the simulated geometrical displacements to the measured geometrical displacements. They used the known configuration for the part's optical measurement based on which the displacement vector for the FE simulation at each node of the CAD mesh was calculated using the intersection of a cylindrical neighborhood of its normal vector and the point cloud.

Figures 1.1 and 1.2 represent the aforementioned methods in a timeline and according to the direction of simulated displacement (scanned part towards CAD model or vice versa).

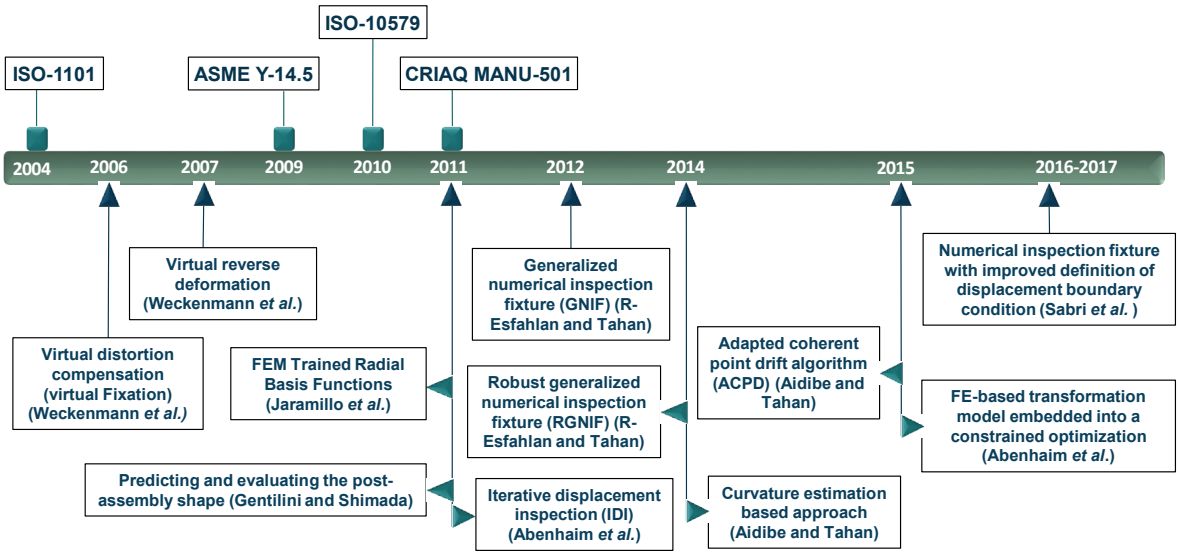

Figure 1.1 Timeline for the simulated displacement methods of fixtureless non-rigid inspection

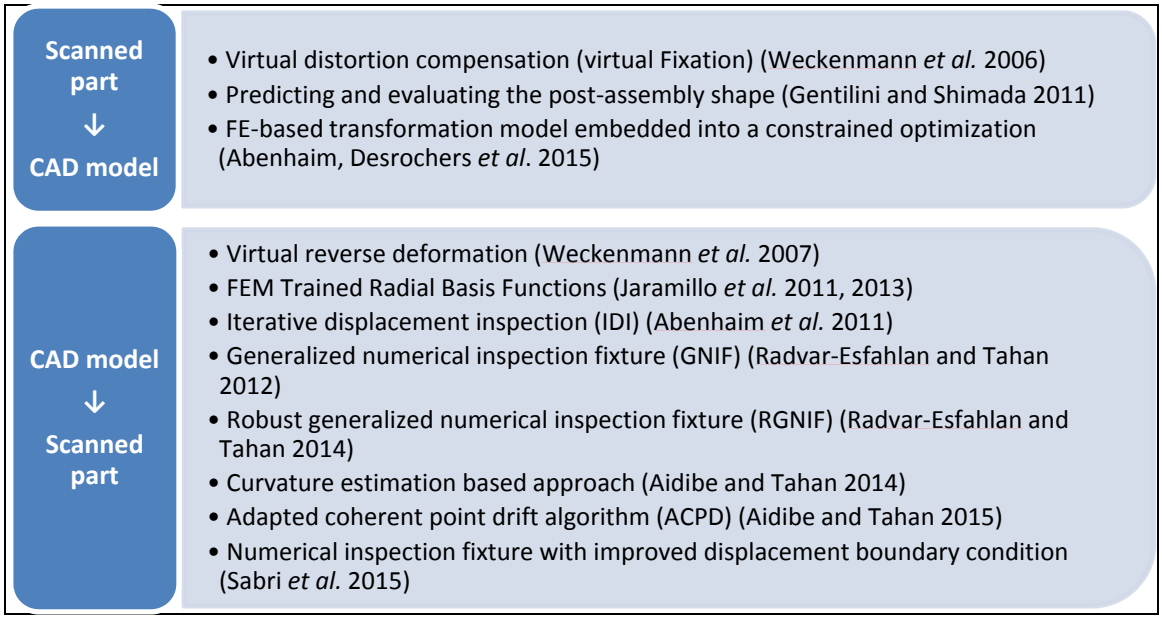

Figure 1.2 Simulated displacement methods of fixtureless non-rigid inspection based on the displacement direction

CHAPTER 2

FIXTURELESS PROFILE INSPECTION OF NON-RIGID PARTS USING THE NUMERICAL INSPECTION FIXTURE WITH IMPROVED DEFINITION OF DISPLACEMENT BOUNDARY CONDITIONS

Vahid SABRI[1], S. Antoine TAHAN[1], X. Tan PHAM[1], Dominic MOREAU[2], and Stephan GALIBOIS[3]

1. Department of Mechanical Engineering, École de Technologie Supérieure (ÉTS), Montreal, Canada
2. Bombardier Aerospace Inc., Montreal, QC, Canada
3. Creaform Inc., Levis, QC, Canada

This chapter has been published in the *"International Journal of Advanced Manufacturing Technology" – Springer London*, February 2016, Volume 82, Issue 5, pages 1343-1352.

2.1 Abstract

Quality control is an important factor for manufacturing companies looking to prosper in an era of globalization, market pressures, and technological advance. The functionality and product quality cannot be guaranteed without this important aspect. Manufactured parts have deviations from their nominal (CAD) shape caused by the manufacturing process. Thus, geometric inspection is a very important element in the quality control of mechanical parts. We have focused here on the profile inspection of non-rigid parts which are widely used in the aeronautic and automotive industries. Non-rigid parts can have different forms in a *free-state* condition compared with their nominal models due to residual stress and gravity loads. To solve this problem, dedicated *inspection fixtures* are generally used in industry to compensate for the displacement of such parts for simulating the use state in order to perform geometric inspections. These fixtures and the inspection process are expensive and time-consuming. Our aim is therefore to develop an inspection method which eliminates the need for specialized fixtures by acquiring a point cloud from the displaced part using a contactless measuring system such as optical scanning and comparing it with the CAD model for the identification of deviations. Using a non-rigid registration method and finite element

analysis, we will numerically inspect the profile of a non-rigid part. To do so, a simulated displacement is performed using an improved definition of boundary conditions for simulating unfixed parts. In this paper, we will apply an improved method on two industrial non-rigid parts with free-form surfaces simulated with different types of displacement, defect, and measurement noise.

Keywords: quality control, geometric inspection, geometric dimensioning and tolerancing, profile tolerance, registration, non-rigid/flexible/deformable part, assembly conditions, metrology.

2.2 Introduction

Geometric inspection has an important role to play in the quality control of mechanical parts since it usually consumes a large portion of production lead time. By means of Geometric Dimensioning and Tolerancing (GD&T), geometric specifications and product design are specified according to functionality. To verify whether manufactured parts meet specifications defined at the design phase, the GD&T inspection process is applied. By using a reliable, efficient, and automated inspection process, product life cycle time will decrease and industrial competition will improve (Gao, Gindy et al. 2006). Although the methods for geometric inspection of rigid parts have significantly improved and are generally available within the industry (Li and Gu 2005), the geometric inspection of non-rigid parts with free-form surfaces has not been well studied.

In mechanical engineering applications, surfaces are allocated a profile tolerance to control manufacturing variations (Li and Gu 2005). A surface profile should be controlled based on the principles established by the *ASME Y14.5-2009* standards (section 8) (ASME-Y14.5 2009). According to these standards (or *ISO 1101:2004*, ISO-GPS standards (ISO-1101: 2004)), unless otherwise specified, all tolerances should be applied in a free-state condition. Exemptions are agreed to this rule for non-rigid parts. In these cases, non-rigid parts may deform significantly from their defined tolerances due to their weight (gravity), or the release

of residual stresses resulting from manufacturing processes (ASME-Y14.5 2009, ISO-10579: 2010).

Generally, to solve the above-mentioned problem, special inspection fixtures with complex setups are used within the industry to compensate for the displacements to simulate use state in order to perform geometric inspection. These dedicated fixtures are expensive, heavy, and complex (Figure 2.1). The process is extremely time-consuming which reduces competitiveness. The mentioned standards also allow for the application of reasonable load (not exceeding the load expected under normal assembly conditions) to displace non-rigid parts to conform to the specified tolerances. The solution is to develop an inspection technique which eliminates the need for specialized fixtures by acquiring a point cloud from the displaced part using a contactless measuring system such as optical scanning and comparing it with the CAD model for the identification of deviations.

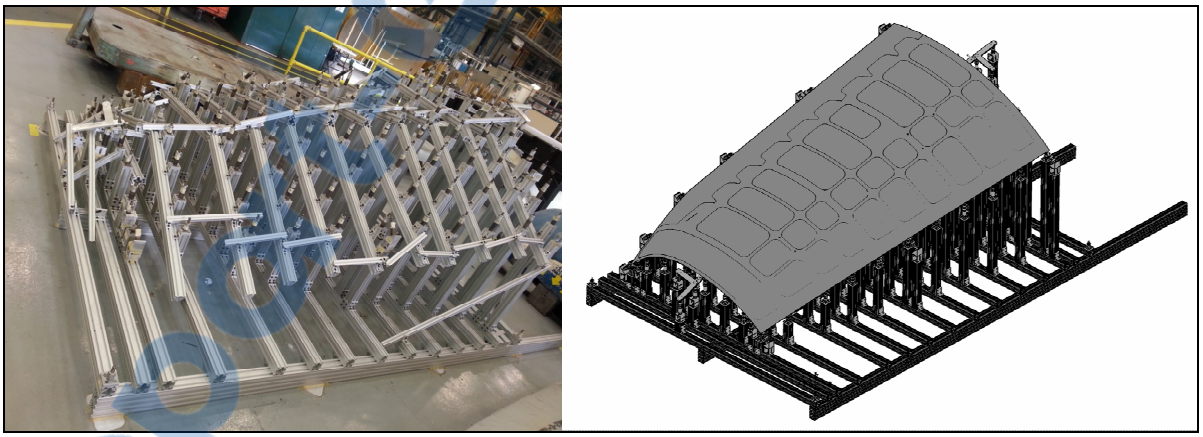

Figure 2.1 A special, expensive, heavy, and complex fixture for the inspection of a flexible plate, Bombardier Aerospace Inc., *left*: the fixture without the part, *right*: the CAD model of the fixture with the part set up on it

For the purpose of comparing the measurement data (point cloud) with the nominal model, it is necessary to dispose these two sets in a joint coordinate system. This procedure is called *registration*. In recent and modern technologies, this registration is mathematically defined using the translation and the rotation of the Design Coordinate System (DCS) with respect to the Measurement Coordinate System (MCS). In application, registration can be done in two steps: searching for the corresponding relationship between scanned and nominal surfaces,

and finding an optimal transformation matrix between the DCS and MCS. The rigid registration methods are only applied for rigid parts whose shapes are similar. Thus, they do not cover flexible parts in which the registration problem requires application of a kind of non-rigid registration method in addition to finding a rigid mapping. The difference between rigid and non-rigid registrations is that a non-rigid registration can align two different shapes (for example, a line with a curve) (Li and Gu 2004, Abenhaim, Tahan et al. 2011). Several rigid and non-rigid registration methods have been developed such as the *Iterative Closest Point (*ICP*)* algorithm (Besl and McKay 1992) and its variants for rigid registration; the *Multi-Dimensional Scaling (*MDS*)* method (Borg and Groenen 2005), and the *Coherent Point Drift (*CPD*)* algorithm (Myronenko and Xubo 2010) for non-rigid registration applied in medical imaging, animation, etc. However, the situation for the registration of a non-rigid mechanical part is different due to the result of its *compliance behavior*.

Compliance behavior of a compliant (flexible) part is an essential issue to study while specifying tolerances and assessing the geometric and dimensional specifications for the part. This factor is a relative concept based on the relation between an imposed force and its persuaded displacement (Abenhaim, Desrochers et al. 2012). Based on the displacements of parts induced by a reasonable force (50°N) during inspection, the parts are considered rigid/non-rigid (flexible)/extremely non-rigid (see Table 2.1). Another method for quantifying flexibility of the mechanical part, from an industrial point of view, was proposed by Aidibe and Tahan (Aidibe and Tahan 2014). Their quantifying method is based on the ratio between the maximum displacement induced by a certain force and the profile tolerance of the non-rigid part. Our research is done on typical non-rigid mechanical parts used in the aeronautic and automotive industries.

The following paper includes four sections: a review of previous researches for the fixtureless geometric inspection of non-rigid parts, the developed method, case studies including the presentation of metrological performances of our method, and finally, a conclusion.

Table 2.1 Displacement of parts in each zone induced by a force during inspection and their compliance behavior

δ/tol by a reasonable force during inspection (≈ 50 N)	**Compliance behavior**
$\delta/tol <$ 5-10 %	Rigid
$\delta/tol >$ 5-10 % (e.g. thin shell, skin in aeronautic and automotive parts)	Non-rigid (flexible)
$\delta/tol \gg$ 10 % (the shape depends on the part's weight and position, such as thin seals and paper)	Extremely non-rigid

2.3 Review of previous research

Ascione and Polini (Ascione and Polini 2010) dealt with the free-form surface inspection of non-rigid parts using inspection fixtures combined with CMM. Abenhaim *et al.* (Abenhaim, Desrochers et al. 2012) presented a review of the previous researches for the fixtureless inspection of non-rigid parts and proposed a classification of the specification methods used for the GD&T of non-rigid parts under the ASME and ISO standards. In the following, we will introduce the primary methods, based on the simulated displacement approach, developed for the geometric inspection of non-rigid parts without the use of inspection fixtures.

For the first time in 2006, Weckenmann *et al.* (Weckenmann and Gabbia 2006, Weckenmann and Weickmann 2006) made strides in the fixtureless inspection of non-rigid parts by proposing the *virtual distortion compensation* method in which they virtually displaced the distorted part into the nominal model by displacing the point cloud captured by a contactless scanning device. A triangle mesh of the surface from the point cloud was generated and transformed into a finite element analysable (FEA) model. Afterwards, the fixation process was simulated using information about the assembly features' deviation from the actual (measured) to the ideal (nominal) position. This method requires human intervention to recognize the correlation between some determined points and assembly conditions in order to define the boundary conditions of the FEA problem. Therefore, boundary conditions can be improved to simulate a real model of the fixation system. In addition, converting the point

cloud into a FE model is a time-consuming process with many uncertainties. In 2007, Weckenmann *et al.* (Weckenmann, Weickmann et al. 2007) improved the shortcomings of their previous work by displacing a CAD model towards the measurement data in the *virtual reverse deformation* method. They enforced the boundary conditions on the CAD model using the known position of the fixation points on the scanned part. Therefore, a pre-processing of the measurement data is not needed. Through this method, they decreased inspection time and obtained more precise results. FE simulation of the displacement boundary conditions on the geometrically ideal CAD model is clearly more accurate. However, this method still required human intervention to find the corresponding relationship between the CAD model and the measurement data. Moreover, the modeling of the boundary conditions in the FE dataset needs to be improved to simulate the unfixed part.

Similar to the virtual reverse deformation method, Jaramillo *et al.* (Jaramillo, Boulanger et al. 2009, Jaramillo, Boulanger et al. 2011) proposed an approach which requires significantly less computing power, using the Radial Basis Functions (RBFs) to minimize the finite element mesh density required to correctly predict part behavior. Recently in (Jaramillo, Prieto et al. 2013), they improved their method by performing flexible part registration using only partial views from areas that have to be inspected. They applied an interpolation technique based on RBFs to estimate positions of the missing fixation points since the partially scanned data may not contain all of them.

Gentilini and Shimada (Gentilini and Shimada 2011) proposed a method for the shape inspection of a flexible assembly part by virtually mounting it into the assembly. First, the dense measured mesh is smoothed and reduced to become suitable for FEA. If not available, material properties are defined by a calibration process. Then, specific displacement boundary conditions are defined and applied for FE simulation of the assembly process. Once FEA is performed, quality inspection of the simulated post-assembly shape is done using visualization tools. In addition, the virtual post-assembly shape is compared with the real post-assembly shape for method accuracy validation. This method can predict the final assembled shape of a flexible part, but it has the shortcomings mentioned in the virtual distortion compensation method. The polygonal mesh data suffers from uncertainties, noise,

and a high quantity of polygons; therefore, it needs post-processing steps, smoothing, and decimation.

Recently, Radvar-Esfahlan and Tahan (Radvar-Esfahlan and Tahan 2012) introduced the *Generalized Numerical Inspection Fixture (*GNIF*)* method which is based on the property that the shortest path (*geodesic distance*) between any two points on the surfaces does not change during an isometric displacement (*distance preserving* property of non-rigid parts) in spite of large displacement. Taking advantage of this property, the method looks for some correspondence between the part and the CAD model. The authors used *Multidimensional Scaling* in order to find a correspondence between two metric spaces (CAD model and scanned part). Then knowing some boundary conditions, finite element non-rigid registration (FENR) was executed. The geometric deviations between the displaced CAD model and the measurement data can be calculated after the FENR. Correspondence search is completely automatic. The GNIF dealt with a very general case of non-rigid inspection. In the absence of assembly conditions, the authors used the borders for FENR purposes. This situation may not conform to assembly conditions and real use state. Boundary conditions for the simulated displacements can be improved based on assembly conditions. The authors in (Radvar-Esfahlan and Tahan 2014) robustified the GNIF method by filtering out points that cause incoherent geodesic distances. The improved method is able to handle parts with missing data sets.

In contrast to the aforementioned methods, Abenhaim *et al.* (Abenhaim, Tahan et al. 2011) proposed the *Iterative Displacement Inspection (*IDI*)* algorithm that is not based on the FEA module. This method iteratively displaces the meshed CAD model until it matches the scanned data. The IDI algorithm is based on optimal step non-rigid ICP algorithms (Amberg, Romdhani et al. 2007) which combine rigid and non-rigid registration methods. As well, a developed identification method distinguishes surface deviations from the part's displacement. This method principally displaces the mesh regarding its smoothness and prevents concealing surface defects and measurement noise during the matching process. Aidibe *et al.* (Aidibe, Tahan et al. 2012) improved the identification module of the IDI algorithm by proposing the application of a maximum-normed residual test to automatically

set the identification threshold. However, the IDI method has some drawbacks. Due to a lack of FE analysis, the method depends on identifying some flexibility parameters which are dependent on thickness. In addition, they use the same number of nodes in the two point clouds.

Aidibe and Tahan (Aidibe and Tahan 2014) presented an approach that combines the curvature properties of manufactured parts with the extreme value statistic test as an identification method for comparing two data sets and to recognize profile deviation. This approach was tested on simulated typical industrial sheet metal with satisfactory results in terms of error percentage in defect areas and in the estimated peak profile deviation. As the core of the algorithm is based on the Gaussian curvature comparison, application of the method is limited to relatively-flexible parts where small displacements are predictable. The authors in (Aidibe and Tahan 2015) proposed the ACPD method for optimization of the CPD algorithm in order to adapt it to the relatively-flexible parts problem, introducing two criteria: the stretch criterion between the nominal model and the aligned one, and the Euclidian distance criterion between the aligned nominal model and the scanned part.

2.4 Proposed approach

In terms of registration problems, the literature tells us that the best approach seems to be to search for the correspondence between two data sets (in our case, the CAD model and the scanned data). As mentioned in the previous section, the GNIF method based on the isometric displacement (Radvar-Esfahlan and Tahan 2012) has some advantages that encourage us to use it to search for corresponding points between two data sets. In this paper, a new formulation of boundary conditions is defined, and the developed method is implemented on two industrial case studies with free-form surfaces.

2.4.1 Proposed approach based on the improvement of displacement boundary conditions

In the present method, we calculate the Cartesian coordinates of the matching points in both the data sets; then, we will improve the boundary conditions for the finite element analysis, by searching for the correspondents inside the predefined boundary areas.

The Generalized MDS method of non-rigid registration, applied in the GNIF approach, represents the corresponding points in the data sets based on the barycentric coordinate system (Radvar-Esfahlan and Tahan 2012) (Figure 2.2). But, to use these points for future purposes, their barycentric coordinates should be converted into Cartesian coordinates. Given a point with the barycentric coordinates $(\lambda_1, \lambda_2, \lambda_3,$ where $\lambda_1 + \lambda_2 + \lambda_3 = 1)$ inside a triangle, and knowing the Cartesian coordinates of the vertices (the nodes of an element in the finite element mesh), the Cartesian coordinates can be obtained at the point through the following equations:

$$\begin{cases} x_P = \lambda_1 . x_1 + \lambda_2 . x_2 + \lambda_3 . x_3 \\ y_P = \lambda_1 . y_1 + \lambda_2 . y_2 + \lambda_3 . y_3 \\ z_P = \lambda_1 . z_1 + \lambda_2 . z_2 + \lambda_3 . z_3 \end{cases} \tag{2.1}$$

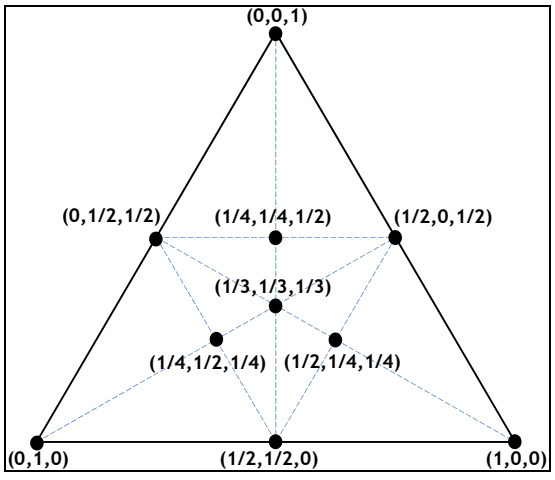

Figure 2.2 Barycentric coordinates $(\lambda_1, \lambda_2, \lambda_3)$ on an equilateral triangle

By substituting $\lambda_3 = 1 - \lambda_1 - \lambda_2$ into the equations above:

$$\begin{cases} x_P = \lambda_1 . x_1 + \lambda_2 . x_2 + (1 - \lambda_1 - \lambda_2) . x_3 \\ y_P = \lambda_1 . y_1 + \lambda_2 . y_2 + (1 - \lambda_1 - \lambda_2) . y_3 \\ z_P = \lambda_1 . z_1 + \lambda_2 . z_2 + (1 - \lambda_1 - \lambda_2) . z_3 \end{cases} \quad (2.2)$$

Using Equations 2.2, the Cartesian coordinates of the corresponding points in each data set can be calculated.

Figure 2.3 shows schematically the different steps of our approach. First, we put the scanned part surface ($S_{Scan} = p'_i , i = 1 \dots m$) close enough to the CAD surface ($S_{CAD} = p_i , i = 1 \dots n$) (pre-alignment) to achieve a satisfactory result for rigid registration by ICP (Besl and McKay 1992). Then, the pre-aligned surface is rigidly registered to the CAD surface by the ICP algorithm. In this step, the GNIF method is used to find a set of correspondent pairs between the two surfaces:

$$C_{CAD} = \{p_k \in S_{CAD} | k = 1 \dots q\} \; C_{Scan} = \{p'_k \in S_{Scan} | k = 1 \dots q\}, \quad q \ll m, n \quad (2.3)$$

To define a set of displacement boundary conditions for simulating the displacement from the CAD model to the rigidly registered scanned part surface, the constrained areas on the CAD model, such as fixation positions (e.g. hole) or contact surfaces (e.g. target datums) according to ASME Y14.5, are first recognized (Gentilini and Shimada 2011). Then, the corresponding points (with the Cartesian coordinates) inside each constrained area (with the index of *j*), and consequently their correspondents in the scanned data, are identified among all the correspondents obtained by the GNIF method as follows:

$$B_j = \{p_t \in C_{CAD} | t = 1 \dots s_j \ll q\}, \; B'_j = \{p'_t \in C_{Scan} | t = 1 \dots s_j \ll q\} \quad (2.4)$$

Next, for each area and its corresponding area on the scanned surface, we define a centre of mass by fitting a plane through the identified corresponding points (B_j, B'_j). To register each pair of the identified correspondents in the two data sets by simulated displacement using finite element analysis, the displacement boundary conditions should be defined by local translation law (Gentilini and Shimada 2011): (Figure 2.4)

- The centre of mass (C_{m_j}) is translated to the corresponding centre of mass on the corresponding plane (C'_{m_j}):

$$\overrightarrow{\Delta r_j} = \begin{Bmatrix} x_{c'} - x_c \\ y_{c'} - y_c \\ z_{c'} - z_c \end{Bmatrix}_j \tag{2.5}$$

Having defined the displacement boundary conditions, the finite element analysis is performed between the two data sets based on the simulated displacement approach. Using ANSYS®, the CAD model is displaced towards the scanned surface applying the defined boundary conditions. Finally, the profile deviations are identified based on the shortest 3D distance between each point of the scanned data and the displaced CAD surface ($\delta_i = \vec{\Delta} \cdot \vec{n}$).

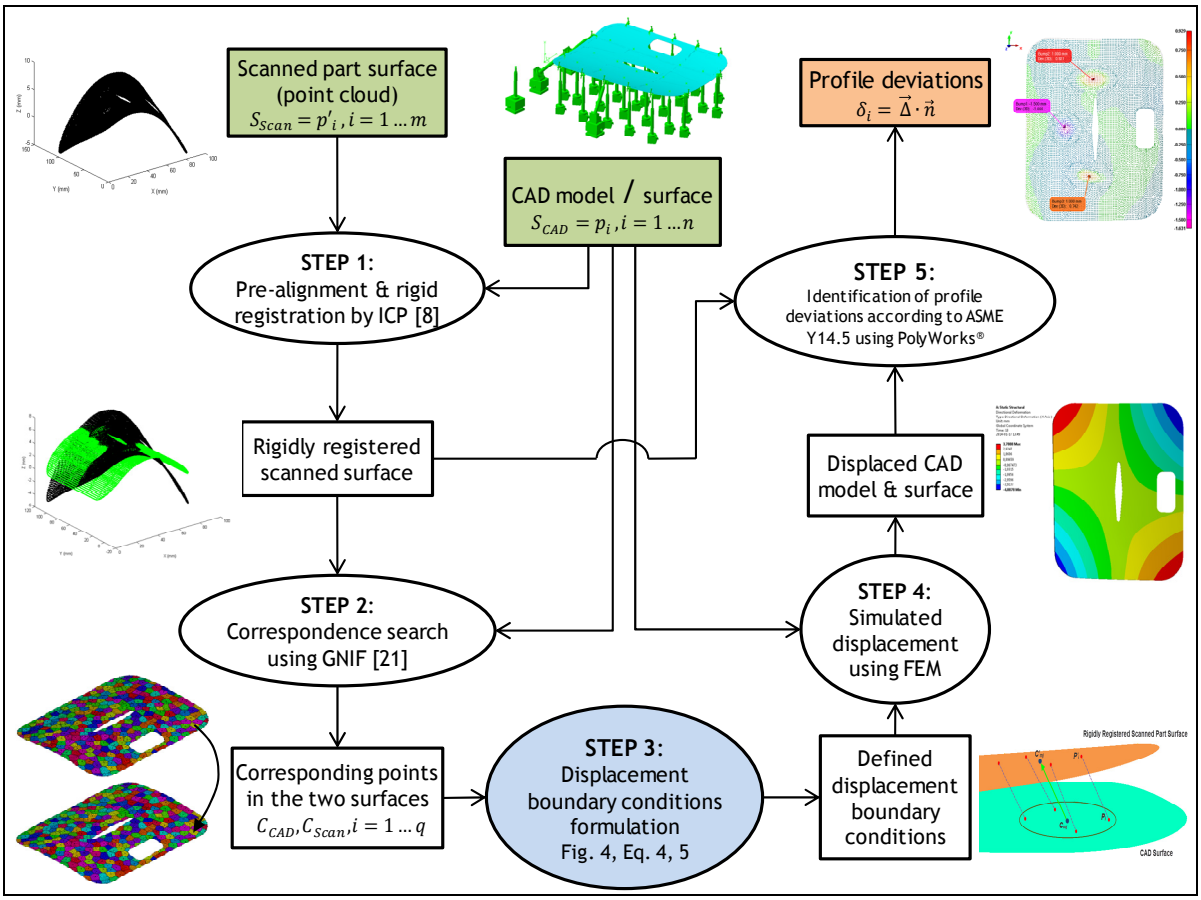

Figure 2.3 Flowchart of the proposed approach

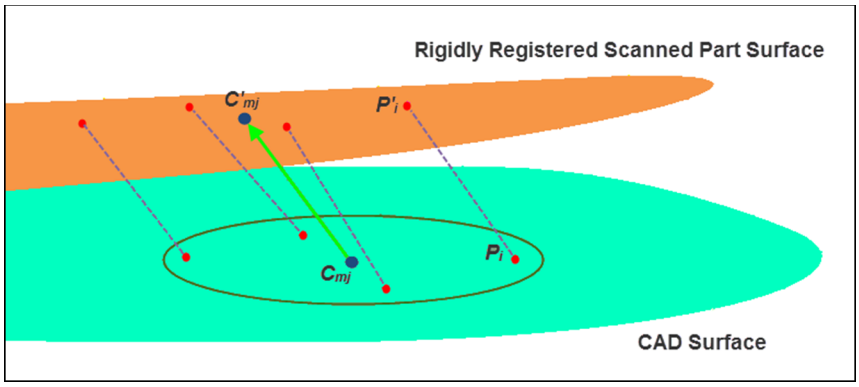

Figure 2.4 Definition of boundary conditions (step 3); correspondence points inside each constraint area and their correspondents on the scanned surface, centres of mass, and a displacement vector are illustrated (case A)

2.5 Case studies

We evaluated our approach on two industrial non-rigid part models from our aerospace industrial partner, Bombardier Aerospace. The parts are illustrated in Figure 2.5. For each model, different virtual parts with different (but known) displacements and deviations (bumps) are simulated, and their point clouds are extracted. To simulate the parts, we applied two types of displacement (torsional or flexural), two types of defect area (small or big), and different amplitudes (1, 1.5, or 2 mm) on each model (A and B): A.S.F, A.S.T, A.B.F, A.B.T, B.S.F, B.S.T, B.B.F, B.B.T (case A or B, S: small defects, B: big defect, F: flexural displacement, T: torsional displacement). There is one defect in the cases with big area defects, and there are two or more defects with different amplitudes in the cases with small area defects.

To evaluate repeatability of the approach, Gaussian measurement noise $N(0, \sigma_{noise})$ was introduced three times on the case B.B.F where $\sigma_{noise} = 0.02\ mm$ that is a typical value of the measurement noise for a non-contact scanning device. Therefore, the proposed approach was applied on eleven (11) case studies.

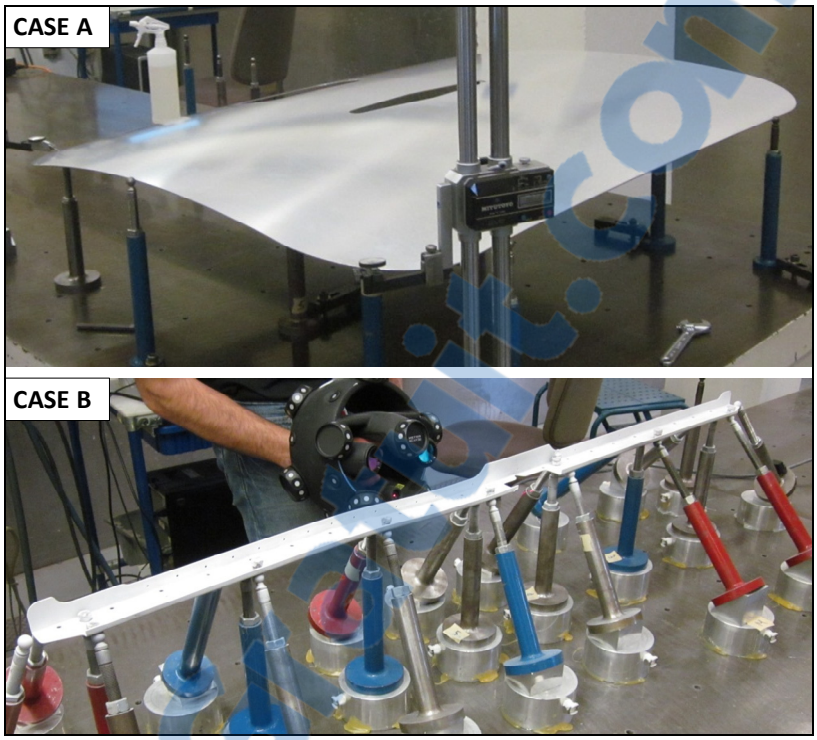

Figure 2.5 Non-rigid parts, Bombardier Aerospace Inc.

In each case, first the pre-alignment and the rigid registration using the ICP algorithm are performed. Figure 2.6 shows the simulated parts after this step. Using the GNIF method, the correspondents between the CAD surface and the rigidly registered surface are recognized. (Figure 2.7)

Knowing the constrained areas and the corresponding points, the boundary conditions are defined. Then using ANSYS®, the CAD model is displaced to the rigidly registered scanned surface for the FE non-rigid registration applying the linear elastic FEA method. The material is *aluminum alloy 7050-T7451*. Figure 2.8 shows the displacement results by FEM and the resulting displaced CAD surface.

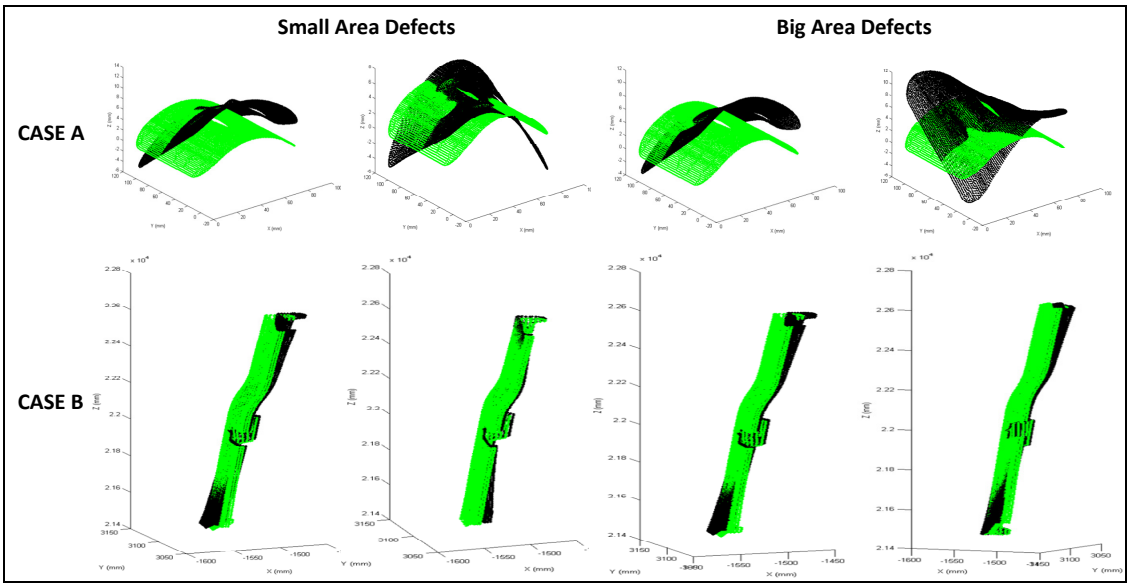

Figure 2.6 Simulated parts with different (but known) displacements and deviations, after pre-alignment and rigid registration (step 1)

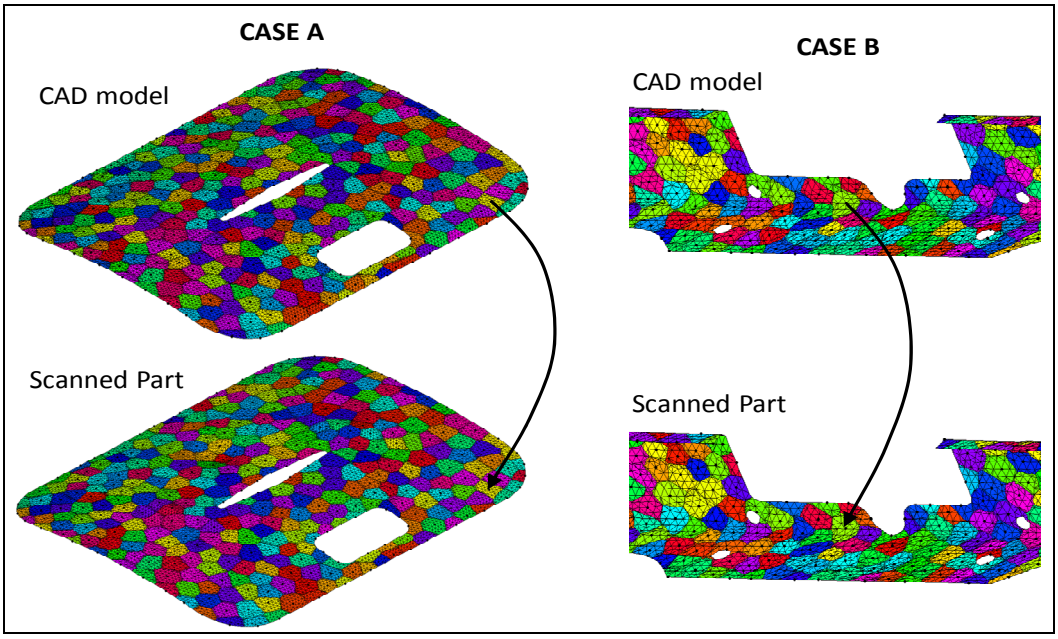

Figure 2.7 Correspondence search by GNIF (step 2) – example: cases A.S.T (case A, small defects, torsional displacement) and B.S.T (case B, small defects, torsional displacement)

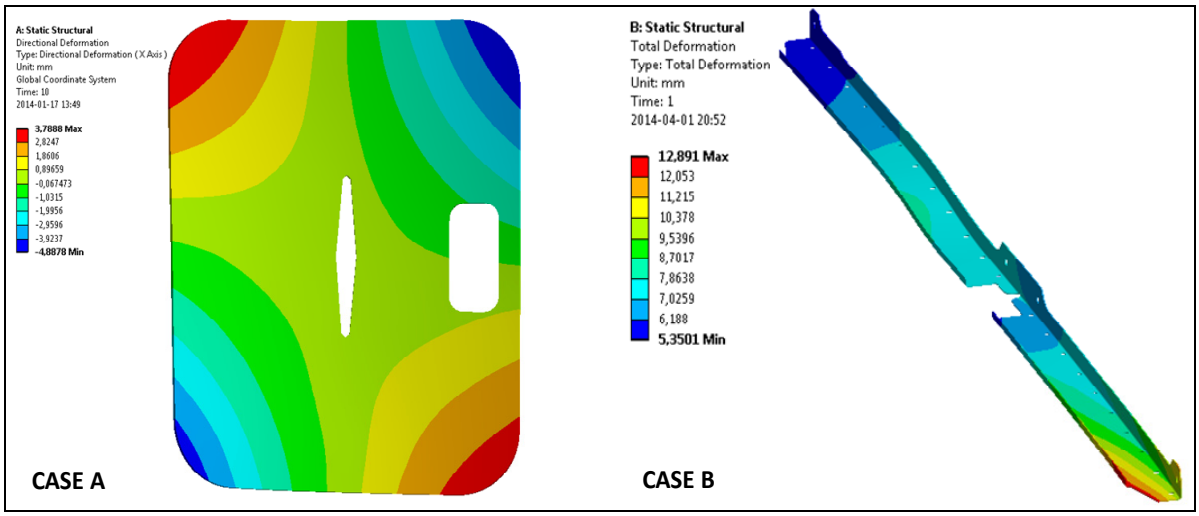

Figure 2.8 Displacement compensation by finite element analysis with defined boundary conditions between the CAD model and the rigidly registered surface, in ANSYS® (step 4) – example: cases A.S.T and B.S.T

Comparing the displaced CAD surfce and the rigidly registered scanned surface, the known deviations are recognized, using PolyWorks®. Table 2.2 represents a summary of the amplitude results in each defect compared between the nominal (simulated) amplitude and the detected (calculated) amplitude. The displacements are, on average, about 10 mm. These values, as well as defect positions and areas, are illustrated in Figure 2.9 (Case A), Figure 2.10 (Case B) and Figure 2.11 (Case B.B.F with Gaussian measurement noise) using the inspection color maps in PolyWorks®.

By improving the definition of boundary conditions, the error percentage generally decreases. A precise and complete definition of boundary conditions eventuates in precise results. Also, the accuracy of the correspondence searching method (GNIF in our paper) definitely affects the results. In a case where a defect (like the defect in the cases A.B.F and A.B.T) is located on a boundary area (a contact surface for example), its position and amplitude can be detected and calculated by studying and filtering the neighborhood area.

Table 2.2 Results of defect's amplitude

Case studies			Case A			Case B		
Type of Defects	Displacement Type	Defect number	Nominal Amplitude (mm)	Detected Amplitude (mm)	Error (%)*	Nominal Amplitude (mm)	Detected Amplitude (mm)	Error (%)*
Small Area	Flexural	1	1.500	1.562	4.1	1.500	1.286	14.3
		2	1.000	0.756	24.4	2.000	1.770	11.5
		3	1.000	0.926	7.4	2.000	1.993	0.3
		4	-	-	-	1.000	0.780	22.0
	Torsional	1	1.500	1.444	3.7	1.500	1.360	9.3
		2	1.000	0.921	7.9	2.000	2.080	4.0
		3	1.000	0.742	25.8	2.000	1.773	11.3
		4	-	-	-	1.000	0.908	9.2
Big Area	Torsional	1	1.500	1.148	23.5	1.000	0.982	1.8
	Flexural	1	1.500	1.228	18.1	1.000	1.113	11.3
	Flexural + $N_1(0, \sigma_{noise})$**	1	-	-	-	1.000	1.126	12.6
	Flexural + $N_2(0, \sigma_{noise})$	1	-	-	-	1.000	0.917	8.3
	Flexural + $N_3(0, \sigma_{noise})$	1	-	-	-	1.000	0.942	5.8

* Error percentage in the result of defect amplitude
** $\sigma_{noise} = 0.02\ mm$

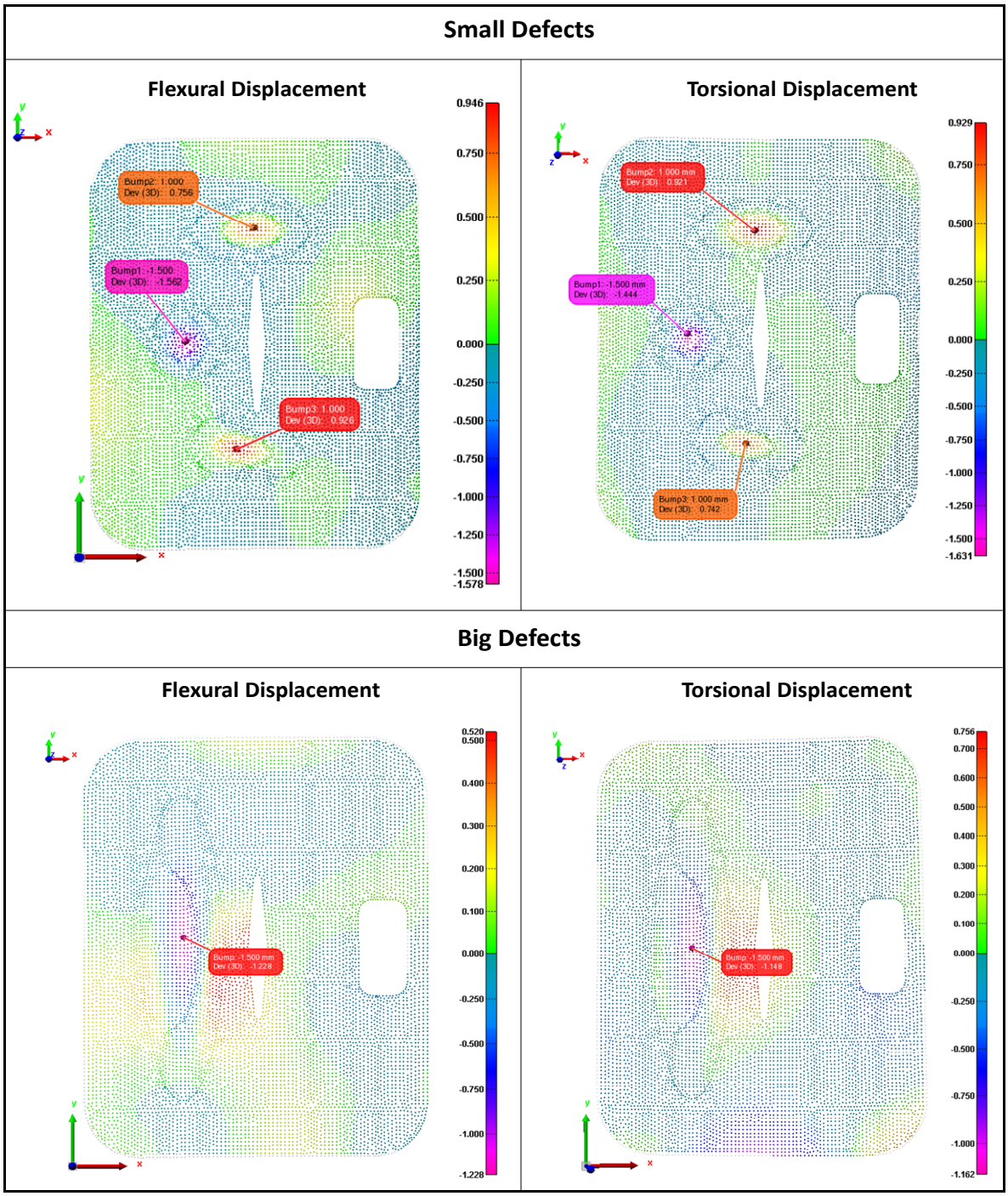

Figure 2.9 Defect amplitudes (mm), positions, and areas, using inspection color map – case A

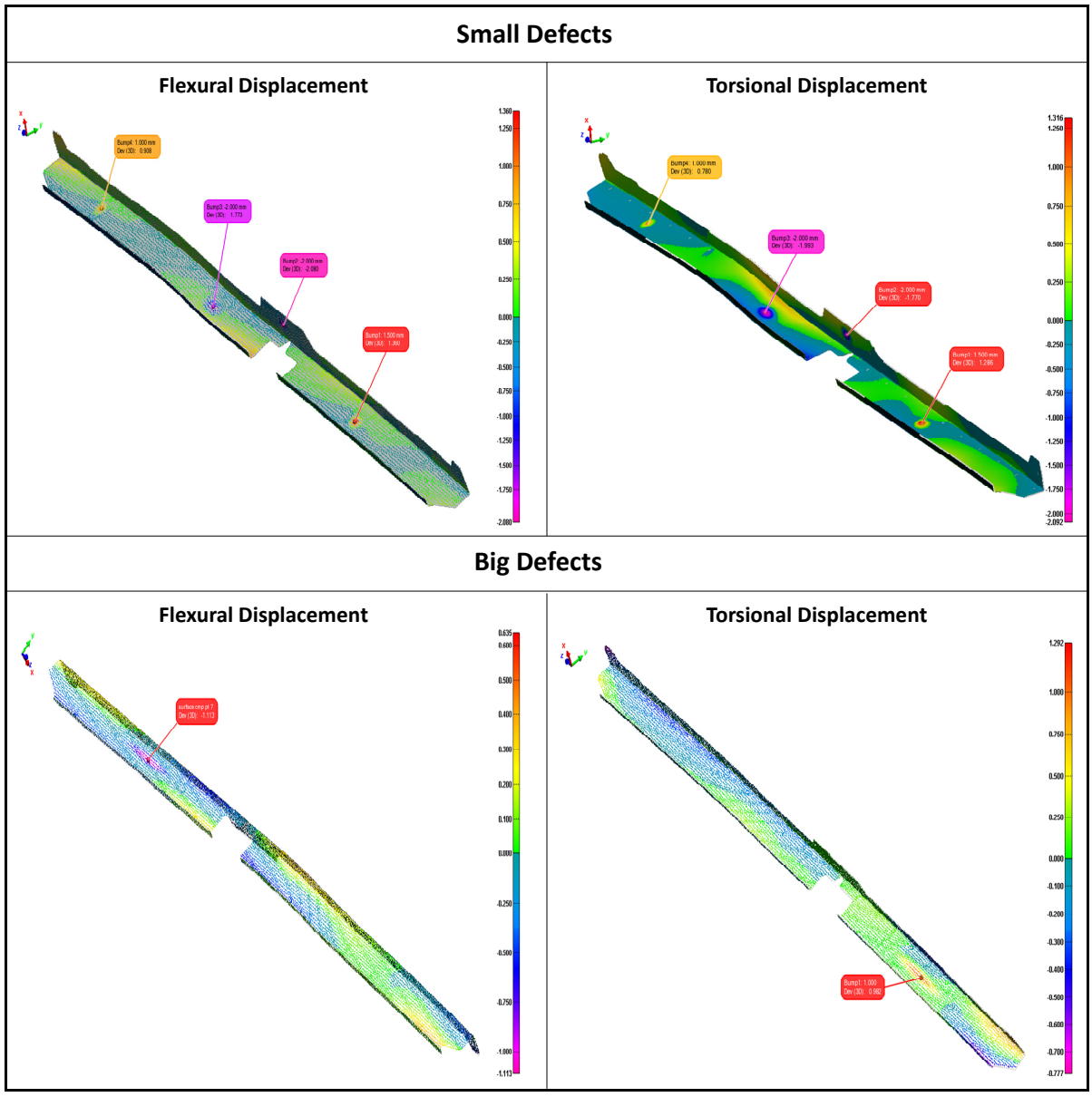

Figure 2.10 Defect amplitudes (mm), positions, and areas, using inspection color map – case B

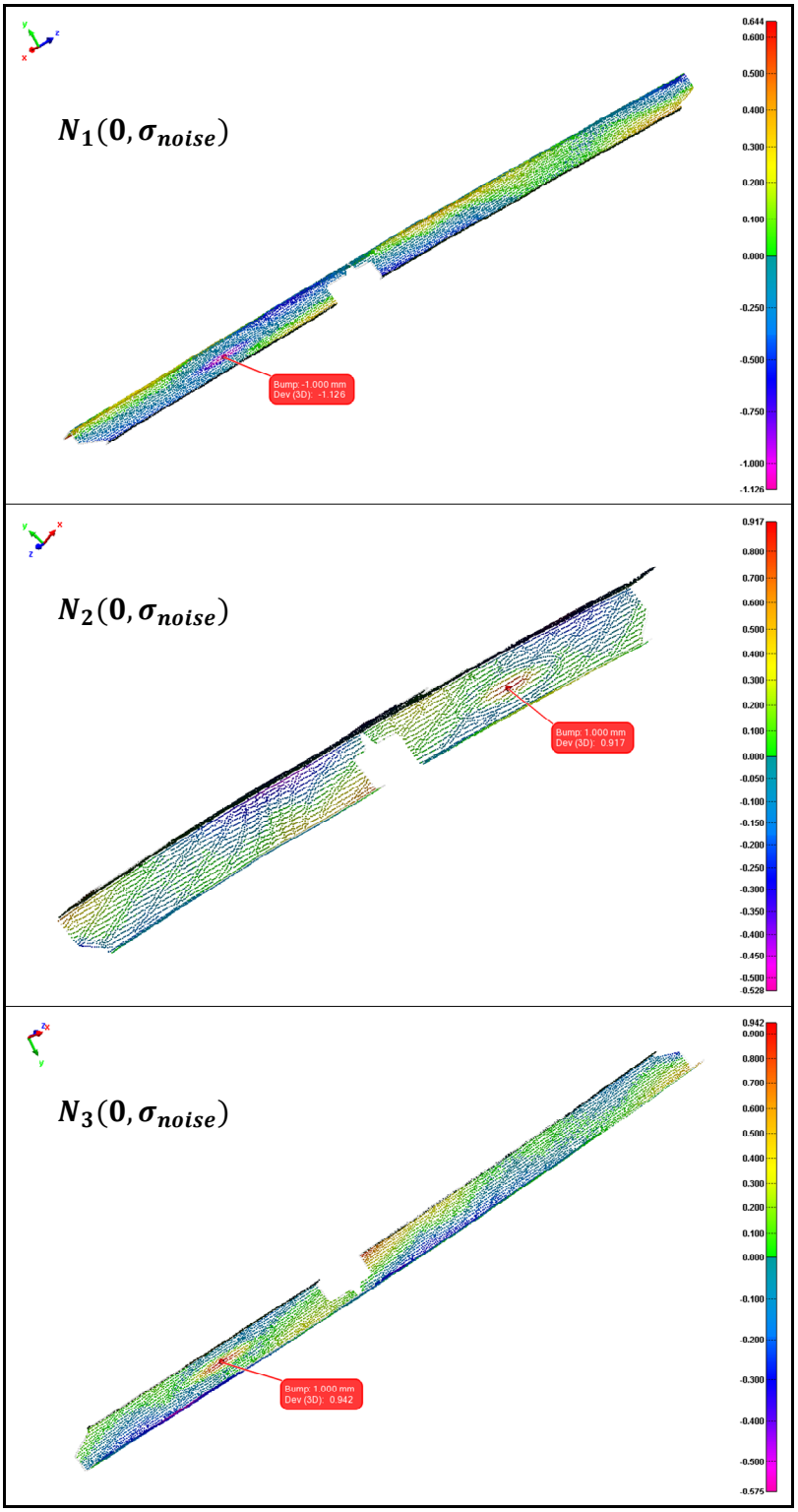

Figure 2.11 Defect amplitudes (mm), positions, and areas, using inspection color map – case B.B.F with Gaussian measurement noise $N(0, \sigma_{noise})$, $\sigma_{noise} = 0.02\ mm$

2.6 Conclusion

In this paper, a technique for the profile inspection of flexible parts was developed to eliminate the need for specialized inspection fixtures. This approach was studied and evaluated on two industrial non-rigid part models from our industrial partner, Bombardier Aerospace Inc. To compare a point cloud (extracted from a simulated part containing known displacement and deviations) with the CAD model, a pre-alignment and a rigid registration (using the ICP method) were performed first. Next, applying the GNIF method, correspondents between the two data sets were found. Knowing the constrained areas such as contact surfaces and fixation areas on the CAD model, planes were fitted through the points inside each area as well as their correspondents on the scanned data. Then, the displacement boundary conditions were completely defined by local translation laws for finite element simulation. The deviation amplitudes, areas, and positions were identified comparing the scanned data with the displaced CAD model. In this paper, the improved method was applied on two industrial case studies with free-form complex surfaces. A definition of boundary conditions, and consequently, an identification of deviations were improved using our approach. If the boundary conditions are completely and exactly defined, more precise results will inevitably be obtained. Repeatability of the proposed approach was evaluated by introducing Gaussian measurement noise on a case. In the future work, repeatability of the approach as well as the detection of defect areas will be studied precisely. Our research advances to implement this approach on real point clouds acquired from part surfaces in order to improve the definition of, and to consider different kinds of, boundary conditions.

2.7 Acknowledgments

The authors would like to thank the National Sciences and Engineering Research Council (NSERC) and our industrial partners for their support and financial contribution.

CHAPTER 3

A ROBUST AND AUTOMATED FE-BASED METHOD FOR THE FIXTURELESS DIMENSIONAL INSPECTION OF NON-RIGID PARTS USING AN IMPROVED NUMERICAL INSPECTION FIXTURE

Vahid SABRI[1], Sasan SATTARPANAH K.[2] S. Antoine TAHAN[1],
Jean-Christophe CUILLIÈRE[2], Vincent FRANÇOIS[2], X. Tan PHAM[1]

1. Products, Processes, and Systems Engineering Laboratory (P2SEL), Department of Mechanical Engineering, Ecole de Technologie Superieure (ÉTS), Montreal, QC, Canada
2. Équipe de Recherche en Intégration Cao-Calcul (ERICCA), Department of Mechanical Engineering, Université du Québec à Trois-Rivières, Trois-Rivières, QC, Canada

This chapter has been accepted for the publication in the *"International Journal of Advanced Manufacturing Technology" – Springer London* (submission ID: JAMT-D-16-02890).

3.1 Abstract

Dimensional inspection is an important element in the quality control of mechanical parts that have deviations from their nominal (CAD) model resulting from the manufacturing process. The focus of this research is on the profile inspection of non-rigid parts which are broadly used in the aeronautic and automotive industries. In a *free-state* condition, due to residual stress and gravity loads, a non-rigid part can have a different shape compared with its assembled condition. To overcome this issue, specific *inspection fixtures* are usually allocated in industry to compensate for the displacement of such parts in order to simulate the use state and accomplish dimensional inspections. These dedicated fixtures, their installation, and the inspection process consume a large amount of time and cost. Therefore, our principal objective has been to develop an inspection plan for eliminating the need for specialized fixtures by digitizing the displaced part's surface using a contactless (optical) measuring device and comparing the acquired point cloud with the CAD model to identify deviations. In our previous work, we developed an approach to numerically inspect the profile of a non-rigid part using a non-rigid registration method and finite element analysis. To do so, a simulated displacement was performed using an improved definition of boundary conditions

for simulating unfixed parts. In this paper, we will improve on the method and save time by increasing the accuracy of displacement boundary conditions and using automatic node insertion and finite element analysis. The repeatability and robustness of the approach will be also studied and its metrological performance will be analyzed. We will apply the improved method on two industrial non-rigid parts with free-form surfaces simulated with different types of displacement, defect, and measurement noise (for evaluation of robustness).

Keywords: quality control, geometric / dimensional inspection, geometric dimensioning and Tolerancing (GD&T), profile tolerance, registration, non-rigid / flexible / deformable / compliant part, assembly conditions, dimensional metrology.

3.2 Introduction

Dimensional inspection plays a significant role in the quality control of mechanical parts since it usually consumes a large portion of production lead time. By means of Geometric Dimensioning and Tolerancing (GD&T), geometric specifications and product design are specified with respect to functionality. To verify if the specifications defined at the design phase are respected, the GD&T inspection procedure is applied. Using a reliable, efficient, and automated inspection process will result in decreased product life cycle time and improved industrial competition (Gao, Gindy et al. 2006). The dimensional inspection, in the case of rigid parts, has significantly improved and the developed methods are generally applied within the industry (Li and Gu 2005), whereas the dimensional inspection of non-rigid parts with free-form surfaces is still an ongoing and challenging field of research.

In mechanical engineering applications, surfaces are allocated a profile tolerance to control manufacturing variations (Li and Gu 2005). A surface profile should be controlled based on the norms established by the *ASME Y14.5-2009* standards (section 8) (ASME-Y14.5 2009). According to these standards (or *ISO 1101:2004*, ISO-GPS standards (ISO-1101: 2004)), unless otherwise specified, all tolerances should be applied in a free-state condition. Exemptions are agreed to this rule for non-rigid parts that may deform significantly from

their defined tolerances due to their weight (gravity) or the release of residual stresses resulting from manufacturing processes (ASME-Y14.5 2009, ISO-10579: 2010).

To overcome the above-mentioned issue, specialized inspection fixtures with complex installations are usually used within the industry to compensate for the displacements in order to simulate the use state and perform dimensional inspections of non-rigid parts. These dedicated fixtures are costly, heavy, and complex (Figure 3.1). The installation and inspection processes are extremely time-consuming which reduces competitiveness. The mentioned standards also agree with the application of reasonable load (not exceeding the load expected under normal assembly conditions) to displace non-rigid parts to conform to the defined tolerances. The solution is to develop an inspection technique for eliminating the need for specialized fixtures by digitizing the displaced part's surface using a contactless (such as optical) measuring device and comparing the obtained point cloud with the nominal model to identify deviations.

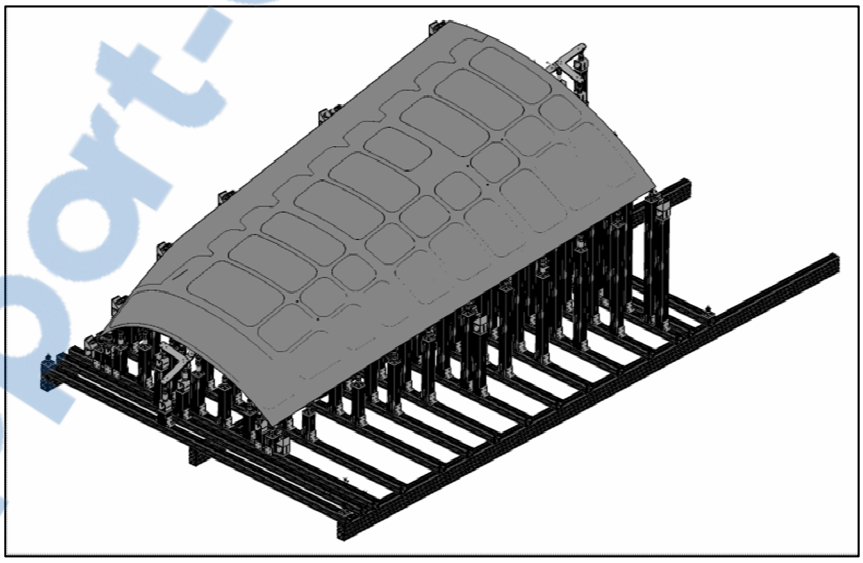

Figure 3.1 A costly, heavy, and complex fixture dedicatedly installed for the dimensional metrology of a non-rigid plate mounted on it, Bombardier Aerospace Inc.

To compare the digitized data (point cloud) with the nominal (CAD) model, it is essential to dispose these two data sets in a joint coordinate system. This procedure is termed

registration. In modern technologies, registration is mathematically defined using the translation and the rotation of the Design Coordinate System (DCS) with respect to the Measurement Coordinate System (MCS). In application, registration can be done in two stages: searching for the correspondence relationship between nominal and digitized surfaces; and, defining an optimum transformation matrix between the DCS and MCS. The rigid registration methods are applied only for rigid parts. In flexible parts, the registration problem requires the application of a non-rigid registration method on top of finding a rigid mapping. The difference between rigid and non-rigid registrations is that a non-rigid registration can align two different shapes (for example, a line with a curve) (Li and Gu 2004, Abenhaim, Tahan et al. 2011). Numerous methods have been developed for rigid and non-rigid registration such as the *Iterative Closest Point (ICP)* algorithm (Besl and McKay 1992) and its variants for rigid registration; the *Multi-Dimensional Scaling (MDS)* method (Borg and Groenen 2005), and the *Coherent Point Drift (CPD)* algorithm (Myronenko and Xubo 2010) for non-rigid registration applied in medical imaging, animation, etc. However, for the registration of a non-rigid mechanical part, the situation is different due to the result of its *compliance behavior*.

Compliance behavior of a compliant (flexible) part is a vital issue to study while specifying tolerances and assessing the geometric and dimensional specifications for the part. This element is a relative concept based on the relation between an imposed force and its resulting displacement (Abenhaim, Desrochers et al. 2012). Based on the displacements of parts stemming from a reasonable force (50 N) during dimensional inspection, the parts are considered rigid / non-rigid (flexible) / extremely non-rigid (see Table 3.1). For quantifying the flexibility of a mechanical part from an industrial point of view, another method was proposed by Aidibe and Tahan (Aidibe and Tahan 2014). Their quantifying method is based on the ratio between the maximum displacement (δ) induced by a certain force and the profile tolerance of the non-rigid part. Our research is on typical non-rigid mechanical parts used in the aeronautic and automotive industries.

A review of previous research on the fixtureless dimensional inspection of non-rigid parts is discussed in the next section. In this paper, we present an improved version of a previous

approach proposed by our team (Sabri, Tahan et al. 2016). This new approach is improved mainly with respect to the displacement boundary conditions used in FE-based non-rigid registration and to the automation of node insertion. This improved inspection method is described in section 3. Case studies along with an evaluation of repeatability and an analysis of metrological performance are presented in section 4. The paper ends with a conclusion.

Table 3.1 The ratio δ/tol in each zone induced by a force during inspection and their compliance behaviour

δ/tol by a reasonable force during inspection (≈ 50 N)	**Compliance behavior**
$\delta/tol <$ 5-10 %	Rigid
$\delta/tol >$ 5-10 % (e.g. thin shell, skin in aeronautic and automotive parts)	Non-rigid (Flexible)
$\delta/tol \gg$ 10 % (the shape depends on the part's weight and position, such as thin seals and paper)	Extremely non-rigid

3.3 Review of previous research

Ascione and Polini (Ascione and Polini 2010) discussed the dimensional inspection of non-rigid parts with free-form surface using inspection fixtures combined with Coordinate Measuring Machine (CMM). Abenhaim *et al.* (Abenhaim, Desrochers et al. 2012) presented a review of previous research on the fixtureless inspection of non-rigid parts and proposed a classification of the specification methods used for the GD&T of non-rigid parts under the ASME and ISO standards. In the following, we will introduce the primary methods, based on a simulated displacement approach, developed for the dimensional inspection of non-rigid parts without the use of inspection fixtures.

A first attempt at the fixtureless inspection of non-rigid parts was undertaken in 2006 by Weckenmann *et al.* (Weckenmann and Gabbia 2006, Weckenmann and Weickmann 2006). The authors proposed the *virtual distortion compensation* method in which they virtually displaced the distorted manufactured part into the nominal model by displacing the point

cloud acquired using a contactless measuring device. A triangle surface mesh was generated from the point cloud and transformed into a finite element analysable (FEA) model. Afterwards, the positioning process was simulated using information about the assembly features' deviation from the actual (measured) to the ideal (nominal) position. In this method, human intervention is needed to recognize the correlation between some determined points and assembly conditions in order to define the boundary conditions of the FEA problem. Hence, boundary conditions can be improved to simulate a real model of the positioning system. Moreover, converting the digitized data (point cloud) into a FE model is a time-consuming process loaded with uncertainties. One year later in 2007, Weckenmann *et al.* (Weckenmann, Weickmann et al. 2007) improved on the shortcomings of their previous work by displacing a CAD model towards the measurement data in the *virtual reverse deformation* method. They enforced the boundary conditions on the CAD model using the known position of the fixation points on the scanned part. Thus, a pre-processing of the digitized data is not required. Through this method, they decreased inspection time and achieved more precise results. The FE simulation of the displacement boundary conditions on the geometrically ideal CAD model is evidently more accurate. Nevertheless, this method still required human intervention to find the corresponding relationship between the CAD model and the measurement data. Furthermore, the modelling of the boundary conditions in the FE dataset needs to be improved to simulate the unfixed part.

Analogous to the virtual reverse deformation method, Jaramillo *et al.* (Jaramillo, Boulanger et al. 2009, Jaramillo, Boulanger et al. 2011) presented an approach which requires less calculation power, using the Radial Basis Functions (RBFs) to minimize the finite element mesh density required to correctly predict part behavior. Recently in (Jaramillo, Prieto et al. 2013), they improved upon their method by performing the registration of flexible part using only partial views from areas that needed inspected. They applied an interpolation technique based on RBFs to estimate positions of the missing fixation points since the partially digitized data may not contain all of them.

Gentilini and Shimada (Gentilini and Shimada 2011) proposed an approach for the shape inspection of a flexible assembly part by virtually mounting it into the assembly. First, the

dense measured mesh is smoothed and reduced to become suitable for FEA. Material properties, if not available, are defined by a calibration process. Then, specific displacement boundary conditions are defined and applied for the FE simulation of the assembly process. Once FEA is performed, quality inspection of the simulated post-assembly shape is done using visualization tools. Moreover, the virtual post-assembly shape is compared with the real one for an evaluation of method accuracy. This method can predict the final assembled shape of a flexible part, but it has the drawbacks mentioned in the virtual distortion compensation method. The polygonal mesh data suffers from uncertainties, noise and a high quantity of polygons, therefore it needs post-processing steps, smoothing and decimation.

In 2012, Radvar-Esfahlan and Tahan (Radvar-Esfahlan and Tahan 2012) presented the *Generalized Numerical Inspection Fixture (GNIF)* method based on the *distance preserving* property of non-rigid parts: the shortest path (*geodesic distance*) between any two points on the surfaces does not change during an isometric displacement in spite of large displacement. By taking advantage of this property, the algorithm looks for some correspondence between the scanned part and the CAD model. The authors used the *Multidimensional Scaling (MDS)* approach in order to find a correspondence between two metric spaces (CAD model and scanned part). Then, finite element non-rigid registration (FENR) was executed knowing some boundary conditions. The dimensional deviations between the displaced CAD model and the digitized data can be identified after the FENR. Correspondence search is completely automatic. The GNIF dealt with a very general case of non-rigid inspection. The authors used the borders for FENR in the absence of assembly conditions. This situation may not conform to assembly conditions and real use state. Boundary conditions for the simulated displacements can be improved based on assembly conditions. The authors in (Radvar-Esfahlan and Tahan 2014) robustified the GNIF method by filtering out points that cause incoherent geodesic distances. The improved method is able to handle parts with missing digitized data sets.

In contrast to the aforementioned methods, Abenhaim *et al.* (Abenhaim, Tahan et al. 2011) proposed the *Iterative Displacement Inspection (IDI)* method that is not based on the FEA module. This method iteratively displaces the meshed CAD model until it matches to the

digitized data. The IDI algorithm is based on optimal step non-rigid ICP algorithms (Amberg, Romdhani et al. 2007) which combine rigid and non-rigid registration methods. Also, an identification method was developed for distinguishing surface deviations from the part's displacement. This method displaces the CAD mesh regarding its smoothness and prevents covering surface defects and measurement noise during the mapping process. Aidibe *et al.* (Aidibe, Tahan et al. 2012) improved the identification module of the IDI algorithm by proposing the application of a maximum-normed residual test to automatically set the identification threshold. However, the IDI method has certain drawbacks. Due to a lack of FE analysis, the method depends on identifying some flexibility parameters which are reliant on thickness. In addition, they use the same number of nodes in the two data sets.

Aidibe and Tahan (Aidibe and Tahan 2014) presented an approach that integrates the curvature properties of manufactured parts with the extreme value statistic test as an identification method for comparing two data sets and to recognize profile deviation. This approach was tested on simulated typical industrial sheet metal with satisfactory results in terms of error percentage in defect areas and in the estimated peak profile deviation. As the fundamental of the algorithm is based on the Gaussian curvature comparison, application of the method is limited to relatively-flexible parts where small displacements are predictable. The authors in (Aidibe and Tahan 2015) proposed the ACPD method for optimization of the CPD algorithm in order to adapt it to the relatively-flexible parts problem, introducing two criteria: the stretch criterion between the nominal model and the aligned one; and the Euclidian distance criterion between the aligned nominal model and the scanned part.

Abenhaim *et al.* (Abenhaim, Desrochers et al. 2015) introduced a method that registers the point cloud to the nominal model using information recuperated from the FE model of the CAD model. This is done by embedding a FE-based transformation model into a boundary displacement constrained optimization. This optimization problem tries to minimize a distance-based similarity criterion between points in unconstrained areas whereas this criterion between points in constrained areas is kept in a specified contact distance, and simultaneously, the restraining forces are limited. The latter allows for the inspection of non-rigid parts for which their functional requirements require limiting the restraining forces

imposed during assembly. In addition, the point cloud does not need to be pre-processed into a FE model. Also, there is no need for manual identification of fixation positions in the point cloud. Furthermore, as long as the point cloud includes the restraining areas, a partial view of the part can be enough for the method.

An automatic fixtureless inspection approach based on filtering corresponding sample points was presented in (Sattarpanah Karganroudi, Cuillière et al. 2016), wherein corresponding sample points that are in defect areas are automatically filtered out, based on curvature and von Mises stress criteria. This tends to a more accurate inspection of non-rigid parts.

Recently in (Thiébaut, Lacroix et al. 2017), an approach was proposed to evaluate shape deviations of flexible parts, using optical scanners, in a given measuring configuration for which the setup is known (whatever configuration, independent from the assembly conditions). The CAD model was displaced by the FE simulation of the part's displacement due to its own gravity considering the known configuration used for the measurement. Having applied to a simple part, the form deviations were recognized by subtracting the simulated geometrical displacements to the measured geometrical displacements. They used the known configuration for the part's optical measurement based on which the displacement vector for the FE simulation at each node of the CAD mesh was calculated using the intersection of a cylindrical neighborhood of its normal vector and the point cloud.

3.4 Proposed approach

Searching for correspondence between two data sets, as a primary step, seems to be the best idea in registration problems, according to the literature. As mentioned in the previous section, the GNIF method based on the isometric displacement (Radvar-Esfahlan and Tahan 2012) has some advantages that encourage us to use it to search for corresponding points between two data sets. In our previous work (Sabri, Tahan et al. 2016), we developed an approach to numerically inspect the profile of a non-rigid part using a non-rigid registration method and finite element analysis. To do so, a simulated displacement was performed using an improved definition of displacement boundary conditions for simulating unfixed parts.

The developed method was implemented on two industrial non-rigid parts with free-form surfaces simulated with different types of displacement, defect, and measurement noise (for one case). In the current paper, we will improve our method and save the time using the automatic node insertion and finite element analysis. Also, repeatability and robustness of the improved approach will be studied for all the cases. We will apply the improved method on two industrial non-rigid parts; one from the previous work (case B) and a new one (case C). In addition, for repeatability and robustness evaluation, Gaussian measurement noise will be introduced three times to each case (24 times for 8 cases). Therefore, the improved method will be studied on a total of 32 cases.

The Generalized MDS method of non-rigid registration, applied in the GNIF approach, represents the corresponding points on the data sets based on the barycentric coordinate system (Radvar-Esfahlan and Tahan 2012). To use these points for future purposes, their barycentric coordinates have to be converted into Cartesian coordinates. Using Equations 2.1 and 2.2 in Chapter 2 (Sabri, Tahan et al. 2016), the Cartesian coordinates of the corresponding points in each data set can be calculated.

Figure 3.2 schematically shows the different steps of our approach. First, we displace the scanned part surface ($S_{Scan} = p'_i, i = 1, \dots, m$) close enough to the CAD surface ($S_{CAD} = p_i, i = 1, \dots, n$) (pre-alignment) to achieve a satisfactory result for rigid registration using ICP (Besl and McKay 1992). Then, the pre-aligned surface is rigidly registered to the CAD surface by using the ICP algorithm. The next step is to apply the modified 64-bit version of the GNIF method to find a set of correspondent pairs between the two surfaces (Equation 3.1). We have modified the GNIF code, in MATLAB®, and converted the 32-bit version into a 64-bit version to achieve the capability of dealing with high density data sets. In the 32-bit version, the GNIF code can be only applied on meshes with less than 10,000 nodes; whereas using the modified 64-bit version, we can search for correspondence, and consequently apply the proposed method, on any case study with an enormous number of nodes.

$$C_{CAD} = \{p_i | i = 1, \dots, q\} \; C_{Scan} = \{p'_i | i = 1, \dots, q\}, \quad q \ll m, n \tag{3.1}$$

To define a set of displacement boundary conditions for simulating the displacement from the CAD model to the rigidly registered scanned part surface, the constrained areas on the CAD model, such as fixation positions (e.g. hole) or contact surfaces (e.g. target datums) according to ASME Y14.5, are first recognized (Gentilini and Shimada 2011). Then, the corresponding points (with the Cartesian coordinates) inside each constrained area (with the index of j), and consequently their correspondents in the scanned data, are identified among all the correspondents obtained by the GNIF method:

$$B_j = \{p_i \in C_{CAD} | i = 1, \dots, s_j \ll q\},\ B'_j = \{p'_i \in C_{Scan} | i = 1, \dots, s_j \ll q\} \tag{3.2}$$

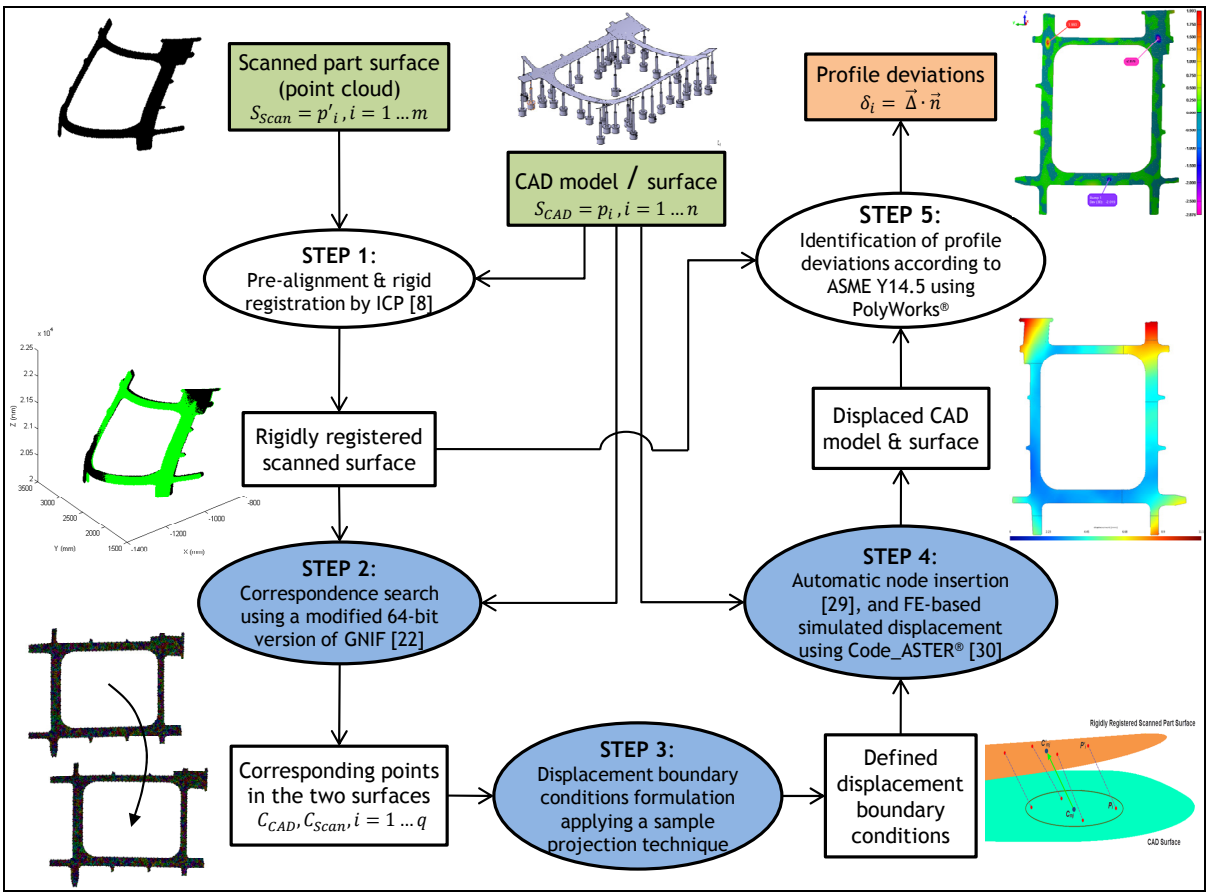

Figure 3.2 Flowchart of the proposed approach

Next, for each area and its corresponding area on the scanned surface, we define a centre of mass by fitting a plane through the identified corresponding points (B_j, B'_j). To register each pair of the identified correspondents in the two data sets by simulated displacement using finite element analysis, the displacement boundary conditions should be defined by local translation law (Gentilini and Shimada 2011):

- the centre of mass (C_{m_j}) is translated to the corresponding centre of mass on the corresponding plane (C'_{m_j}):

$$\overrightarrow{\Delta r_j} = \begin{Bmatrix} x_{c\prime} - x_c \\ y_{c\prime} - y_c \\ z_{c\prime} - z_c \end{Bmatrix}_j \tag{3.3}$$

In the previous paper (Sabri, Tahan et al. 2016), the displacement vectors were calculated based on the difference between the coordinate of each sample point (centre of mass) on the CAD model and its corresponding sample point on the scanned model. However, the generated sample points for CAD and scanned models based on the presented method are not necessarily located on the pertinent CAD or scanned mesh; this is a source of error in finite element calculation. In the current paper, to increase accuracy of the FE calculation and consequently the non-rigid inspection result, the generated centres of mass are projected individually on their related CAD or scanned models. To this end, each generated sample point is moved along its normal direction respect to the mesh surface to coincide with the related mesh triangulation. Then, the displacement vectors are calculated accordingly based on the difference between the coordinate of each projected sample point on the CAD model and its corresponding projected sample point on the scanned part. Therefore using the sample projection technique, the accuracy of the method is improved in step 3.

Having defined the displacement boundary conditions, the finite element analysis can be performed between the two data sets based on the simulated displacement approach to distinguish between displacements and deviations. The goal is to find the maximum profile deviation on each defect comparing the scan data and the displaced CAD model (δ_{max} in Figure 3.3). To this aim, the determined centres of mass are inserted into the CAD mesh, and then the CAD model is displaced towards the scanned surface applying the defined

displacement boundary conditions to the inserted centres of mass. In our previous work (Sabri, Tahan et al. 2016), this node insertion process was performed manually. In the present paper, the nodes (projected centres of mass instead of original ones) are inserted into the CAD mesh automatically using a classical Delaunay point insertion method (Borouchaki, George et al. 1996). Then, each displacement vector is calculated as explained before in the step 3 of the algorithm. Applying FE analysis, the CAD model is deformed towards the scanned model by applying the displacement vectors as the displacement boundary conditions on the projected and inserted sample points on the CAD model. The FEA is performed by applying a new and open source method (Cuillière and Francois 2014). In other words, the step 4 of the algorithm is also improved, and we save time and cost.

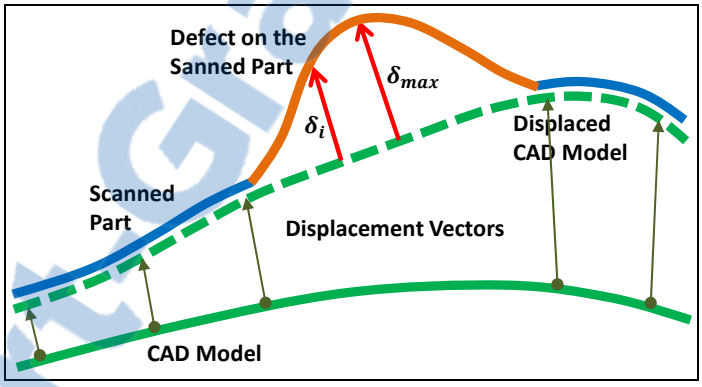

Figure 3.3 Simulated displacement, identification of profile deviations (δ_i) and estimation of maximum profile deviation (δ_{max}) on a defect

We have successfully implemented the methodology using several tools. Mesh generation, mesh transformations, and FEA have been done using the research platform developed by our research team (Cuillière and Francois 2014). This platform is based on C++ code, on Open CASCADE® libraries and on Code_Aster® as FEA solver. Typically, noise generation and point projection as well as FEA takes almost 1 minute on a computer with Intel® Core™ i7 at 3.60 GHz processor in 31.3 GB RAM.

Finally, the profile deviations (δ_i) are identified based on the shortest 3D distance between each point of the scanned data and the displaced CAD surface, as recommended by ASME

Y14.5-2009 (ASME-Y14.5 2009), using PolyWorks® Software. Then on each defect, the maximum profile deviation (δ_{max}) is estimated.

3.5 Case studies, repeatability evaluation, and metrological performance analysis

We evaluate our proposed approach on two industrial non-rigid part models (case A and case B) typical in aerospace industries. Parts are illustrated in Figure 3.4. For each model, different virtual parts with different (but known) displacements and deviations (e.g. bumps) are simulated, and their point clouds are extracted. To simulate the parts, we apply two types of displacement: torsional (typical of displacement due to residual stresses) or, flexural (typical of displacement due to gravity). Two types of defect area (small or big) were simulated with different amplitudes (1, 1.5, 2, or 3 mm) on each model (A and B): ASF, AST, ABF, ABT, BSF, BST, BBF, BBT (Case A or B, S: small defects, B: big defect, F: flexural displacement, T: torsional displacement). There is one defect in the cases with big area defects, and there are three or four defects with different amplitudes in the cases with small area defects. The meshing in all the cases is triangular surface mesh with 5mm size. The number of nodes in the CAD model in case B is 9816, and in case A is 29776. Thus, a correspondence search in case C became possible with the modified 64-bit version of the GNIF code in MATLAB®.

The automatic node insertion technique and FE solver in the step 4 makes us able to evaluate repeatability and study robustness of the approach. Gaussian measurement noise $N(0, \sigma_{noise})$ is introduced three times on each of the above-mentioned cases (24 times for 8 cases) where $\sigma_{noise} = 0.01, 0.02, 0.03\ mm$ that is a typical value of the measurement noise for a non-contact scanning device. The noises are generated as random numbers from the normal distribution with mean and standard deviation parameters. These random numbers are added to the nodes coordinate of the scanned mesh in the normal direction respect to the mesh surface. Therefore, the proposed approach is totally applied on 32 case studies: 8 original (noise-free) cases, and 24 cases with noise.

In each case, the pre-alignment and the rigid registration using the ICP algorithm are performed first. Figure 3.5 shows the simulated parts after this step. Using the modified 64-bit version of the GNIF method, the correspondents between the CAD surface and the rigidly registered surface are identified (Figure 3.6). To compare the capability of corresponding search between the 32b and the 64b versions of the GNIF algorithm, the calculation time for each original case, on a computer with Intel® Core™ i7-3770 at 3.40 GHz processor in 16.0 GB RAM, is mentioned in Table 3.2. The number of correspondence sample points is 1000 in the cases B and 2000 in the cases A. There is an insignificant time difference between the 32b and the 64b versions in the case B which is the smaller case (9816 nodes in the CAD model). The main difference is in the case A (29776 nodes in the CAD model) where the 32b version of the GNIF algorithm is inapplicable for the calculation.

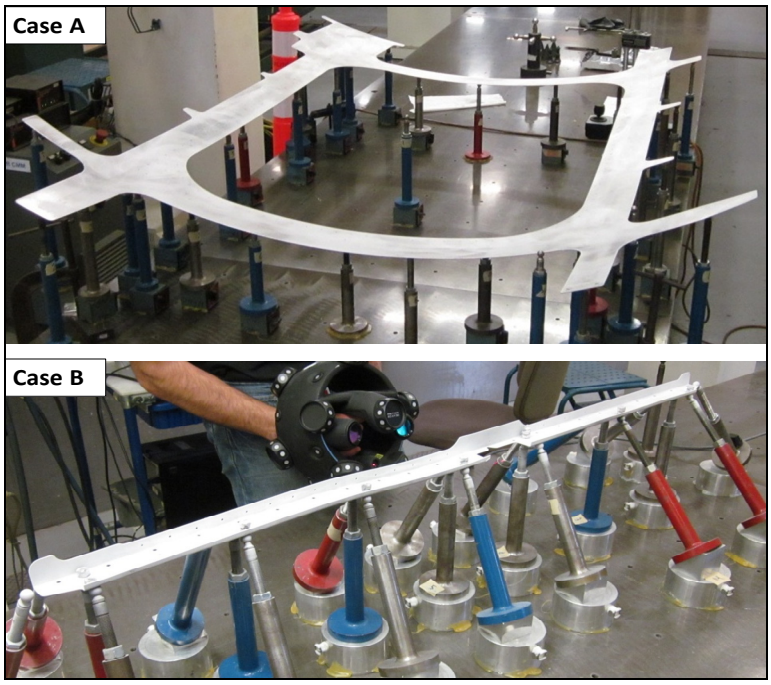

Figure 3.4 Non-rigid parts, Bombardier Aerospace Inc.; dimensions (mm) of case A: 1750 × 1430, and case B: 1153.4 × 38.6; the material is *aluminium alloy 7050-T7451*.

Knowing the constrained areas and the corresponding points, the displacement boundary conditions are formulated taking advantage of the sample projection technique as described earlier. The projected centres of mass are inserted into the CAD mesh using the automatic

node insertion method (Borouchaki, George et al. 1996). Having defined the displacement boundary conditions, using the recently developed FE-based platform (Cuillière and Francois 2014), the CAD mesh is modified and displaced to the rigidly registered scanned surface (for registration purpose) applying the linear elastic FEA method (Figure 3.7).

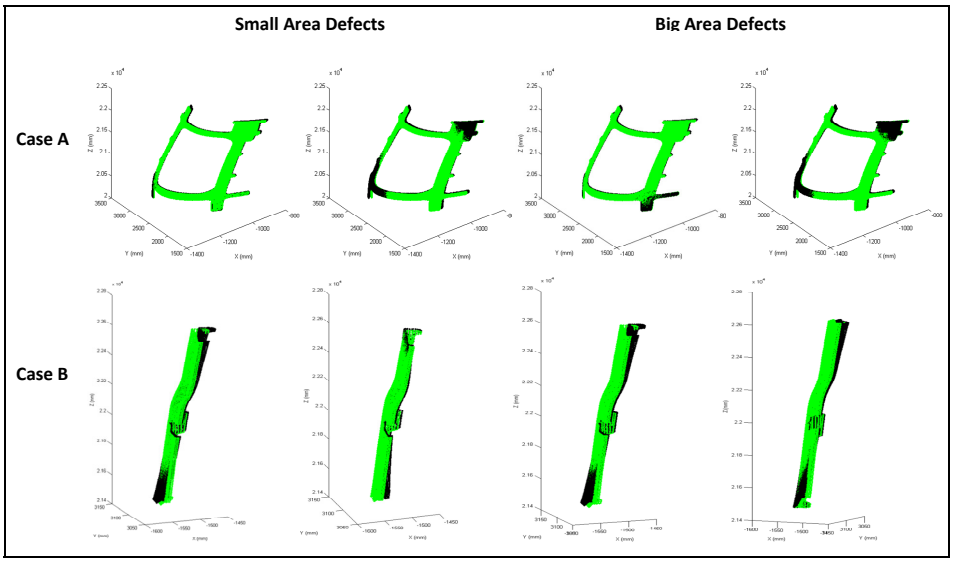

Figure 3.5 Simulated parts with different (but known) displacements and deviations, after pre-alignment and ICP rigid registration (step 1)

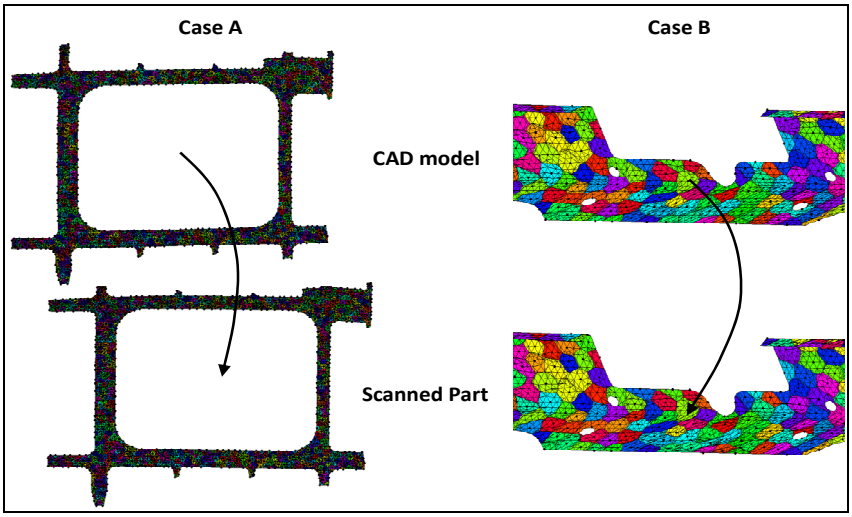

Figure 3.6 Correspondence search by the modified GNIF (step 2) – Examples: ABF and BST

Table 3.2 Capability and calculation time of corresponding search compared between the 32b and the 64b versions of the GNIF algorithm

Cases	Calculation time (minutes)	
	32b GNIF	64b GNIF
ASF	Inapplicable	126
AST	Inapplicable	156
ABF	Inapplicable	98
ABT	Inapplicable	96
BSF	17	20
BST	23	20
BBF	16	17
BBT	26	19

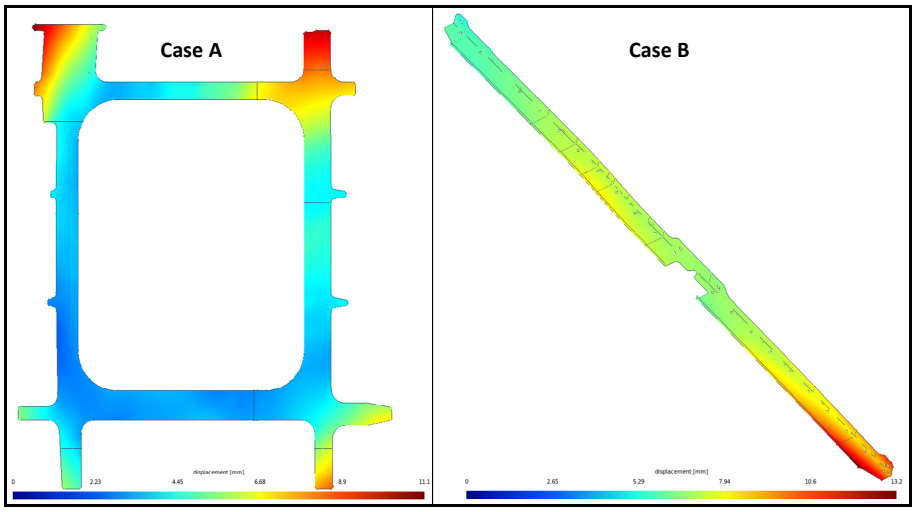

Figure 3.7 FE-based simulated displacement using Code ASTER® (Cuillière and Francois 2014) (step 4) – Examples: ABF and BST

Comparing the displaced CAD surface and the rigidly registered scanned surface, the known deviations are recognized, using PolyWorks®. Table 3.3 summarizes the amplitude results by the automatic method in each defect compared between the nominal amplitude and the

detected (estimated) amplitude in the original noise-free cases A and B. These values, as well as defect positions and areas, are illustrated in Figure 3.8 (Case A) and Figure 3.9 (Case B) using the inspection color maps in PolyWorks®. There is a comparison between the results of the original and the automatic method in the noise-free case B in Table 3.3 as well. For repeatability evaluation, Table 3.4 is dedicated to the results of defect's amplitude in the cases A and B with added noise for repeatability evaluation. The maximum displacement in all of the cases is around 10 mm.

Table 3.3 Results of defect amplitudes in cases A and B (noise-free), and a comparison between the original and the automatic method in case B

Case Studies			Case B					Case A		
Type of Defects	Displacement Type	Defect Index	Nominal Amplitude (mm)	Original Method (Sabri, Tahan et al. 2016)		Automatic Method		Nominal Amplitude (mm)	Automatic Method	
				Detected Amplitude (mm)	Error (%)*	Detected Amplitude (mm)	Error (%)*		Detected Amplitude (mm)	Error (%)*
Small Area	Flexural	1	1.500	1.286	-14.3	1.286	-14.3	2.000	1.974	1.3
		2	2.000	1.770	-11.5	1.559	-22.0	2.500	2.005	19.8
		3	2.000	1.993	-0.3	1.783	-10.8	3.000	2.902	3.3
		4	1.000	0.780	-22.0	0.907	-9.3	-	-	-
	Torsional	1	1.500	1.360	-9.3	1.309	-12.7	2.000	2.019	0.9
		2	2.000	2.080	4.0	1.667	-16.6	2.500	1.993	20.3
		3	2.000	1.773	-11.3	2.100	5.0	3.000	2.876	4.1
		4	1.000	0.908	-9.2	0.779	-22.1	-	-	-
Big Area	Torsional	1	1.000	0.982	-1.8	0.963	-3.7	3.000	3.285	9.5
	Flexural	1	1.000	1.113	11.3	0.936	-6.4	3.000	3.207	6.9

* Error percentage in the result of defect amplitude

Table 3.4 Results of defect amplitudes in cases A and B with added noise for repeatability evaluation ($N_i(0, \sigma_{noise_i})$)**

Case Studies			Case A			Case B		
Type of Defects	Displacement Type	Defect Index	Nominal Amplitude (mm)	Detected Amplitude (mm)	Error (%)	Nominal Amplitude (mm)	Detected Amplitude (mm)	Error (%)
Small Area	Flexural	1	2.000	1) 2.011 2) 1.982 3) 1.990 Av) 1.994	1) 0.5 2) 0.9 3) -0.5 Av) -0.3	1.500	1) 1.212 2) 1.272 3) 1.253 Av) 1.246	1) -19.2 2) -15.2 3) -16.5 Av) -16.9
		2	2.500	1) 2.004 2) 2.008 3) 2.001 Av) 2.004	1) -19.8 2) -19.7 3) -20.0 Av) -19.8	2.000	1) 1.614 2) 1.569 3) 1.560 Av) 1.581	1) -19.3 2) -21.5 3) -22.0 Av) -20.9
		3	3.000	1) 2.935 2) 2.902 3) 2.924 Av) 2.920	1) -2.2 2) -3.3 3) -2.5 Av) -2.6	2.000	1) 1.772 2) 1.743 3) 1.792 Av) 1.77	1) -11.4 2) -12.8 3) -10.4 Av) -11.5
		4	-	-	-	1.000	1) 0.905 2) 0.900 3) 0.873 Av) 0.893	1) -9.5 2) -10.0 3) -12.7 Av) -10.7
	Torsional	1	2.000	1) 2.041 2) 2.018 3) 2.050 Av) 2.036	1) 2.0 2) 0.9 3) 2.5 Av) 1.8	1.500	1) 1.075 2) 1.044 3) 1.069 Av) 1.063	1) -28.3 2) -30.4 3) -28.7 Av) -29.1
		2	2.500	1) 1.992 2) 1.996 3) 1.994 Av) 1.994	1) -20.3 2) -20.2 3) -20.2 Av) -20.2	2.000	1) 1.424 2) 1.412 3) 1.569 Av) 1.468	1) -28.8 2) -29.4 3) -21.5 Av) -26.6
		3	3.000	1) 2.873 2) 2.867 3) 2.890 Av) 2.876	1) -4.2 2) -4.4 3) -3.7 Av) -4.1	2.000	1) 2.042 2) 2.089 3) 1.978 Av) 2.036	1) 2.1 2) 4.4 3) -1.1 Av) 1.8
		4	-	-	-	1.000	1) 0.859 2) 0.867 3) 0.885 Av) 0.870	1) -14.1 2) -13.3 3) -11.5 Av) -13.0
Big Area	Flexural	1	3.000	1) 3.289 2) 3.270 3) 3.283 Av) 3.280	1) 9.6 2) 9.0 3) 9.4 Av) 9.4	1.000	1) 0.928 2) 0.919 3) 0.914 Av) 0.921	1) -7.2 2) -8.1 3) -8.6 Av) -8.0
	Torsional	1	3.000	1) 3.253 2) 3.159 3) 3.193 Av) 3.201	1) 8.4 2) 5.3 3) 6.4 Av) 6.7	1.000	1) 1.033 2) 1.081 3) 1.062 Av) 1.033	1) 3.3 2) 8.1 3) 6.2 Av) 5.9

** $\sigma_{noise_i} = i \times 0.01\ mm,\ \mathrm{i} = 1,2,3$

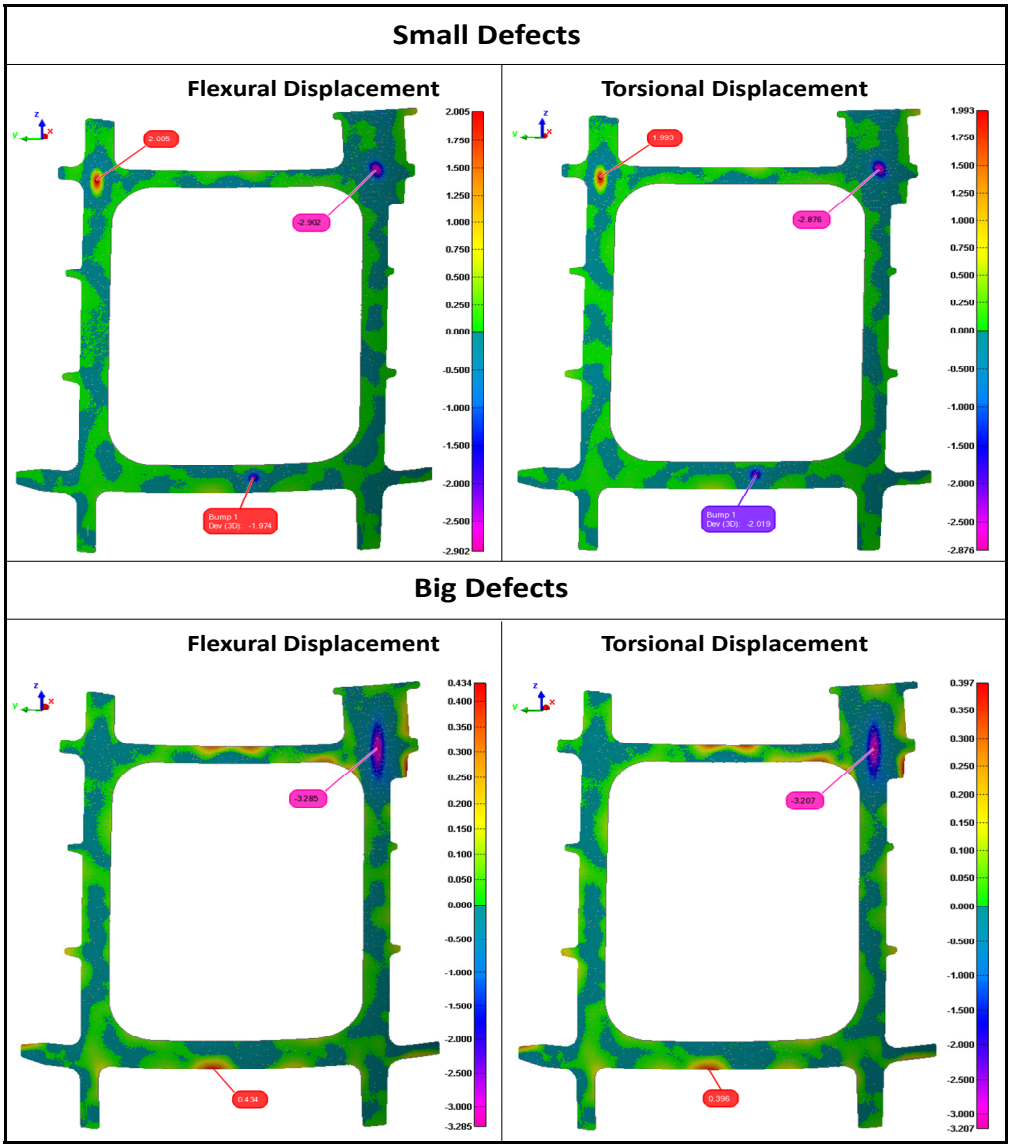

Figure 3.8 Defect amplitudes (mm), positions and areas, using inspection color map – Case A (original, noise-free)

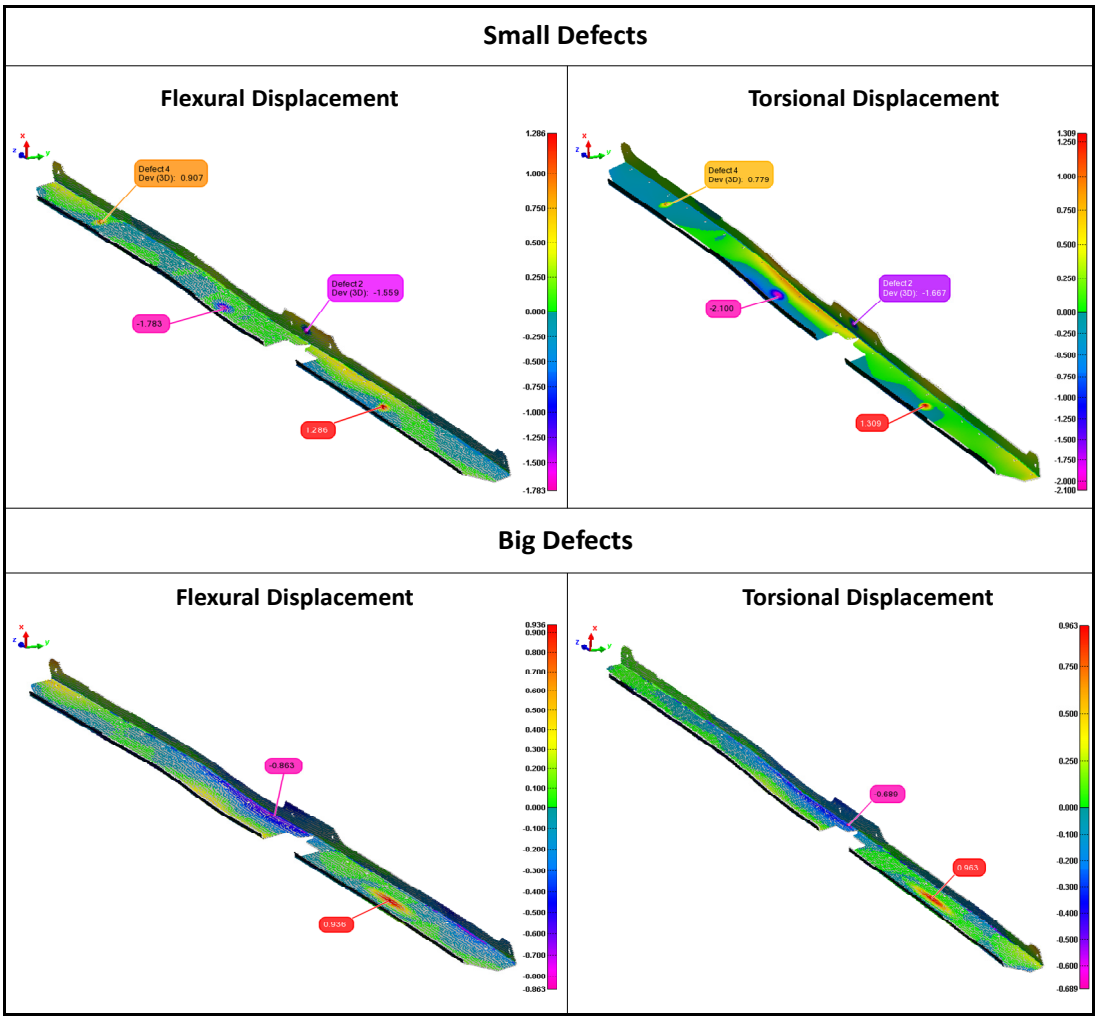

Figure 3.9 Defect amplitudes (mm), positions and areas, using inspection color map – Case B (original, noise-free)

The error percentage generally decreases by improving the definition of boundary conditions. A precise and complete definition of boundary conditions leads to precise results. Also, the accuracy of the correspondence searching method (the modified GNIF method in our paper) definitely affects the results. The modified 64-bit version of the GNIF algorithm lets us to deal with large flexible parts with very dense point clouds. Satisfactory results can be achieved in a very short time compared to the original approach, by taking advantage of the recently developed platform for automatic node insertion and FE solver.

To explain the various values of the algorithmic error in different (and even the same) defects, uncertainty sources should be identified. Regarding the different steps of the algorithm, the developed method's accuracy is limited by the uncertainty of these elements: the correspondence search, the displacement boundary condition formulation, and the FE solver. The only known source of error is the Gaussian measurement noise added numerically for the simulation of scanned parts to study the method's robustness. The algorithmic error is the combination of the mentioned uncertainty errors whose values are not known or predictable to us. A validation research is needed to study and quantify these uncertainties. Figure 3.10 illustrates the different uncertainty sources in the presented approach.

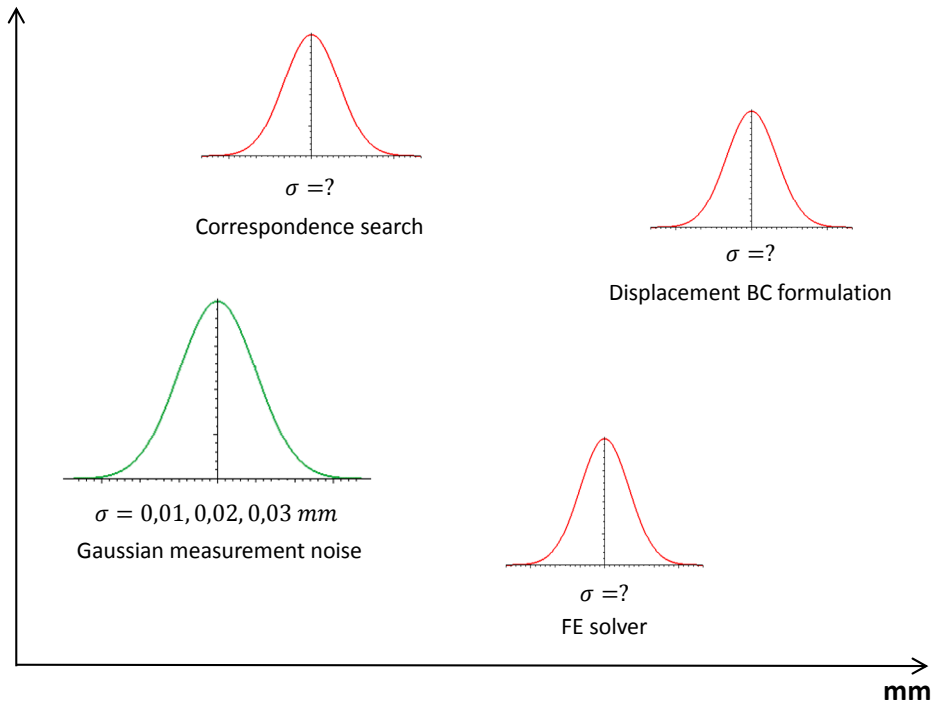

Figure 3.10 Different uncertainty sources in the developed algorithm

Figure 3.11 represents Box Plots for the results of the maximum error (%) relative to σ_{noise} in each case A and B. Comparing the results in different values of σ_{noise}, the developed algorithm can be considered repeatable and robust to the typical measurement noise

forasmuch as there is an insignificant difference between intervals respect to the different values of σ_{noise}. This is because the centres of mass (based on which the displacement vectors for the FE simulation are calculated) are defined as the average of the neighborhood points in each area. Therefore, the noise is quite averagely compensated in a centre of mass.

A small bias is seen in the case B that could be because of some reasons such as the part's high length relative to its width and maybe insufficient or inaccurate definition of displacement boundary conditions and areas. This bias is not significant in the case A that is not too long relative to its width, and the boundary conditions in which are defined, in quantity and quality, better than in the case B.

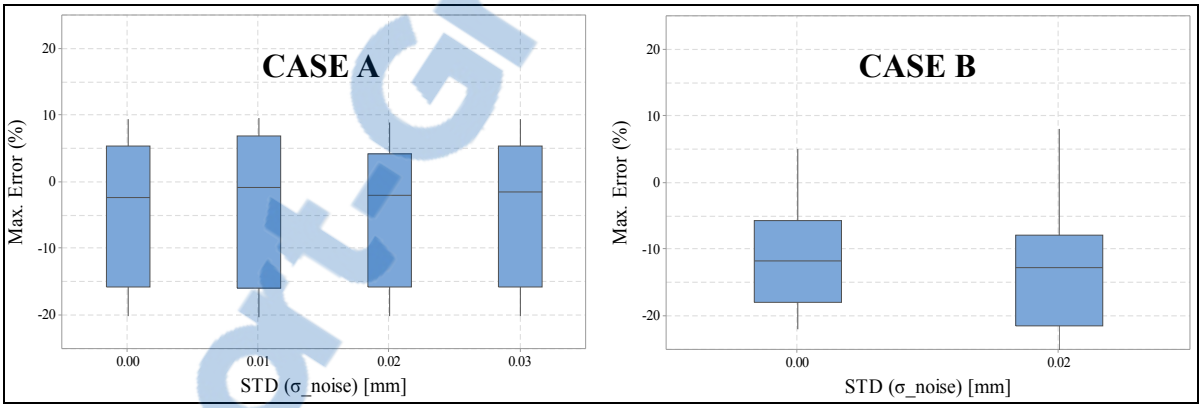

Figure 3.11 Box Plots for the results of the maximum algorithmic error on profile deviation (%) relative to $\boldsymbol{\sigma_{noise}}$ in the cases A and B

3.6 Conclusion

In the present paper, an automatic method for the profile inspection of flexible parts was developed to eliminate the need for dedicated inspection fixtures. This approach was studied and evaluated on two industrial non-rigid part models from our industrial partner, Bombardier Aerospace Inc. To compare a point cloud (extracted from a simulated part containing known displacement and deviations) with the CAD model, a pre-alignment and a rigid registration (using the ICP method) were done first. Then, correspondents between the

two data sets were found applying our modified 64-bit version of the GNIF method. Next, knowing the constrained areas such as contact surfaces and fixation areas on the CAD model, planes were fitted through the points inside each area as well as their correspondents on the digitized data. Then, the displacement boundary conditions were completely defined by local translation laws for finite element simulation. The deviation amplitudes, areas, and positions were identified comparing the scanned data with the displaced CAD model. In this paper, the improved method was applied on two industrial flexible parts with free-form complex surfaces. A definition of boundary conditions, and consequently, an identification of deviations were improved using our approach. If the boundary conditions are completely and exactly defined, more precise results will inevitably be achieved. The 64-bit version of the GNIF algorithm made us able to apply the method on large flexible parts with dense point clouds (e.g. the case C). Accuracy of the algorithm was improved by using a sample projection technique for the formulation of displacement boundary conditions. Time was saved, compared to the original approach, using an automatic node insertion technique and FE solver. The latter allowed us to study repeatability of the proposed method by introducing Gaussian measurement noise three times on each case. Metrological performance of the approach was analyzed using Box Plots that proved the robustness of the method to the typical measurement noise according to the results of the repeatability evaluation. Our research advances to implement this approach on real point clouds acquired from part surfaces in order to improve the definition of, and to consider different kinds of, boundary conditions.

3.7 Acknowledgments

The authors would like to thank the National Sciences and Engineering Research Council (NSERC) and our industrial partners for their support and financial contribution.

CHAPTER 4

A METHOD FOR DIMENSIONAL METROLOGY OF NON-RIGID PARTS BASED ON ARC LENGTH MEASUREMENT AT FREE-STATE CONDITION

Vahid SABRI[1], Gad N. ABENHAIM[2], S. Antoine TAHAN[1], X. Tan PHAM[1]

1. Products, Processes, and Systems Engineering Laboratory (P2SEL), École de Technologie Superieure (ÉTS), Montreal, QC, Canada
2. Ford, Detroit, MI, USA

This chapter has been accepted with revisions for the publication in the *"International Journal of Advanced Manufacturing Technology" – Springer London* (submission ID: JAMT-D-16-03929).

4.1 Abstract

Deviations from nominal shape resulting from manufacturing process are inevitable for mechanical parts. Through the use of dimensional metrology tools and techniques, these deviations can be identified. In the particular case of non-rigid parts, which are extensively used in the aeronautic and automotive industries, the dimensional inspection is particularly delicate because their form in the free-state condition is greatly affected by gravity and residual stress. The use of dedicated fixtures is a frequently used solution to conform the component in industry but this is also very costly and time-consuming. In this paper, we propose a method for performing the inspection of arc length tolerance, and we show the potential of this fast and easy method to identify many types of defects. Indeed, the inspection of arc length with measuring tapes is a very old technique used in industry for measuring the curvilinear distance (arc length) along the surface. Typically, this method was not precise enough and time effective. This research proposes a numerical solution for the virtual dimensional metrology of arc length along free-form surfaces using the *Fast Marching Method* (FMM) based on the *Geodesic Distance* (length of the shortest path) between any two points on the surface. The main idea behind this paper is that the geodesic distance between any pair of points on a non-rigid surface remains practically constant

during an isometric displacement in spite of large displacement. Taking advantage of the *distance preserving* property of non-rigid parts, the presented approach enables us to virtually inspect the non-rigid parts without the need for specialized fixtures for conformation. Therefore, any deviation on the geodesic distance, bigger than a priori arc length tolerance, means that there is a defect on the part. This is the concept behind our work. This algorithm is tested on several case studies with different configurations, and its accuracy is compared with a recently developed method in the domain.

Keywords: dimensional metrology, geometrical inspection, geometrical dimensioning and tolerancing, arc length measure, non-rigid / flexible / deformable / compliant mechanical part, Fast Marching Method (FMM).

4.2 Introduction

Generally, mechanical parts have dimensional and geometrical deviations from nominal shape caused by the inherent variations in manufacturing processes. Dimensional metrology is an important step in the quality control of manufactured parts. Geometrical specifications and product design are determined by applying Geometrical Dimensioning and Tolerancing (GD&T) with respect to functionality. To validate if these specifications are met, the dimensional inspection of the product is an obligation. The dimensional metrology procedure consumes a large amount of time and cost. Therefore, a reliable, efficient, and automated procedure will improve the industrial competition (Gao, Gindy et al. 2006).

On the other hand, non-rigid parts (widely used in the aeronautic and automotive industries) may differ from their nominal shape in a free-state condition due to their weight or the release of residual stresses. Thus in industry, they need to be precisely positioned on dedicated fixtures for inspection purposes. These specialized fixtures are expensive and the installment process is time-consuming. Ascione and Polini (Ascione and Polini 2010) dealt with the dimensional metrology of non-rigid parts with free-form surfaces using inspection fixtures combined with CMM. Abenhaim *et al.* (Abenhaim, Desrochers et al. 2012) presented a review of previous research for the fixtureless dimensional metrology of non-rigid parts

and proposed a classification of the specification methods used for the GD&T of non-rigid parts under the ASME (e.g. Y14.5 (ASME-Y14.5 2009)) and ISO (e.g. 1101 (ISO-1101: 2004)) standards. The researchers in (Weckenmann and Weickmann 2006, Weckenmann, Weickmann et al. 2007, Abenhaim, Tahan et al. 2011, Jaramillo, Boulanger et al. 2011, Radvar-Esfahlan and Tahan 2012, Jaramillo, Prieto et al. 2013, Aidibe and Tahan 2014, Radvar-Esfahlan and Tahan 2014, Abenhaim, Desrochers et al. 2015, Aidibe and Tahan 2015, Sabri, Tahan et al. 2016) proposed approaches for the dimensional inspection of non-rigid mechanical parts in a free-state condition without the need for specialized fixtures.

Historically, by performing the inspection of arc length tolerance with flexible measuring tape, deviation on the profile (such as contour) and localization (e.g. distance between two holes) can be easily identified. For example in aeronautic industry, to ensure a good quality for the joining of two fuselage sections (which may be considered non-rigid), their circumference lengths must fit inside the predefined tolerance (Figure 4.1). Of course, the traditional methods (such as measuring tape) contain uncertainties due to their dependence on human intervention. They also do not have enough accuracy and time efficiency. Thus, they have become obsolete with the introduction of digital inspection tools (CMM, laser scan, photogrammetry, etc.). However, the basic idea remains valid. This method is an alternative that allows for validating the dimensional integrity of the non-rigid parts without using a conformation fixture. This paper seeks to explore the opportunity of proposing an inspection methodology based on the estimation of geodesic distances from a 3D scanner.

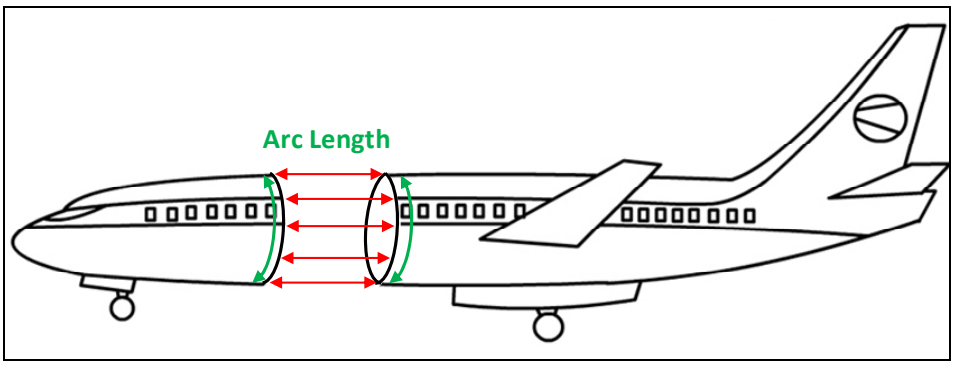

Figure 4.1 Joint of two sections of a fuselage by considering the arc length tolerance

Several approaches have been proposed for measuring the length along the surface. In 2013, Hunt and Niphakis (John and Nathan 2013) presented a method for characterizing the shape of *Lighter Than Air* (LTA) vehicles more accurately and completely using photogrammetry and stretch functions. The actual inflated shapes of LTA vehicles have traditionally been determined using measuring tapes and plumb bobs to measure the projected profile and surface lengths. Photogrammetry overcomes some of the shortages of the traditional method that uses measuring tapes and plumb bobs.

Aidibe and Tahan (Aidibe and Tahan 2015) proposed an approach that combines the optimization of the smoothness regularization parameters of the *Coherent Point Drift* (CPD) non-rigid registration method alongside the Thompson-Biweight statistical test as an identification method to distinguish profile and localization defects from a part's displacement. The nominal model is smoothly modified to fit the scanned part by minimizing two criteria. The first criterion is the conservation of the curvilinear (or geodesic) distance (isometric transformation), with the condition that the stretch difference between the original nominal model and the modified one should be very small. The second criterion is the minimization of the Euclidian distance between the modified nominal model and its corresponding scanned part.

The original definition of the geodesic distance comes from the length of a geodesic path between a pair of points on the surface of the Earth that is considered the shortest path for traveling between these two points. The concept of geodesic distance can be generalized to any kind of surface, and applied as the length of the shortest path between any pair of points on the surface. If the point cloud on the surface is dense enough, a simple solution for the estimation of the geodesic distance between a pair of points is the *shortest path algorithm* proposed by Dijkstra (Dijkstra 1959), but this solution is not accurate enough because in this algorithm, it is allowed to move in the graph using only vertices (nodes). The popular fast marching method (FMM) (Sethian 1996, Sethian 1999, Sethian 2008) is a numerical algorithm for the approximation of the geodesic distance on a rectangular orthogonal mesh. Kimmel and Sethian (Kimmel and Sethian 1998) extended the fast marching method to triangulated mesh with the same computational complexity. FMM allows one to solve the

boundary value problem without iteration unlike the standard methods. For more details, the reader should refer to (Sethian 1999, Bronstein, Bronstein et al. 2007). Bose *et al* (Bose, Maheshwari et al. 2011) presented a survey that gives a brief overview of theoretically and practically relevant algorithms to compute geodesic paths and distances on three-dimensional polyhedral surfaces.

The main idea of the current paper is inspired by the following fact: assuming an isometric displacement, the geodesic distance on a non-rigid surface does not change in spite of large displacement (Figure 4.2). Thus, the identification of this distance is independent from the condition in which the measurement was taken (free-state or constrained). Our objective is to develop a virtual method for dimensional metrology of arc length along the surface to use it instead of traditional and physical techniques and tools (measuring tape), particularly in the case of non-rigid parts without the need for specialized fixtures for conformation (in a free-state condition).

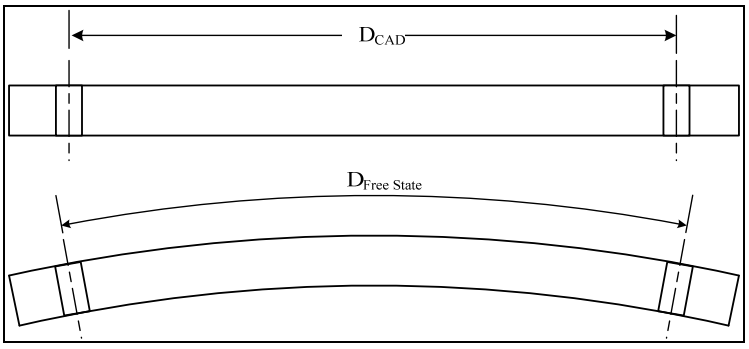

Figure 4.2 Distance preserving property of non-rigid parts

4.3 Methodology

In the present paper, we propose a low-cost numerical approach for dimensional inspection of arc length along the surface using the fast marching method (FMM) based on the geodesic distance (length of the shortest path) between any two points on the surface. To compare between the nominal (CAD) surface and the scanned part surface for evaluation of the arc length tolerance, the first step is to define a matrix of geodesic distances between all pairs of

strategic points on the part surface which can be holes, intersection between functional features, etc. In Figure 4.3, a skin panel is illustrated. In this typical case as an example, the featured points (e.g. P_i and P_j) are on the contours and the curvilinear (geodesic) distance between them must meet the arc length tolerance.

All geodesic distances can be grouped in a symmetric square matrix:

$$GD_{n\times n} = \begin{bmatrix} 0 & \cdots & GD_{n1} \\ \vdots & \ddots & \vdots \\ GD_{1n} & \cdots & 0 \end{bmatrix}_{n\times n} \tag{4.1}$$

where n is the size of the sampling domain that is, in our case, the strategic points on the part surface. And by definition, we have $GD_{ii} = 0$ and $GD_{ij} = GD_{ji}$.

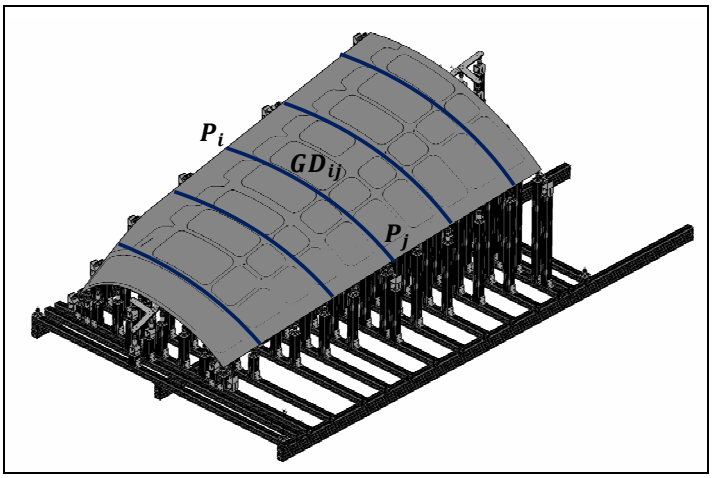

Figure 4.3 Featured points on a skin panel and their geodesic distances (e.g. P_i, P_j, GD_{ij})

Knowing the nominal geodesic distance between the two determined points or features on the CAD surface (GD_{ij}^{CAD}), we have estimated the geodesic distance between their corresponding points or features on the scanned part surface (GD_{ij}^{SCAN}). If the difference between the nominal and estimated values is inside the defined tolerance ($Tol_{\,arc\,length}$) for all dimensions, the part is considered accepted:

$$\forall i,j \in S: \left|GD_{ij}^{SCAN} - GD_{ij}^{CAD}\right| < Tol_{\,arc\,length} \tag{4.2}$$

where S is a set of featured points. The deviation metrics will be estimated by the followings:

$$\begin{cases} e_{ij} = GD_{ij}^{SCAN} - GD_{ij}^{CAD} \\ e_{ij}(\%) = 100 \times \frac{GD_{ij}^{SCAN} - GD_{ij}^{CAD}}{GD_{ij}^{CAD}} \end{cases} \tag{4.3}$$

As mentioned before, to calculate the geodesic distance between pairs of points, as mentioned before, the Dijkstra shortest path algorithm (Dijkstra 1959) is a simple idea if the sampling domain is dense enough; however, the result is not always the real shortest path because it is allowed to move in the graph using only nodes. This inconsistency in the Dijkstra algorithm was resolved by the fast marching method introduced by Sethian (Sethian 1996) as a numerical method for solving boundary value problems of the *Eikonal* equation:

$$|\nabla T(x)|F(x) = 1 \tag{4.4}$$

which represents the evolution of a closed curve in $\mathbb{R}^2$(or a surface in $\mathbb{R}^3$) with speed F in its normal direction so that the speed function never changes in sign. T is the shortest traveling time. Kimmel and Sethian (Kimmel and Sethian 1998) proposed an improved version of the FMM on triangulated mesh with the same computational complexity. The geodesic (shortest) path in the FMM can pass through the mesh unlike the Dijkstra algorithm.

In the cases where the features are holes and we need to study the dimensions between holes centers, there is not an exact or specified node to represent the centers. Therefore, we estimate an average geodesic distance between each pair of holes by taking the nearest nodes around the circle profile of each hole. Let us assume hole i and hole j; there are m and n nearest nodes around hole i and hole j. The average geodesic distance between these holes is estimated by the following:

$$Ave.\ GD_{ij} = \frac{1}{m \times n} \sum_{r=1}^{m} \sum_{s=1}^{n} GD_{rs} \tag{4.5}$$

The application of the proposed method will be generally in the case of non-rigid parts since they are more likely to have arc length error along the surface because of their manufacturing

processes and small thickness. Non-rigid parts may differ from their nominal shape in a free-state condition due to their weight or the release of residual stresses resulting from manufacturing processes. During an isometric displacement, the geodesic distance between any pair of points on the surface of a non-rigid part remains constant in spite of large displacement (Figure 4.2). Taking advantage of this *distance preserving* property of non-rigid parts (Radvar-Esfahlan and Tahan 2012), the presented approach enables us to virtually inspect the non-rigid parts without the need for specialized fixtures for conformation. Thus, this method saves time and cost. For the purpose of evaluation, we will apply our method on a non-rigid case study with different types of displacement in the next section.

4.4 Case studies

We evaluated the FMM performance (algorithmic error) on several case studies (Figure 4.4) with different shape (flat or free-form), dimensions, and mesh size ($1 - 5\ mm$). A flat plate (case A) with the dimensions $1000 \times 100 \times 2$ mm is studied with the nominal maximum geodesic distance $NGD = 1004.99\ mm$ and for different sizes of mesh from $1\ mm$ to $5\ mm$.

Table 4.1 Algorithmic error (e_{ij} in mm and $e_{ij}(\%)$) of the FMM in different cases

	Mesh Size (mm)	1.0	1.5	2.0	2.5	3.0	3.5	4.0	4.5	5.0
A	e_{ij} (mm)	0.27	0.39	0.47	0.58	0.63	0.69	0.78	0.99	1.00
	e_{ij} (%)	0.02	0.03	0.04	0.05	0.06	0.06	0.07	0.09	0.10
	e_{ij} (% Mesh Size)	27.08	26.49	23.90	23.20	21.31	19.86	19.54	22.22	20.15
B	e_{ij} (mm)	0.19	0.27	0.31	0.36	0.41	0.48	0.49	0.55	0.46
	e_{ij} (%)	0.02	0.03	0.03	0.03	0.04	0.05	0.05	0.06	0.05
	e_{ij} (% Mesh Size)	19.45	18.32	15.96	14.49	13.81	13.77	12.26	12.37	9.24
C	e_{ij} (mm)	0.35	0.47	0.63	0.71	0.81	0.91	1.03	1.16	1.16
	e_{ij} (%)	0.03	0.04	0.06	0.07	0.08	0.08	0.10	0.11	0.11
	e_{ij} (% Mesh Size)	35.19	31.43	31.55	28.49	27.24	26.01	25.86	25.81	23.30

Two other cases B and C (free-form plates) are also studied for different sizes of mesh like the case A. In the case B, the dimensions are $900 \times 40 \times 1$ mm and the nominal maximum geodesic distance $NGD = 908.65\, mm$. The dimensions are $1000 \times 100 \times 2$ mm for the case C, and the nominal maximum geodesic distance $NGD = 1013.50\, mm$.

The results (Table 4.1) show that the maximum percentage (%) of the algorithmic error is around 0.10, 0.06, and 0.11 in the cases A, B, and C.

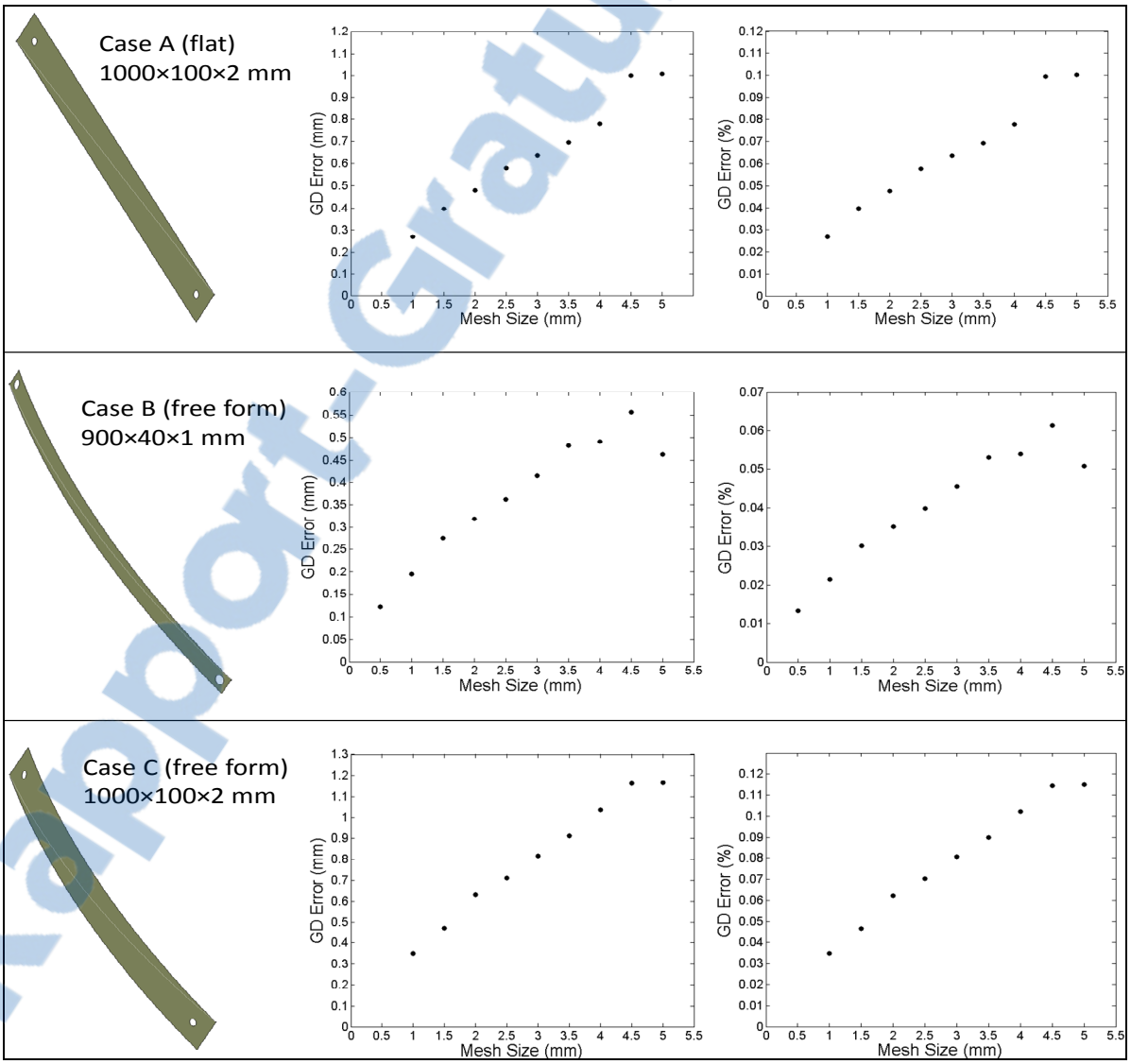

Figure 4.4 Cases A, B, and C; algorithmic error (e_{ij} in mm and $e_{ij}(\%)$) of the FMM in plots

Accuracy of the proposed method based on the FMM is also compared to another method, adapted CPD developed by Aidibe and Tahan (Aidibe and Tahan 2015), on a same case study used in their paper (Figure 4.5). Defects are imposed in three different positions and with different values. Fifteen (15) cases are generated with different defects combining different positions and values. Table 4.2 represents these cases as well as the nominal values and the position of the imposed defects, estimated values of the defects by the adapted CPD method and by our adapted FMM. Table 4.3 represents the algorithmic error percentage for each method. In this case study, the maximum of the algorithmic error is 0.12 % for the adapted FMM and 0.24 % for the adapted CPD.

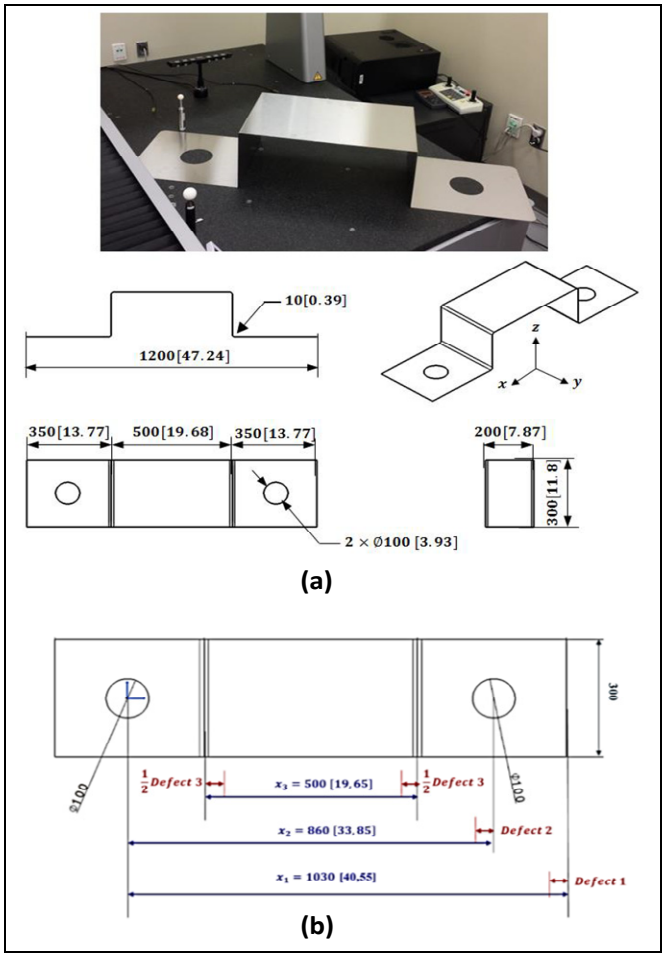

Figure 4.5 Case study applied in the adapted CPD (Aidibe and Tahan 2015); a) CAD model with the nominal dimensions, and the manufactured part, b) positions of the imposed defects

Table 4.2 Case studies with the position and the nominal values of the defects, and estimated values of the defects by each method

Case		Nominal value of defects (mm)			Estimated value of defects (mm)					
					Adapted CPD (Aidibe and Tahan 2015)			Adapted FMM		
		Δx_1	Δx_2	Δx_3	Δx_1	Δx_2	Δx_3	Δx_1	Δx_2	Δx_3
B1	V1	3.5	-	-	3.57	-	-	3.79	-	-
	V3	17.5	-	-	17.93	-	-	17.84	-	-
	V5	35.0	-	-	35.45	-	-	35.40	-	-
B2	V1	0	1.8	-	-	1.9	-	-	2.17	-
	V3	0	9.0	-	-	8.8	-	-	9.34	-
	V5	0	18.0	-	-	17.37	-	-	18.35	-
B3	V1	3.5	1.8	-	3.46	1.17	-	3.80	2.02	-
	V3	17.5	9.0	-	17.59	8.37	-	17.87	9.30	-
	V5	35.0	18	-	34.58	17.13	-	35.44	18.36	-
B4	V1	-	-	5.0	-	-	4	-	-	5.60
	V3	-	-	25.0	-	-	25.86	-	-	25.57
	V5	-	-	50.0	-	-	48.6	-	-	50.54
B5	V1	3.5	1.8	5.0	3.3	1.51	4.12	3.75	1.96	5.35
	V3	17.5	9.0	25.0	17.6	8.35	24.27	17.94	9.34	25.64
	V5	35.0	18.0	50.0	34.47	18.61	48.73	35.39	18.30	50.07

Table 4.3 Case studies with the position and the nominal values of the defects, and the algorithmic error percentage (%) for each method

Case		Nominal value of defects (mm)			Algorithmic error ÷ nominal distance (e_{ij}) (%)					
					Adapted CPD (Aidibe and Tahan 2015)			Adapted FMM		
		Δx_1	Δx_2	Δx_3	Δx_1	Δx_2	Δx_3	Δx_1	Δx_2	Δx_3
B1	V1	3.5	-	-	0.004	-	-	0.02	-	-
	V3	17.5	-	-	0.03	-	-	0.02	-	-
	V5	35.0	-	-	0.03	-	-	0.02	-	-
B2	V1	0	1.8	-	-	0.008	-	-	0.02	-
	V3	0	9.0	-	-	-0.01	-	-	0.02	-
	V5	0	18.0	-	-	-0.01	-	-	0.02	-
B3	V1	3.5	1.8	-	-0.002	-0.05	-	0.02	0.01	-
	V3	17.5	9.0	-	0.006	-0.05	-	0.02	0.02	-
	V5	35.0	18	-	-0.02	-0.02	-	0.03	0.02	-
B4	V1	-	-	5.0	-	-	-0.19	-	-	0.11
	V3	-	-	25.0	-	-	0.16	-	-	0.10
	V5	-	-	50.0	-	-	-0.24	-	-	0.09
B5	V1	3.5	1.8	5.0	-0.01	-0.02	-0.17	0.01	0.01	0.06
	V3	17.5	9.0	25.0	0.006	-0.05	-0.13	0.03	0.02	0.12
	V5	35.0	18.0	50.0	-0.03	0.04	-0.22	0.02	0.02	0.01
Range					0.002-0.24			0.01-0.12		

Another case (a plate with free-form surface) is represented where the features are holes (Figure 4.6). The geodesic distance between each pair of points is calculated using Equation 4.5 and the FMM. The nominal geodesic distances as well as the error percentages are shown in Figure 4.6. The algorithmic error varies between $0.19\,\text{mm}$ and $0.30\,\text{mm}$ ($0.26-0.72\,\%$). The results are shown on a plot in Figure 4.7.

NGD = [0 45 90 33.173 95.919 66.346 80.167 111.812
0 0 45 55.906 55.906 80.167 66.346 80.167
0 0 0 95.919 33.173 111.812 80.167 66.346
0 0 0 0 90 33.173 55.906 95.919
0 0 0 0 0 95.919 55.906 33.173
0 0 0 0 0 0 45 90
0 0 0 0 0 0 0 45]

EGD = [0 0.25 0.28 0.23 0.26 0.25 0.28 0.28
0 0 0.25 0.28 0.26 0.30 0.23 0.29
0 0 0 0.27 0.23 0.29 0.30 0.25
0 0 0 0 0.19 0.24 0.30 0.27
0 0 0 0 0 0.26 0.30 0.23
0 0 0 0 0 0 0.25 0.27
0 0 0 0 0 0 0 0.25]

Nominal GD = 45 - 111.81 mm

Error of GD = 0.19 - 0.30 mm
= 0.26 - 0.72 %

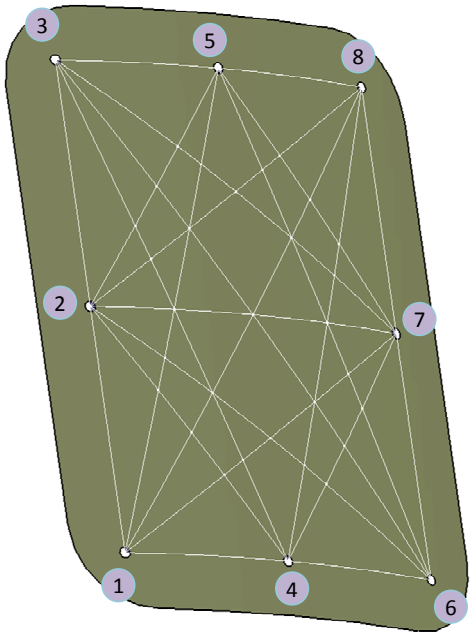

Figure 4.6 A skin with free-form surface and hole features

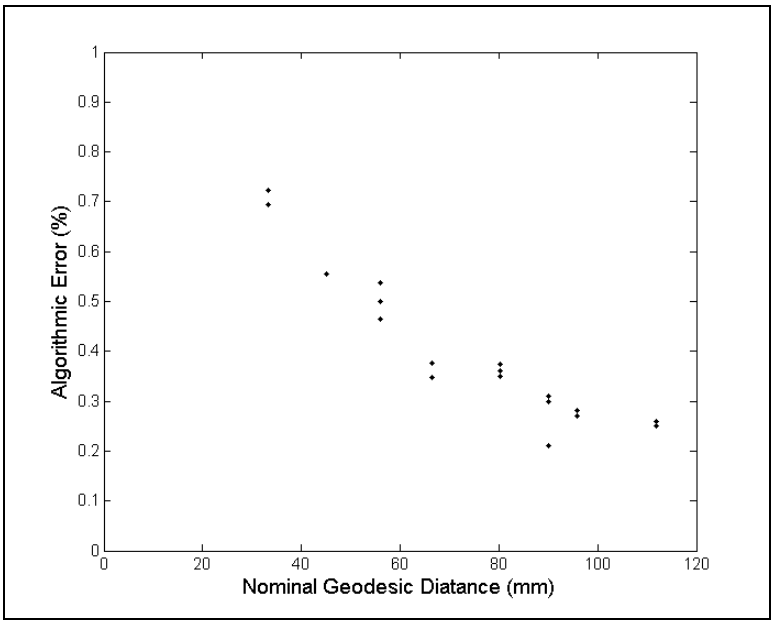

Figure 4.7 Nominal geodesic distance (mm) – Algorithmic error (e_{ij}) (%)

The general application of the proposed approach will be for the inspection of non-rigid parts in the free-state condition. Therefore, a non-rigid case study with different types of (isometric) displacement is evaluated to validate the level of systematic error (bias) induced by the algorithm. To verify if the geodesic distances remain the same during different configurations of displacement, a part is considered without any defect. There are two types of displacement and two values for the maximum displacement, so there are totally 4 configurations other than the nominal shape (Figure 4.8). The results indicate that the maximum algorithmic error is around 0.10 % in the case with flexural displacement and maximum displacement of 25 mm which is much bigger than a typical displacement for a non-rigid mechanical part in the free-state condition.

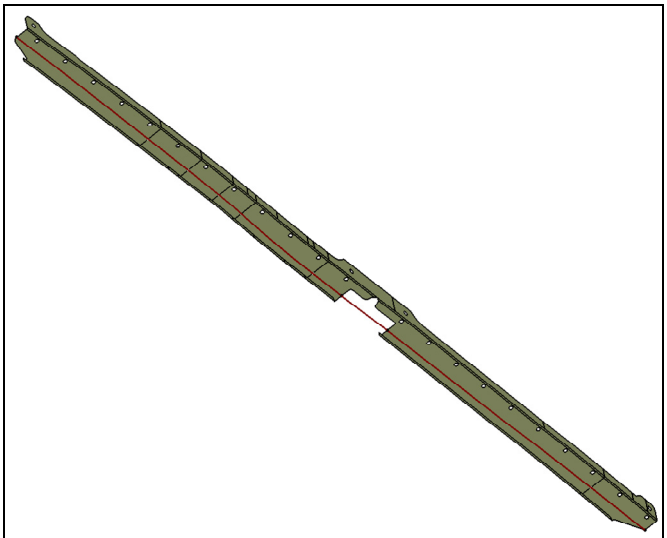

Maximum Displacement (mm)	Estimated Geodesic Distance (mm)	Error (%)
0 (Nominal)	1156	0
12 (Flexural)	1156.43	0.04
25 (Flexural)	1157.12	0.10
12 (Torsional)	1156.14	0.01
25 (Torsional)	1156.21	0.02

Figure 4.8 Algorithmic error (e_{ij}) (%) in different displacement configurations induced to a defect-free case

4.5 Conclusion

In this paper, a virtual technique was proposed for the dimensional metrology of non-rigid parts based on the conservation of arc length distance. The method applied the fast marching method to identify the geodesic distance between each preselected pair of points on the surface of the part. The approach was tested on several case studies, inspired from aviation applications, with different configurations such as different shapes (flat or free-form), dimensions, and mesh size ($1 - 5\ mm$). The maximum algorithmic error was $0.11\ \%$. As well, its accuracy was compared to a recently developed method of adapted CPD on a case study. The maximum percentage of the algorithmic error was 0.12 for our adapted FMM and 0.24 for the adapted CPD. This algorithm was also extended for use in skins with hole features by computing the average geodesic distance. In this case, the maximum algorithmic error was $0.72\ \%$. Since the general application of the proposed approach will be for the inspection of non-rigid parts in free-state condition, a non-rigid defect-free case study with different types of displacement was evaluated. The results indicated that the maximum algorithmic error was $0.10\ \%$. As observed in several cases, the satisfying results prove that the FMM is a highly accurate method for the dimensional metrology of arc length along the surface. The presented approach can be used for a fast and efficient dimensional inspection of non-rigid parts through point cloud acquisition in a free-state condition, without the need for dedicated fixtures. Therefore, instead of using manual measuring tapes, we can apply the presented numerical approach to measure the arc length automatically with a very high accuracy.

4.6 Acknowledgments

The authors would like to thank the National Sciences and Engineering Research Council (NSERC) and our industrial partners for their support and financial contribution.

CONCLUSION

In this thesis, we studied on the dimensional inspection of non-rigid (flexible) mechanical parts virtually to eliminate the need for dedicated inspection fixtures which consume much time and cost. Several approaches have been developed for the above-mentioned objective. These developed approaches save time and cost by acquiring point clouds from non-rigid parts' surface in a free-state condition (without positioning on dedicated fixtures) by means of optical scanners in a very short time, and applying numerical techniques and simulations for the aim of the dimensional inspection using the virtual inspection fixtures instead of the physical ones.

A numerical method was developed in Chapter 1 for the profile inspection of flexible parts without the need for specialized inspection fixtures. This approach was studied and evaluated on two industrial non-rigid part models from our industrial partner, Bombardier Aerospace Inc. To compare a point cloud (extracted from a simulated part containing known displacement and deviations) with the CAD model, a pre-alignment and a rigid registration (using the ICP method) were performed first. Next, applying the GNIF method, correspondents between the two data sets were found. Knowing the constrained areas such as contact surfaces and fixation areas on the CAD model, planes were fitted through the points inside each area as well as their correspondents on the scanned data. Then, the centre of mass inside each area was inserted into the related mesh. Next, the displacement vectors were calculated accordingly based on the difference between the coordinate of each centre of mass on the CAD model and its corresponding centre of mass on the scanned part. Therefore, the displacement boundary conditions (BC) were completely defined by local translation laws for finite element simulation. Applying FE analysis, the CAD model was deformed towards the scanned model by applying the displacement vectors as the displacement boundary conditions on the inserted nodes (centres of mass) on the CAD model. The deviation amplitudes, areas, and positions were identified by comparing the scanned data with the displaced CAD model. In this chapter, the developed method was applied on two industrial case studies with free-form surfaces. A definition of boundary conditions, and consequently,

an identification of deviations were improved using our approach. If the boundary conditions are completely and exactly defined, more precise results will inevitably be obtained. Repeatability of the proposed approach was evaluated by introducing Gaussian measurement noise on a case.

In Chapter 2, we improved our approach in the main steps (2, 3, and 4) of the algorithm:

Step 2: The GNIF code, in MATLAB®, was modified and the 32-bit version was converted into a 64-bit version to achieve the capability of dealing with high density data sets. In the 32-bit version, the GNIF code can be only applied on meshes with less than 10,000 nodes; whereas using the modified 64-bit version, we can search for correspondence, and consequently apply the proposed method, on any case study with an enormous number of nodes. The improvement in the step 2 (the 64-bit version of the GNIF algorithm) enabled us to apply the method on large flexible parts with dense point clouds.

Step 3: To increase accuracy of the FE calculation and consequently the non-rigid inspection result, the generated centres of mass were projected individually on their related CAD or scanned models. To this end, each inserted centre of mass was moved along its normal direction respect to the mesh surface to coincide with the related mesh triangulation. Then, the displacement vectors were calculated accordingly based on the difference between the coordinate of each projected sample point (centre of mass) on the CAD model and its corresponding projected sample point on the scanned part. Therefore using the sample projection technique, the accuracy of the method improved in the step 3.

Step 4: The insertion of the added nodes (projected centres of mass instead of original ones) into the related mesh was done automatically using a classical Delaunay point insertion method (Borouchaki, George et al. 1996). The FEA was performed by applying a new and open source method (Cuillière and Francois 2014). In other words, the algorithm also improved in the step 4, and we saved time and cost.

The improved method was applied on two industrial flexible parts with free-form surfaces; one from the previous work and a new larger one. The automatic node insertion technique

and FE solver in the step 4 allowed us to evaluate the repeatability and study the robustness of the approach by introducing Gaussian measurement noise three times on each case. The proposed approach was totally applied on 32 case studies: 8 original (noise-free) cases, and 24 cases with noise. The error percentage generally decreases by improving the definition of boundary conditions. A precise and complete definition of boundary conditions leads to precise results. Also, the accuracy of the correspondence searching method (the modified GNIF method in our paper) definitely affects the results. Metrological performance of the approach was analysed using Box Plots that proved the robustness of the method to the typical measurement noise according to the results of the repeatability evaluation.

Chapter 3 dedicates to a virtual technique proposed for dimensional metrology of non-rigid parts based on the conservation of arc length distance. The method applied the fast marching method to identify the geodesic distance between each preselected pair of points on the part surface. The approach was tested on several case studies, inspired from aviation applications, with different configurations such as different shape (flat or free-form), dimensions, and mesh size ($1 - 5\,mm$). The maximum algorithmic error was $0.11\,\%$. As well, its accuracy was compared with a recently developed method of adapted CPD on a case study. The maximum percentage of the algorithmic error was 0.12 for the adapted FMM and 0.24 for the adapted CPD. This algorithm was also extended to be used in skins with hole features by computing the average geodesic distance. In this case, the maximum algorithmic error was $0.72\,\%$. Since the general application of the proposed approach will be for the inspection of non-rigid parts in the free-state condition, a non-rigid defect-free case study with different types of displacement was evaluated. The results indicated that the maximum algorithmic error was $0.10\,\%$. As studied on several cases, the satisfying results prove that the FMM is a highly accurate method for dimensional metrology of arc length along the surface and the presented approach can be used for a fast and efficient dimensional inspection of non-rigid parts through point cloud acquisition in a free-state condition, without the need for dedicated fixtures. Therefore, instead of using manual measuring tapes, we can apply the presented numerical approach to measure the arc length automatically with a very high accuracy.

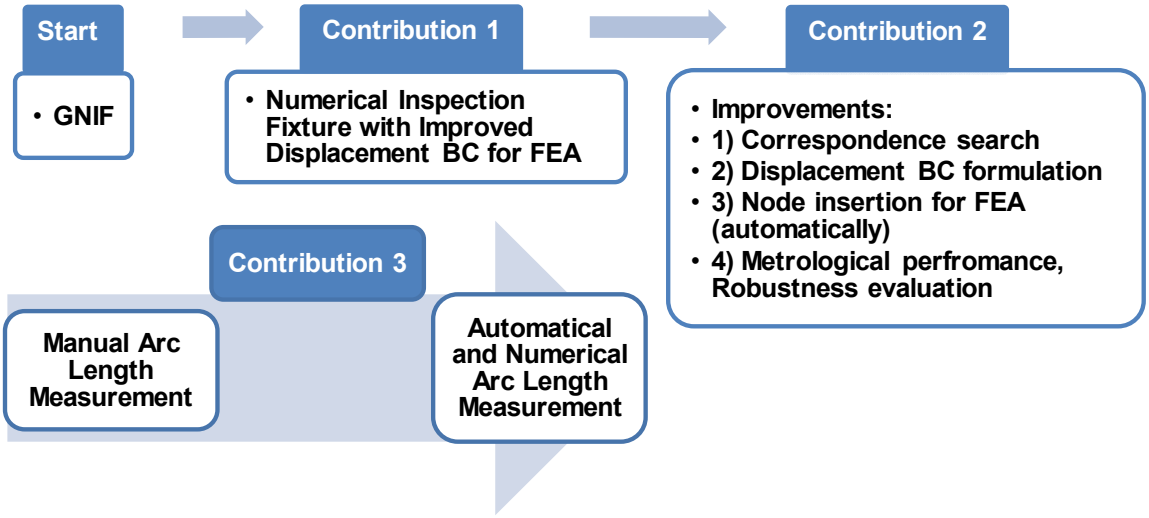

Figure C.1 Thesis contributions

RECOMENDATIONS

1. The presented contributions were applied and validated on several industrial case studies with different shapes and configurations. However, to improve the definition of boundary conditions, the developed methods can be studied and evaluated on **different non-rigid parts with different kinds of boundary conditions and constraints** such as sliding contacts.

2. The flexible parts studied in this thesis have constant thickness (and therefore constant flexibility) so that we considered them skins, captured point clouds from their surface, and applied the triangle shell element for the FEA. In some cases in the industry, the compliance behavior of a non-rigid part is not constant because of its **variable thickness and / or stiffeners**. Dealing with this kind of cases needs to be deeply studied forasmuch as it is very challenging in many aspects such as data acquisition, FEA, and conformation.

3. In our approaches, it has been tried to automatically simulate as closely as possible the real (industrial) procedure (conformation) of the geometric inspection of non-rigid parts. We took into account important factors such as mechanical behavior and flexibility by applying the FEM, and automatized our methods in most of their sections. Although, to improve the approaches applicability, **the limit of the force required for the assembly and the conformation of non-rigid parts must be considered**. The compliance behavior of a non-rigid part is a relative notion based on the ratio between a reasonable force during inspection (around 50 N) and its induced displacement. **Automatization of the approaches can be still improved** (e.g. in determination of boundary areas for the first time in each CAD model).

4. Another challenge is **to establish an assembly strategy** to optimize the conformation of a non-rigid part with known defects for better identification results and to avoid exceeding the limit of the force needed for the flexible part conformation.

5. To apply the correspondence search algorithm in the GNIF method (or GMDS), the CAD and the scanned part should be in triangle surface mesh. It is very easy to generate an ideal mesh for the CAD model. But there are uncertainties in converting a dense point cloud (acquired from a part surface by optical scanner with noise and in some cases only partial capture) to a coherent triangle surface mesh. Therefore, an important challenge is **to apply the proposed approaches on real point clouds acquired from part surfaces** to compare the experimental and the numerical results and to achieve the industrial implementation.

6. The correspondence search algorithm GMDS is accurate enough in most of the cases. But the results in some cases are not accurate or satisfying such as symmetrical parts. One suggestion is **to research on a more accurate and reliable method for the correspondence search**. Several approaches have been developed for the correspondence search in different fields of study such as computer vision and medical imaging. However, their accuracy and applicability should be studied and evaluated especially compared to the GMDS algorithm.

7. **A rigorous validation research** is recommended by the study of the methods' uncertainties and their effects on the results. Two variable groups can be considered:
   - Geometrical specifications and calculations such as the geodesic distance calculation and the correspondence search,
   - Mechanical properties, material behavior, compliance behavior, FE method, boundary condition definition.

   The accuracy of the developed numerical methods is limited by the uncertainty of different elements such as:
   - Data acquisition device (scanner),
   - Simulation of the numerical inspection fixture,
   - Geodesic distance calculation (with FMM algorithm),
   - Correspondence search algorithm (with GMDS algorithm),
   - The FE method and the boundary condition definition,

- Mechanical properties, material, and compliance behavior.

8. The materials of the cases studied in this thesis are Al alloys which have widely been used in the aeronautic production especially because of their light weight. In the newest technologies and developments, application of composite (non-isotropic) materials is growing up. Depending on the functional requirements, this category of materials can have lighter weight and better mechanical properties (e.g., Young's modulus, yield strength). Therefore, the **non-isotropic material** is a highly recommended subject for future researches.

9. The methods developed in / out of this thesis have advantages and shortcomings. Also mostly, each one is applicable for special cases depending on the part's shape and flexibility or the tolerance to be verified. For the aim of an industrial implementation, a highly interesting challenge is **to develop a global approach** taking advantages and considering the shortcomings of the approaches proposed in / out of this thesis.

BIBLIOGRAPHY

Abenhaim, G. N., A. Desrochers, A. S. Tahan and J. Bigeon (2015). "A virtual fixture using a FE-based transformation model embedded into a constrained optimization for the dimensional inspection of nonrigid parts." Computer-Aided Design 62: 248-258.

Abenhaim, G. N., A. Desrochers and S. A. Tahan (2012). "Nonrigid parts' specification and inspection methods: notions, challenges, and recent advancements." The International Journal of Advanced Manufacturing Technology 63(5-8): 741-752.

Abenhaim, G. N., A. S. Tahan, A. Desrochers and R. Maranzana (2011). "A novel approach for the inspection of flexible parts without the use of special fixtures." Journal of Manufacturing Science and Engineering 133(1).

Abenhaim, G. N., S. A. Tahan, A. Desrochers and R. Maranzana (2011). "A Novel Approach for the Inspection of Flexible Parts Without the Use of Special Fixtures." Journal of Manufacturing Science and Engineering 133(1): 011009-011011.

Aidibe, A. and A. Tahan (2014). "The inspection of deformable bodies using curvature estimation and Thompson-Biweight test." The International Journal of Advanced Manufacturing Technology: 1-15.

Aidibe, A. and A. Tahan (2015). "Adapting the coherent point drift algorithm to the fixtureless dimensional inspection of compliant parts." The International Journal of Advanced Manufacturing Technology: 1-11.

Aidibe, A., A. Tahan and G. Abenhaim (2012). "Distinguishing profile deviations from a part's deformation using the maximum normed residual test." WSEAS Transactions on Applied and Theoretical Mechanics 7(1): 18-28.

Aidibe, A., S. A. Tahan and G. N. Abenhaim (2011). Dimensioning control of non-rigid parts using the Iterative Displacement Inspection with the maximum normed residual test.

Amberg, B., S. Romdhani and T. Vetter (2007). Optimal Step Nonrigid ICP Algorithms for Surface Registration. IEEE Conference on Computer Vision and Pattern Recognition, Minneapolis, MN, USA.

Ascione, R. and W. Polini (2010). "Measurement of nonrigid freeform surfaces by coordinate measuring machine." The International Journal of Advanced Manufacturing Technology 51(9-12): 1055-1067.

ASME-Y14.5 (2009). ASME Y14.5-2009. Dimensioning and tolerancing. The American Society of Mechanical Engineers, New York, The American Society of Mechanical Engineers National Standard.

Beraldin, J. A. (2010). Étude sur le hardware de métrologie 3D. I. L. Inc.

Besl, P. J. and N. D. McKay (1992). "A method for registration of 3-D shapes." IEEE Transactions on pattern analysis and machine intelligence 14(2): 239-256.

Borg, I. and P. J. F. Groenen (2005). Modern multidimensional scaling: Theory and applications, Springer Verlag.

Borouchaki, H., P. L. George and S. H. Lo (1996). "Optimal delaunay point insertion." International Journal for Numerical Methods in Engineering 39(20): 3407–3437.

Bose, P., A. Maheshwari, C. Shu and S. Wuhrer (2011). "A survey of geodesic paths on 3D surfaces." Computational Geometry 44(9): 486-498.

Bronstein, A., M. Bronstein, M. Bronstein and R. Kimmel (2007). Numerical geometry of non-rigid shapes, Springer-Verlag New York Inc.

Cuillière, J.-C. and V. Francois (2014). "Integration of CAD, FEA and Topology Optimization through a Unified Topological Model." Computer-Aided Design and Applications 11(5): 493-508.

Dijkstra, E. (1959). "A note on two problems in connexion with graphs." Numerische mathematik 1(1): 269-271.

Fan, J., J. Yang, F. Lu, D. Ai, Y. Zhao and Y. Wang (2016). "3-Points Convex Hull Matching (3PCHM) for fast and robust point set registration." Neurocomputing 194: 227-240.

Gao, J., N. Gindy and X. Chen (2006). "An automated GD&T inspection system based on non-contact 3D digitization." International journal of production research 44(1): 117-134.

Garrido, S., L. Moreno, D. Blanco and P. P. Jurewicz (2011). "Path Planning for Mobile Robot Navigation Using Voronoi Diagram and Fast Marching." International Journal of Intelligent Systems and Applications in Robotics 2(1): 42-64.

Gentilini, I. and K. Shimada (2011). "Predicting and evaluating the post-assembly shape of thin-walled components via 3D laser digitization and FEA simulation of the assembly process." Computer-Aided Design 43(3): 316-328.

ISO-1101: (2004). ISO 1101:2004. Geometrical product specifications (GPS)—geometrical tolerancing—tolerances of form, orientation, location and run-out. Geneva, International Organization for Standardization (ISO).

ISO-10579: (2010). ISO 10579:2010. Geometrical product specifications (GPS)—dimensioning and tolerancing—non-rigid parts. Geneva, International Organization for Standardization (ISO).

Jaramillo, A., F. Prieto and P. Boulanger (2013). "Fast dimensional inspection of deformable parts from partial views." Computers in Industry(0).

Jaramillo, A., F. Prieto and P. Boulanger (2013). "Fixtureless inspection of deformable parts using partial captures." International Journal of Precision Engineering and Manufacturing 14(1): 77-83.

Jaramillo, A. E., P. Boulanger and F. Prieto (2009). On-line 3-D inspection of deformable parts using FEM trained radial basis functions. IEEE 12th International Conference on Computer Vision Workshops (ICCV Workshops), Kyoto, Japan, IEEE.

Jaramillo, A. E., P. Boulanger and F. Prieto (2011). "On-line 3-D system for the inspection of deformable parts." The International Journal of Advanced Manufacturing Technology 57(9-12): 1053-1063.

John, D. H. and N. Nathan (2013). Characterizing the Shape of LTA Vehicles Using Photogrammetry and Stretch Functions. AIAA Lighter-Than-Air Systems Technology (LTA) Conference, American Institute of Aeronautics and Astronautics.

Kimmel, R. and J. Sethian (1998). "Computing geodesic paths on manifolds." Proc. Natl. Acad. Sci. USA 95(15): 8431–8435.

Kimmel, R. and J. A. Sethian (1998). "Computing geodesic paths on manifolds." Proceedings of the National Academy of Sciences 95(15): 8431.

Li, Y. and P. Gu (2004). "Free-form surface inspection techniques state of the art review." Computer-Aided Design 36(13): 1395-1417.

Li, Y. and P. Gu (2005). "Inspection of free-form shaped parts." Robotics and Computer-Integrated Manufacturing 21(4-5): 421-430.

Martínez, S., E. Cuesta, J. Barreiro and B. Álvarez (2010). "Analysis of laser scanning and strategies for dimensional and geometrical control." The International Journal of Advanced Manufacturing Technology 46(5): 621-629.

Myronenko, A. and S. Xubo (2010). "Point Set Registration: Coherent Point Drift." Pattern Analysis and Machine Intelligence, IEEE Transactions on 32(12): 2262-2275.

Radvar-Esfahlan, H. and S.-A. Tahan (2014). "Robust generalized numerical inspection fixture for the metrology of compliant mechanical parts." The International Journal of Advanced Manufacturing Technology 70(5-8): 1101-1112.

Radvar-Esfahlan, H. and S. A. Tahan (2012). "Nonrigid geometric metrology using generalized numerical inspection fixtures." Precision Engineering 36(1): 1-9.

Sabri, V., S. A. Tahan, X. T. Pham, D. Moreau and S. Galibois (2016). "Fixtureless profile inspection of non-rigid parts using the numerical inspection fixture with improved definition of displacement boundary conditions." The International Journal of Advanced Manufacturing Technology 82(5): 1343-1352.

Sattarpanah Karganroudi, S., J.-C. Cuillière, V. Francois and S.-A. Tahan (2016). "Automatic fixtureless inspection of non-rigid parts based on filtering registration points." The International Journal of Advanced Manufacturing Technology 87(1): 687-712.

Savio, E., L. De Chiffre and R. Schmitt (2007). "Metrology of freeform shaped parts." CIRP Annals - Manufacturing Technology 56(2): 810-835.

Sethian, J. (1996). "A fast marching level set method for monotonically advancing fronts." Proceedings of the National Academy of Sciences 93(4): 1591.

Sethian, J. (1999). Level set methods and fast marching methods, Cambridge university press Cambridge.

Sethian, J. (2008). "Theory, algorithms, and applications of level set methods for propagating interfaces." Acta numerica 5: 309-395.

Sethian, J. A. (1996). "A fast marching level set method for monotonically advancing fronts." Proceedings of the National Academy of Sciences 93(4): 1591.

Thiébaut, F., C. Lacroix, L. Andolfatto and C. Lartigue (2017). "Evaluation of the shape deviation of non rigid parts from optical measurements." The International Journal of Advanced Manufacturing Technology 88(5): 1937-1944.

Wang, H., J. Zhou, T. Zhao and Y. Tao (2016). "Springback compensation of automotive panel based on three-dimensional scanning and reverse engineering." The International Journal of Advanced Manufacturing Technology 85(5): 1187-1193.

Weckenmann, A. and A. Gabbia (2006). Testing formed sheet metal parts using fringe projection and evaluation by virtual distortion compensation. Fringe 2005. W. Osten, Springer Berlin Heidelberg: 539-546.

Weckenmann, A. and J. Weickmann (2006). "Optical inspection of formed sheet metal parts applying fringe projection systems and virtual fixation." Metrology and Measurement Systems 13(4): 321-334.

Weckenmann, A., J. Weickmann and N. Petrovic (2007). Shortening of Inspection Processes by Virtual Reverse Deformation. Proceedings of the CIRP 4th International Conference and Exhibition on Machines and Design and Production of Dies and Molds, Cesme, Izmir, Turkey.